Binding Studies of Neuronal Nicotinic Acetylcholine Receptors Expressing Unnatural Amino Acids

Thesis by:

Ximena Da Silva Tavares

In Partial Fulfillment of the Requirements

for the Degree of

Doctor of Philosophy

California Institute of Technology

Pasadena, CA 91125

2015

(Defended August 5th, 2014)

Dedicated to my husband, Nicolas L. Rossi.

I could not have done this without you.

Thank you for sharing in this adventure.

Acknowledgements

This section was challenging, there are quite a few people who have enriched my graduate (and regular) life. My years of graduate study have in some ways been the hardest of my life and I am very grateful for all the support I have received throughout them. In hopes of acknowledging all of the pertinent people I have subdivided this section into several categories: PhD Committee, Dougherty and Lester Labs, Caltech Resources and Administration, Education Outside of Caltech, Friends and Family, Funding.

PhD Committee

I can confidently say that I would not have completed my PhD degree without the unwavering support of Professor Dennis Dougherty. He was there for me every step of the way. Dennis is not only a very gifted scientist but also a caring and dedicated advisor and leader. His ability to tailor his leadership style to the needs of his students as well as the character insight necessary to do so amaze me. I always felt like I could talk to Dennis about anything, whether work or life, and come out feeling better for it. He is also a great speaker and has a witty sense of humor. Our lab meetings were often a source of entertainment in addition to being a source of good science. A couple of times a year, Dennis and his wife, Ellen, would have the whole group over at his house, I would like to thank them both for making me feel like I had a family away from home. Dennis makes some great fudge that I will miss. He jokes that we are not allowed to tell him that we do not like it and still pass candidacy. In my first year, I thought he was serious. I did really like it, though. Since then, I have had quite a few chuckles over the

subsequent grad students' reactions to the joke. I consider myself lucky to have had Dennis as an advisor and will miss him.

Professor Sarah Reisman is my committee chair. She started her lab at Caltech on my first year as a graduate student so I feel a certain kinship with her and, while Dennis' lab was absolutely the right fit for me, I almost joined Sarah's lab and I often wonder what could have been. Sarah is a very dedicated and talented scientist and I thank her for sharing her enthusiasm for science. I also thank her for her advice on job searching. Professors Peter Dervan and David Tirrell always asked some thoughtful questions about my research. I felt they were genuinely interested in my research and the types of questions they asked have helped me develop the way I think about my projects and science.

I consider Professor Henry Lester an honorary member of my committee. Henry has significantly impacted my research. Henry's knowledge in the field of neuroscience, specifically on electrophysiology and ion channels, is unfathomable (at least to me). I think he has forgotten more about these topics than I know about them. He has provided many suggestions that have helped me overcome the myriad of issues arising when doing innovative research, often making the difference between being able to collect usable data or not. Henry has a quirky sense of humor and, between him and Dennis, our progress report meetings were never dull. Since those "unnaturals" meetings could sometimes last over 4 hours; that is saying a lot. I will always fondly remember Henry calling for "inverse coffee breaks."

Dougherty and Lester Labs

I have shared my six years in the Dougherty Lab with a remarkable group of people. Dr. Angela Blum was my mentor during my first year and showed me the proverbial ropes of the lab. A fellow animal lover, she is a very dedicated and thorough scientist. I am thankful for her attention to detail when training me, it served me well over the years. Dr. Nyssa Puskar also taught me a lot about science in the Dougherty group, specifically nicotinic receptors. My work and Nyssa's was closely related and she was a big help in those early years. I enjoyed weekly swimming workouts with Nyssa.

Besides Dennis, Dr. Jai Shanata was the single most influential person on my life in the Dougherty group. I consider Jai a good friend and I have no doubt that we will continue to be friends for years to come. Jai and I collaborated on the singles project and he trained me in the use and maintenance of the Dougherty singles electrophysiology rig as well as on single-channel data analysis. We would often spend over 24 consecutive hours collecting and/or analyzing singles data and would talk about science and life in general. We share many of the same views on the nature of consciousness. A great listener, Jai has been a steadfast source of support over these years and, much like Dennis, he never lost faith in me even when I lost faith in myself. After graduating, Jai accepted a teaching and research position at Loyola University; students working with him should consider themselves lucky, I have no doubt he will make and exceptional advisor.

Drs. Kristina Daeffler and Ethan Van Arman were my year-mates. Kristina is a fellow cat lover and crazy cat lady in training. I always admired her ability to

balance work and life. I thank her for listening to me prattle for years, I do not know how she put up with me. Ethan is a great scientist, he brought a passion for science to the lab that I found contagious. His knack for imitating accents provided much entertainment, he could easily pursue stand-up comedy as an alternative career. Dr. Noah Duffy was our resident MacGyver, he was the go to person whenever something broke in lab. I enjoyed our many conversations about horses. Clint Reagan and Matt Rienzo are excellent chemists. I thank Matt for his collaboration in the deschloroepibatidine project. Chris Marotta is a very hard worker and a prolific scientist, I have no doubt he will be successful at anything he tries. I admire his resourcefulness and dedication. Mike Post greatly enhanced social life at the Dougherty group (and Caltech) since he joined. He is a talented baker and I greatly enjoyed all the treats he brought in to lab. Tim Miles and I sat next to each other for the latter half of my graduate life. He managed the feat of graduating in 4 years and I wish him all the best in his new teaching job. Matt Davis is famous among the group for his puns. Betty Wong has an inquisitive nature that I believe will serve her well in graduate research. David Paul Walton brings a quirky sense humor to the group. Kayla Busby is a dedicated scientist and a cheerful person. Catriona Blunt, Annet Blom and Bryce Jarman joined the group in this last year. I wish them all the best in their graduate journey.

I would like to thank Jonathan Wang, Elisha Mackey and Purnima Deshpande of the Lester Lab for their tireless work to keep us supplied with oocytes.

Caltech Resources and Administration

Caltech is an amazing place where groundbreaking science is almost an everyday occurrence. It is easy to get “desensitized” to it when living it every day, but Caltech truly is amazing. There are a lot of people beyond the science who help keep Caltech running, from the President and Deans to the custodians. I would like to thank everyone involved in administration and some people especially for making my life at Caltech easier. Chemistry department secretary, Agnes Tong and Joe Drew at the Chemistry Stockroom. Steve Gould from the Purchasing Department. When I first joined Caltech, I was amazed that, when I needed something for the lab, I could just hand in an order form to Steve and the stuff would simply show up in lab some time later, like magic, no phone calls to companies or dealing with online ordering.

I would also like to thank Laura Flower Kim and Daniel Yoder at International Student Programs. Daniel and Laura work very hard to make sure every international student feels at home on campus (and in the US). I enjoyed working with Daniel and Laura when volunteering at International Student Orientation every year during my time at Caltech. I consider Laura and Daniel as my friends.

Dr. Felicia Hunt, Assistant Dean for Graduate Studies, was also a big help throughout my graduate career. I saw Dr. Lee Coleman at the Counseling Center for most of my graduate life. I can confidently say that Lee made a big difference on my mental health, something I am deeply grateful for. Perhaps the kindest thing Lee did for me, was to be an impartial listener when I most needed one.

Though the experience of grad school is different for everyone, it is seldom an easy path. I always felt that the staff and faculty at Caltech truly cared about my success and happiness in grad school. Beyond one's research Advisor, there are resources at Caltech, such as the Counseling Center and the Office of Graduate Studies, to help students deal with pretty much anything. I fear that many students are often shy about seeking help from these sources, and I wish this could be otherwise because I can honestly say it made a big difference for me.

Education Outside of Caltech

The first person to foment my love of chemistry and science in general was my High School chemistry teacher in Uruguay, Susana Ferrando. I would like to thank her for my first glimpse into the world of chemistry. Professor Georgina Hart at Miami Dade College was also an influential person in my career choice. She is an exceptional teacher and I greatly enjoyed her lectures. Dr. Frank Mari at Florida Atlantic University introduced me to ion-channels. Little did I know at the time how familiar I was to become with them, I was planning on focusing in synthetic organic chemistry back then.

Friends and Family

Naturally, I made some friends at Caltech outside of the Dougherty Lab. I met Mark Kendall through my good friend and lab-mate, Jai. Mark has since become a good friend too. Though both Mark and Jai have moved to other states, we remain close and I thank them for their friendship and support. I also thank Mark for his help with installing a new computer on the Dougherty

electrophysiology rig. During this process, Mark and I had to often fight our urge to defenestrate that computer, but we got it done. Boram Hong and Dr. Bernardo Sosa Padilla are also good friends of mine, except when Uruguay plays Argentina in soccer. They are both from Argentina, so we share much culture and being around them always made me feel closer to home.

Those who know me, know how much I love horses. Horses and science are my two lifelong passions. My husband, Nicolas Rossi, is a horse trainer. When we first moved to Pasadena in 2008 he got a job with Grand Prix rider Jenni Martin-McAllister. I would like to thank Jenni and her husband, Steve for sharing their horses and knowledge with me. Jenni is an amazingly talented rider who recently represented the US at the FEI World Cup Finals (a big deal in the horse world). Even though I have been riding since I was 4, next to her, I am beginner. I am grateful that she chose to share her knowledge about horses with me. Steve taught me a lot about equine biomechanics; we also enjoyed many philosophical debates about science and religion over the years. Gretchen Tank is a phenomenal horse-woman and trainer, I would like to thank her for many, many riding lessons. I would also like to thank Marnye and Larry Langer for opening their house and their hearts to my husband and I. Marnye and Larry are well known for their epic Halloween parties, but they also host great Thanksgiving dinners. Though he now focuses on horses, Larry has an engineering degree, so we share both horses and science. We have had many talks about science and horses and he has given me some great professional advice.

Next, I would like to thank David Sterckx and his sister, Caroline, at San Pascual Stables. In 2012, my husband got a job as David's assistant trainer and David and Caroline welcomed us into the "barn family." I found that I had as many horses to ride as I had time for and a place where I felt like I belonged. I have since made many more friends at the barn, including Jennifer Sims who is now one of my closest friends.

I have now been in the US for 10 years and, even with the advent of social media, I have lost touch with many of my friends from Uruguay. There are two people, Alejandro Martinez and Dr. Lorena Dentella, with whom I share very special friendships; the kind of friendships that not even time and distance can mitigate. Alejandro and I have been friends since we were five years old, we went through elementary, middle and high school together. Lorena and I met during my years in Medical School in Uruguay, she is now pursuing a specialization in anesthesiology.

Next, I have to thanks my parents, Armando and Alicia Da Silva Tavares, for giving me a great education which ultimately lead me to Caltech. My Dad taught me that success is a consequence, not a goal. For example, that getting an A in a class or passing an exam is not the goal, but the consequence of learning the material. My Mom taught me to believe in my dreams; that nothing was out of reach.

Finally, I would like to thank my husband, Nicolas Rossi, for everything. It is challenging to find the words to describe what a difference he has made in my life. We have been together for 12 years, which is more than 1/3 of our lives. We left

Uruguay together and have been through many tough times and have come out stronger for it. Nicolas brings meaning to my life, for what point is there to life if you have no one to share it with? I look forward to our daughter being born, I have no doubt Nicolas will be an exceptional dad. Besides starting a family together, our latest adventure involves adopting a mare, Agnes, which was found almost starved to death in a field. The incredible coincidence is that Nicolas had worked with Agnes a few years back, before the unfortunate circumstances that lead to her abuse. I am happy to say that Agnes is now fully rehabilitated and that she loves going to horse shows with Nicolas (see Picture below). She also quickly learnt that I am the treat provider and is quite adept at successful begging. Seeing Agnes' progress has brought much joy to my life as well as reminded me of how noble horses are and why I love them so much.

Nicolas and Agnes at the Flintridge Horse Show in April, 2014

Funding

The work described in the following thesis was supported by the NIH (NS 34407; NS 11756) and the California Tobacco-Related Disease Research Program of the University of California, grant number 16RT-0160.

Abstract

Nicotinic acetylcholine receptors are pentameric ligand-gated ion channels mediating fast synaptic transmission throughout the peripheral and central nervous systems. They have been implicated in various processes related to cognitive functions, learning and memory, arousal, reward, motor control and analgesia. Therefore, these receptors present alluring potential therapeutic targets for the treatment of pain, epilepsy, Alzheimer's disease, Parkinson's disease, Tourette's syndrome, schizophrenia, anxiety, depression and nicotine addiction. The work detailed in this thesis focuses on binding studies of neuronal nicotinic receptors and aims to further our knowledge of subtype specific functional and structural information.

Chapter 1 is an introductory chapter describing the structure and function of nicotinic acetylcholine receptors as well as the methodologies used for the dissertation work described herein. There are several different subtypes of nicotinic acetylcholine receptors known to date and the subtle variations in their structure and function present a challenging area of study. The work presented in this thesis deals specifically with the α4β2 subtype of nicotinic acetylcholine receptor. This subtype assembles into 2 closely related stoichiometries, termed throughout this thesis as A3B2 and A2B3 after their respective subunit composition. Chapter 2 describes binding studies of select nicotinic agonists on A3B2 and A2B3 receptors determined by whole-cell recording. Three key binding interactions, a cation-π and two hydrogen bonds, were probed for four nicotinic

agonists, acetylcholine, nicotine, smoking cessation drug varenicline (Chantix®) and the related natural product cytisine.

Results from the binding studies presented in Chapter 2 show that the major difference in binding of these four agonists to A3B2 and A2B3 receptors lies in one of the two hydrogen bond interactions where the agonist acts as the hydrogen bond acceptor and the backbone NH of a conserved leucine residue in the receptor acts as the hydrogen bond donor. Chapter 3 focuses on studying the effect of modulating the hydrogen bond acceptor ability of nicotine and epibatidine on A3B2 receptor function determined by whole-cell recording. Finally, Chapter 4 describes single-channel recording studies of varenicline binding to A2B3 and A3B2 receptors.

Table of Contents

Chapter 1:

Introduction

1.1 The Brain and the Synapse

Composed of a hundred billion neurons, two million miles of axons and a million billion synapses, the human brain is the most complex natural or artificial object known to man.[1] Thus, it is not surprising that while many advances in neuroscience have been made in the last few decades, we are far from unraveling all the intricacies of the structure and function of the human brain. Much work in the field of neuroscience has focused on the study of the synapse and membrane excitability, since it is generally believed that the regulation of these processes underlies much of higher brain function, including memory, learning, and cognition.[1] Figure 1.1 depicts the relative scale of the synapse and neuroreceptors in the central nervous system (CNS).

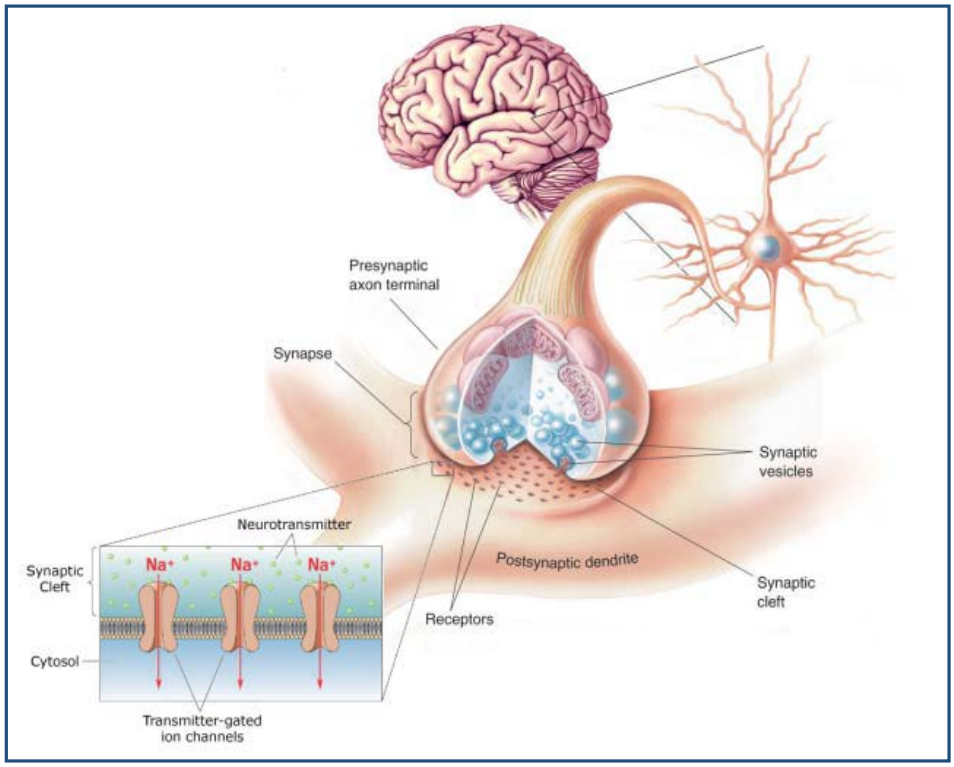

Figure 1.1 The synapse in the CNS

The synapse is defined as the connection between two neurons and can be classified into electrical or chemical depending on the type of communication between cells. Chemical synapses (Figure 1.2) are capable of producing more variable signaling and are associated with the more complex brain functions such as memory and learning.[2] In a chemical synapse an electrical impulse in a presynaptic neuron is converted to a chemical signal mediated by a neurotransmitter that diffuses across the space between the two connecting neurons (synaptic cleft) to activate ligand-gated ion channels (LGICs). Thus, the chemical signal is converted back into an electrical signal at the postsynaptic neuron. LGICs are membrane proteins, which upon binding of a ligand molecule such as a neurotransmitter, undergo a fast conformational change allowing ions to flow across the cell membrane. LGICs mediate fast synaptic transmission that occurs on the order of 1-100ms and corresponds to the majority of synaptic transmission in the brain.[1] Much of the research in the Dougherty lab focuses on the study of LGICs and other membrane receptors at the chemical scale. Two aspects are of special interest to the group; first, how agonist molecules bind to their target receptors and second, how this brings about the conformational changes that activate the receptor. The focus of this thesis will be on a specific type of LGIC: the nicotinic acetylcholine receptor.

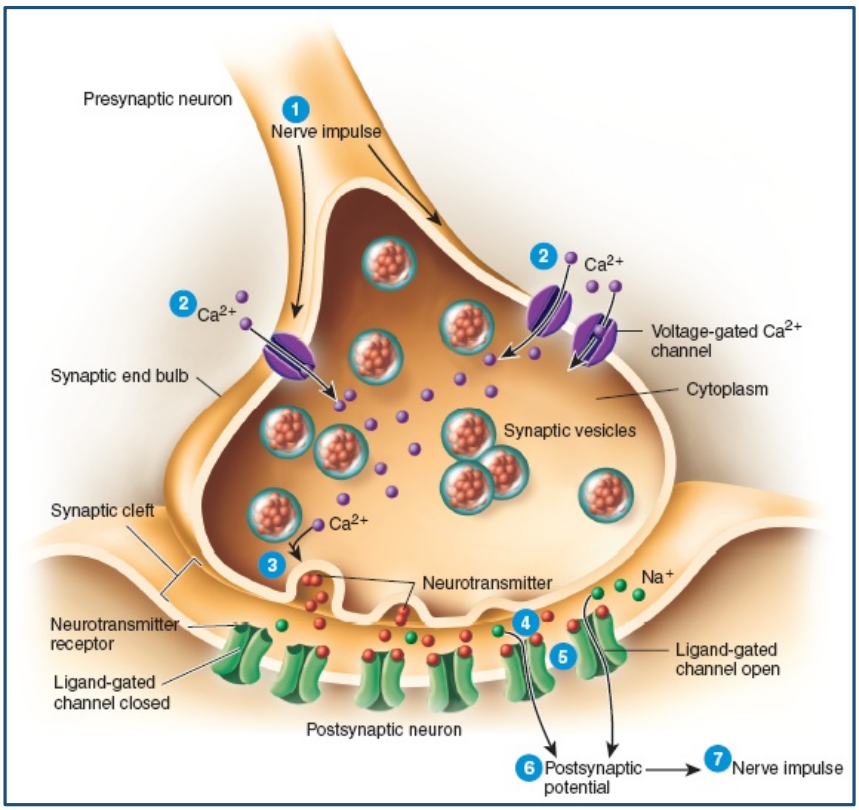

Figure 1.2 Schematic of a Chemical Synapse. An electrical signal (1) in the presynaptic neuron is converted to a chemical signal (neurotransmitter release, 3) and finally back into an electrical signal (7) at the postsynaptic neuron.[3]

1.2 The Nicotinic Acetylcholine Receptor (nAChR)

Nicotinic acetylcholine receptors (nAChRs) owe their name to their activation by the endogenous ligand acetylcholine (ACh) as well as the alkaloid nicotine (Figure 1.3) and are among the most studied neuroreceptors.[4] nAChRs belong to the superfamily of “Cys-Loop” receptors that are so termed due to the presence of a disulfide bond between two conserved cysteine residues separated by 13 amino acids. In addition to nAChRs, other members of the Cys-Loop superfamily include 5-hydroxytryptamine type 3 (5-HT_3) receptors, γ-aminobutyric acid type A and type C ($GABA_A$ and $GABA_C$) receptors, glycine receptors, and invertebrate glutamate

and histidine receptors.[5] Receptors are further classified into excitatory or inhibitory, the former correspond to cation permeable channels (Na^+, K^+ and Ca^{2+}), which promote the firing of an action potential, and the latter conduct anions (Cl^- and HCO_3^-), discouraging the firing of an action potential. nAChRs and 5-HT_3 receptors are excitatory, glycine receptors are inhibitory and GABA are mostly inhibitory.[4] Furthermore, nAChRs mediate fast synaptic transmission and are involved in a wide range of physiological and pathophysiological processes.[6]

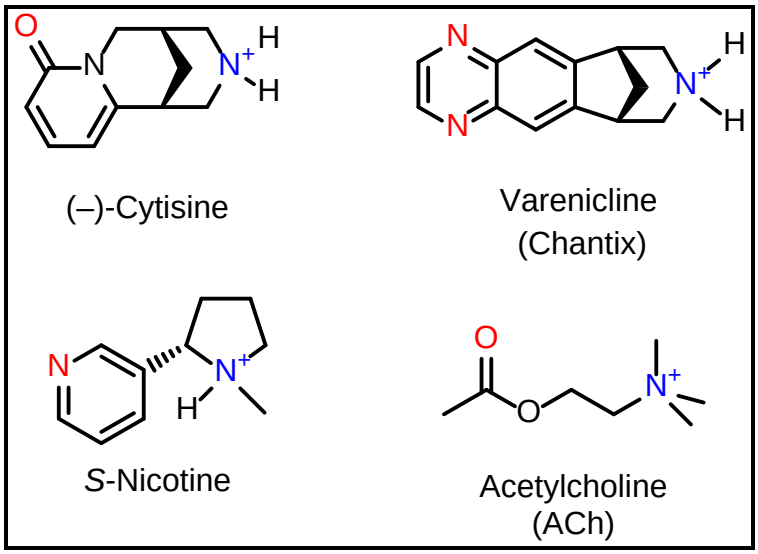

Figure 1.3 nAChR Agonists. These four nicotinic agonists share structural features consisting of a cationic nitrogen (blue) and a hydrogen bond acceptor moiety (red).

nAChRs are distinguished into muscle or neuronal nAChRs according to their localization in the neuromuscular junction or peripheral and central nervous systems, respectively. The muscle-type nAChR is found postsynaptically at the neuromuscular junction where it mediates the chemical to electrical signal transduction resulting in skeletal muscle tone. Neuronal nAChRs have been identified in numerous subtypes that reside at presynaptic and postsynaptic densities in autonomic ganglia and cholinergic neurons throughout the CNS.

These receptors have been implicated in various processes related to cognitive functions, learning and memory, arousal, reward, motor control and analgesia.[6] Due to their role regulating the neurotransmission of dopamine (DA), norepinephrine (NE), serotonin (5-hydroxytryptamine, 5-HT), glutamate (Glu) and γ-aminobutyric acid (GABA), neuronal nAChRs represent potential therapeutic targets for the treatment of pain, epilepsy, Alzheimer's disease, Parkinson's disease, Tourette's syndrome, schizophrenia, anxiety, depression and nicotine addiction.[6] As such, there is considerable interest in gaining nAChR subtype specific structural and functional information. The studies portrayed in this thesis aim to further our knowledge in this area.

Membrane proteins such as the nAChR are notoriously hard to crystallize, and therefore structural information on these proteins is scarce when compared to soluble proteins. Despite the fact that membrane proteins represent ~30% of genetically encoded proteins and ~60% of pharmaceutical targets, they correspond to less than 1% of the structures in the Protein Data Bank (PDB).[7] Presently, structural information on the nAChR stems mainly from two sources, the crystal structure of the acetylcholine binding protein (AChBP) at 2.7Å resolution, and the 4Å resolved cryo-electron microscopy images of the nAChR from the electric organ of *Torpedo californica* (Pacific electric ray) (Figure 1.4C).[8,9] Isolated from the snail *Lymnaea stagnalis*, AChBP is a soluble protein that forms stable homopentamers and shares 20-24% sequence homology with the extracellular domain (ECD) of nAChRs; thus making it a useful model of the nAChR ECD.[8] It is worth noting that since AChBP lacks a transmembrane domain (TMD) it is not an

ion channel and thus no information on nAChR receptor activation can be obtained from this model. However, Unwin et al. solved high resolution cryo-EM images of the muscle-type nAChR, revealing structural insights into the TMD of nAChRs. In conjunction, these studies depict the architecture of nAChR subunits consisting of a large N-terminal extracellular domain comprised mainly of β-sheets, a transmembrane domain consisting of 4 membrane spanning α-helices (M1-M4) and a small extracellular C-terminal domain (Figure 1.3B). nAChRs are pentameric, containing five homologous subunits arranged pseudosymmetrically around a central ion conducting pore lined by the M2 α-helices of each subunit.[9]

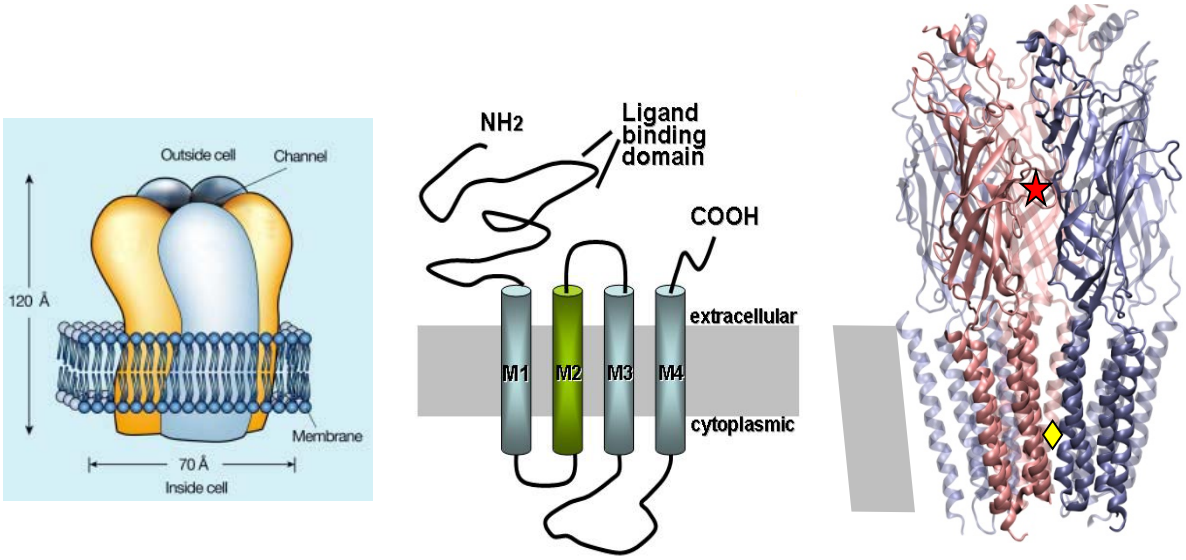

Figure 1.4. nAChR structure. Left: Cartoon depiction of a prototypical pentameric nAChR. **Middle:** Subunit topology showing the pore lining M2 transmembrane domain in green.[10] **Right:** Muscle-type nAChR image based on Unwin's model of the *Torpedo* receptor (pdb file 2BG9). Red star denotes agonist binding site and yellow rhombus indicates channel gate separated by 60Å.[9]

The nAChR family shows considerable diversity. To date, seventeen different vertebrate nAChR subunits have been identified and cloned: α1-α10, β1-β4, γ, δ and ε.[11] The subunits are divided into muscle-type (α1, β1, γ, δ and ε) and neuronal (α2-α10, β2-β4) subunits according to the receptor subtypes that they are known to form. The muscle-type subunits make up the two forms of muscle-type

receptor; $(\alpha1)_2\beta1\gamma\delta$ (embryonic form) and $(\alpha1)_2\beta1\gamma\varepsilon$ (adult form). Subunits are organized clockwise as α1β1γα1δ(or ε) and ACh binds to two orthosteric sites located at the α1/γ and α1/δ interfaces (Figure 1.5). A total of two molecules of ACh must bind, each occupying one of the two binding sites before the channel gate opens and allows the passage of cations, in favor of their electrochemical gradient, thereby translating a chemical signal into an electrical one.[6]

In contrast to the precise stoichiometry of the muscle-type nAChR, the 12 neuronal subunits can form a wide variety of different nAChR subtypes, each of which shows different characteristics in terms of ligand pharmacology, activation and desensitization kinetics as well as cation permeability.[6] Over 20 different neuronal nAChR subtypes have been identified throughout the nervous systems of various vertebrates and at least 22 neuronal subtypes have been successfully expressed in heterologous systems such as *Xenopus laevis* (African clawed frog) oocytes.[11] Of the neuronal subunits, subunits α2-α6 and β2-β4 assemble in heteropentameric complexes of variable stoichiometry, the prevalent stoichiometry being $(\alpha)_2(\beta)_3$ arranged as αβαββ but the $(\alpha)_3(\beta)_2$ stoichiometry has also been reported (Figure 1.5).[12] ACh and other agonists bind at α/β interfaces thereby giving rise to two orthosteric binding sites per receptor. Subunits α3 and α5 are considered structural subunits because they lack the amino acid residues critical for agonist binding and as such cannot participate in the formation of binding sites. It is generally accepted that the more complex neuronal nAChRs are formed by two pairs of α(2,3,4,6)/β(2,4) and only one structural subunit, though there may be exceptions where two structural subunits are present.[6,13]

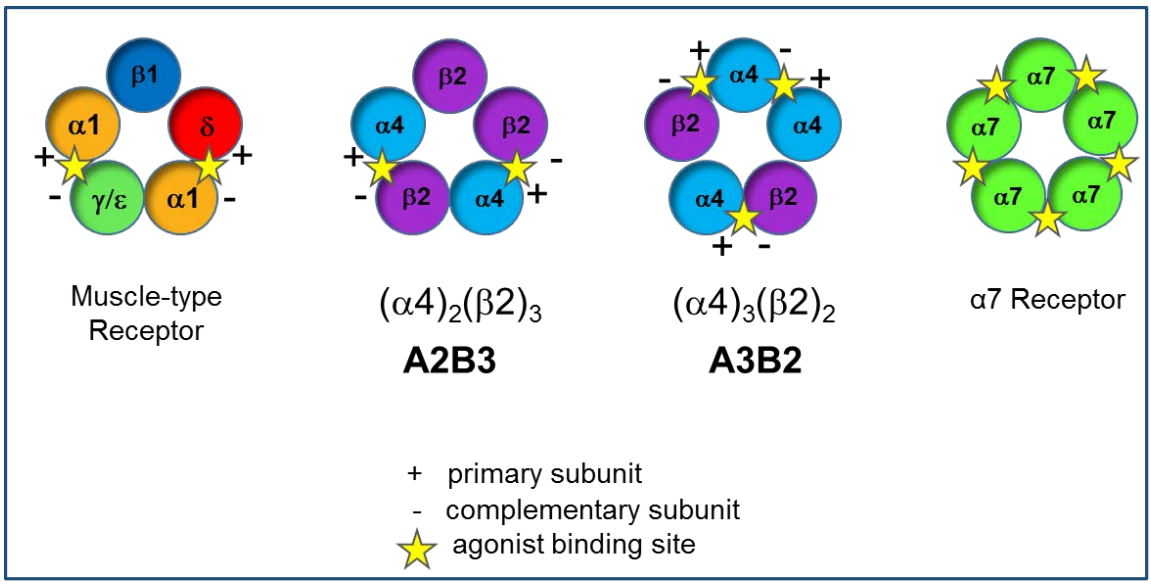

Figure 1.5 nAChR Subtypes. The yellow star denotes the agonist binding sites.

Higher order nAChR subunits α7 (Figure 1.5), α8 and α9 form homopentameric receptors with markedly larger Ca^{2+} permeabilities and faster desensitization kinetics than muscle-type and α/β nAChRs. Whereas the α10 subunit is unable to form functional homomers, it does form functional receptors of unknown stoichiometry in conjunction with α9.[6]

The most prevalent neuronal nAChRs in the CNS are α4β2 and α7, with α4β2 containing receptors comprising ~90% of CNS nAChRs and showing high affinity ACh binding, whereas α7 nAChRs exhibit low affinity ACh binding.[6] The α4β2 receptor is of particular interest due to its implication in nicotine addiction and its therapeutic targeting in smoking cessation.[14-16] This thesis focuses on the α4β2 receptor.

1.2.1 Neuronal α4β2 Receptors

Theoretically, there are six possible pentameric arrangements of α4 with β2, one $(α4)_1(β2)_4$, two combinations of $(α4)_2(β2)_3$, two combinations of $(α4)_3(β2)_2$ and one $(α4)_4(β2)_1$. There is now considerable evidence that α4β2 receptors assemble into two of those possible six stoichiometries, one $(α4)_3(β2)_2$ and one $(α4)_2(β2)_3$ receptor as shown in Figure 1.5.[12,17-20] Throughout this thesis the $(α4)_3(β2)_2$ stoichiometry will be referred to as A3B2 and the $(α4)_2(β2)_3$ as A2B3. These two stoichiometries show different pharmacological properties including differential permeability to Ca^{2+} and agonist sensitivity.[12,19] Since a higher agonist concentration is needed to activate A3B2 receptors than A2B3 receptors, the former are often referred to as the low-affinity form and the latter the high affinity form.

Until recently it was thought that each stoichiometry possessed two binding sites at select α/β interfaces where the α subunit contributed most of the binding residues and was thus termed the principal face and the β subunit was designated the complementary face (Figure 1.5). Recent evidence has challenged this view by showing the existence of a third binding site present for the A3B2 stoichiometry at the α/α interface.[21,22]

The α/β and the α/α binding sites as well as the binding sites of other subtypes of nAChRs share a common structural architecture. Figure 1.6 shows the structure of the agonist binding site based on the AChBP structure and depicts a lidless “aromatic box” (Figure 5) formed by five highly conserved aromatic residues. Four of the five aromatic residues are part of the principal binding subunit

with TyrA forming the bottom of the box and TyrC1, TyrC2 and TrpB forming three of the four sides of the box. The final aromatic residue, TrpD forms the fourth side of the box and is part of the complementary binding subunit (Figure 1.6).[9] The work presented in this thesis focuses on studying the chemical scale binding interactions of select nicotinic agonists to the α4β2 receptor.

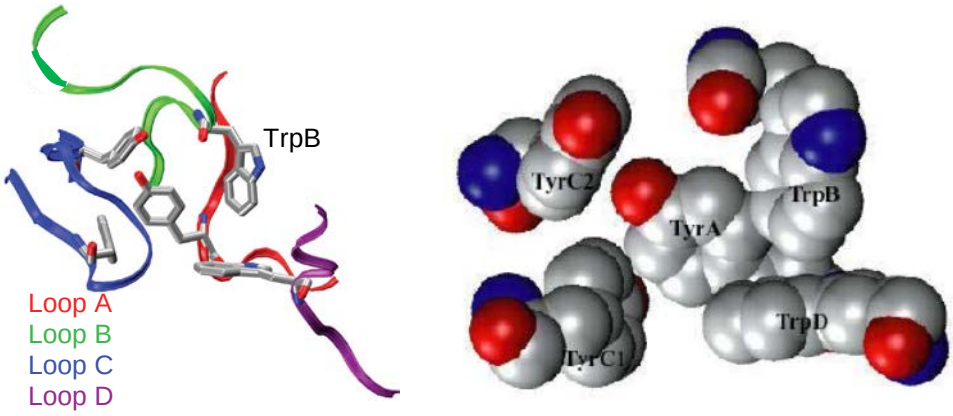

Figure 1.6. Representations of the nAChR binding site modeled from AChBP (PDB 1I9B).[10,23] Residues are designated with their corresponding three letter amino acid code followed by A-D depending on the loop that contributes the residue.

1.3 Expression of nAChRs in *Xenopus* Oocytes

Given the complexity of the human brain, isolating the object of study becomes an attractive strategy to explore a certain aspect of neurobiology. As afore mentioned, structural information on nAChRs is scarce and while valuable, structural imaging techniques such as X-ray crystallography and cryo-EM provide a snapshot of the receptor that is static in nature and cannot yield information on the dynamic events involved in function. Thus, structural information from these sources provides a guide that can be used as a starting point in structure-function studies of physiological significance. The work presented herein involves structure-function studies of the α4β2 receptor and the expression system used is

heterologous protein expression in *Xenopus* oocytes from the frog *Xenopus laevis* (Figure 1.7). *Xenopus* oocytes possess a few inherent properties that make them an ideal candidate for protein expression. First, the oocytes' large 1mm diameter makes them fairly easy to handle, facilitating not only RNA injection but also electrophysiological analysis.[24] Second, oocytes are very amenable to heterologous protein expression by accepting exogenous RNA then translating, assembling and transporting the desired protein to the plasma membrane. Finally, after removal of the follicular membrane of stage V/VI *Xenopus* oocytes, there are no endogenous ion channels that significantly interfere with the electrophysiological functional assays described in this thesis.

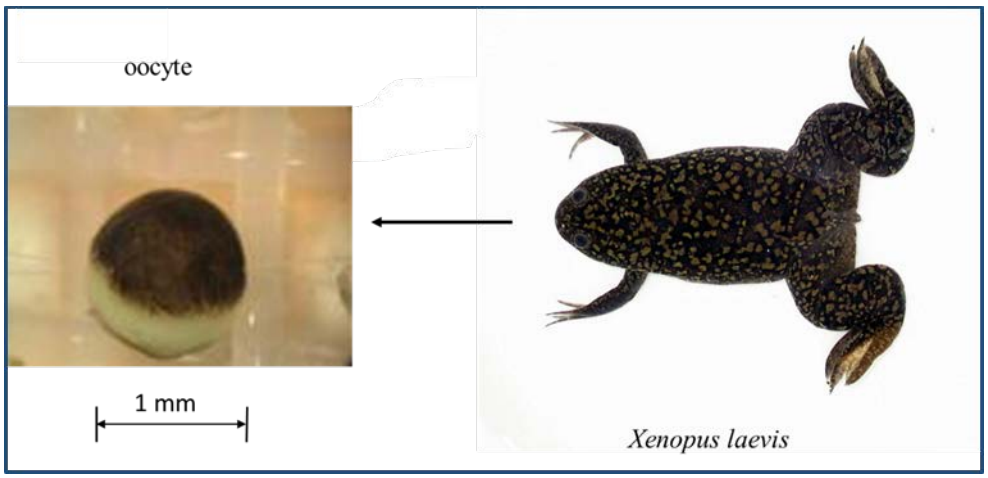

Figure 1.7 *Xenopus laevis* frog and stage V/VI oocyte

The *Xenopus* oocyte expression system certainly lends itself to conventional mutagenesis where the codon of the amino acid of interest is mutated to the codon of the amino acid introduced as a mutation. However, we are severely limited with conventional mutagenesis to the use of the 20 available natural amino acids. Subtle structural perturbations are more often than not beyond the reach of conventional mutagenesis. In 1989 Schultz et al. developed a methodology for the

in vitro incorporation of unnatural amino acids into proteins, which led to the first incorporation of an unnatural amino acid into a protein expressed in a living cell by the Lester and Dougherty labs in 1995.[25,26] Since then our group has used this methodology to incorporate a variety of unnatural amino acids (Figure 1.8) into many different receptors and ion channels, allowing us to probe for subtle functional effects and employ the tools of physical organic chemistry on the brain.[7]

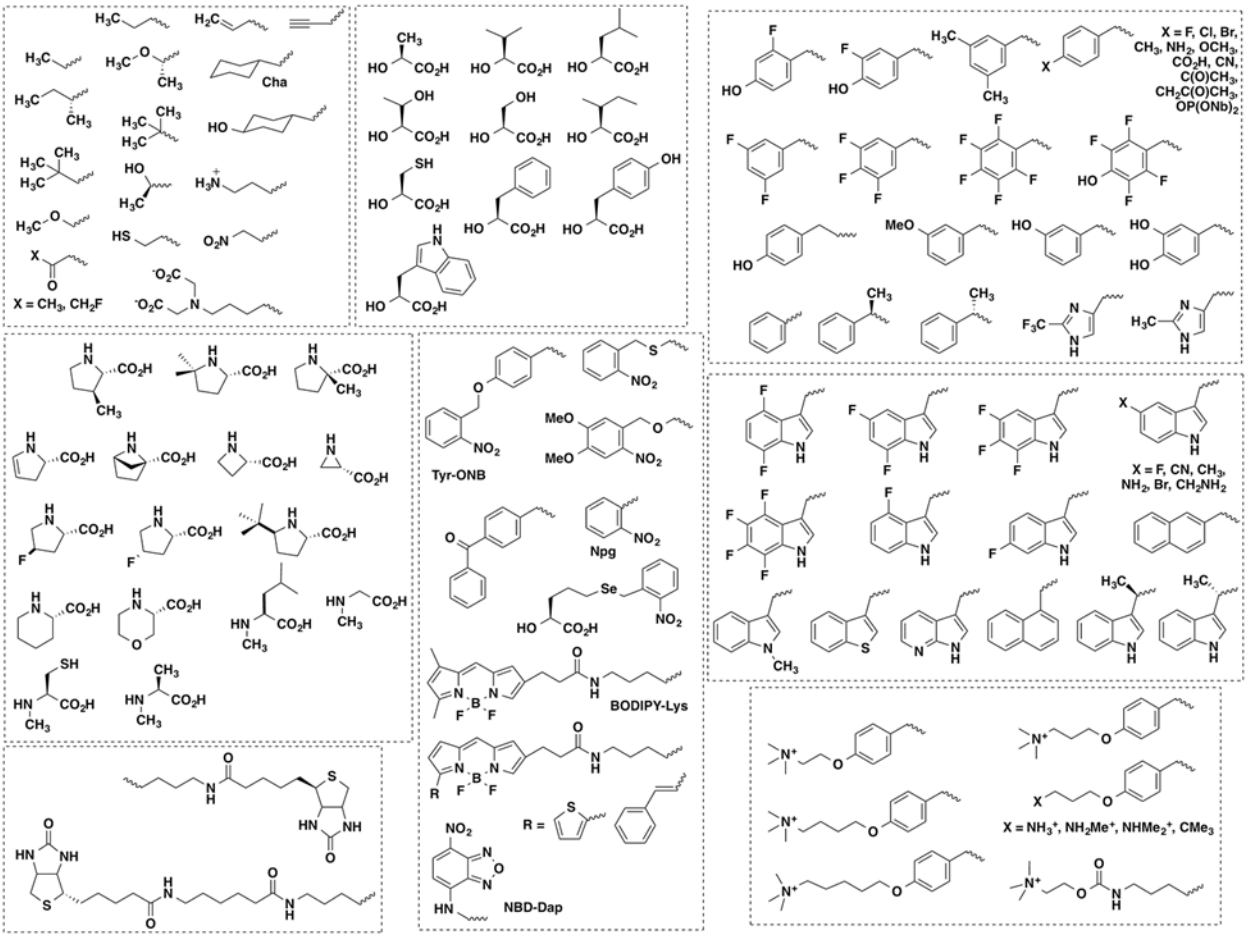

Figure 1.8 Some of the unnatural amino acid side chains that have been incorporated by nonsense suppression in the Dougherty group. The fluorinated tryptophan series residues are predominant throughout this thesis and are shown in the rectangle below the one in the top right-hand corner.

1.3.1 Unnatural Amino Acid Mutagenesis

The methodology for the *in-vivo* incorporation of unnatural amino acids used by the Dougherty group consists of using the nonsense suppression method to hijack the ribosome and thus have the cell's own protein synthesis machinery produce, assemble and fold the desired protein (Figure 1.9).[27] The nonsense suppression method consists of mutating the codon at the site of interest to a stop codon (TAG, TGA or TAA), which as its name suggests, does not code for any natural amino acids and is instead used to terminate protein synthesis. The desired unnatural amino acid is chemically appended to an "orthogonal" suppressor tRNA possessing the corresponding anticodon (CUA, UCA or UUA respectively). An orthogonal tRNA is not recognized by any of the endogenous aminoacyl-tRNA synthetases, the enzymes that append natural amino acids onto their corresponding tRNAs. Thus, orthogonality is a key requirement for tRNAs used in the nonsense suppression method. If endogenous aminoacyl-tRNA synthetases were to recognize the tRNA used for nonsense suppression and append one of the natural amino acids (reaminoacylation) then the result would be expression of a mixture of proteins, some with the desired unnatural amino acid originally appended to the tRNA and others with the natural amino acid resulting from reaminoacylation. The Dougherty group uses several different tRNAs and employs a reaminoacylation control (see Section 1.3.2) to ensure orthogonality.

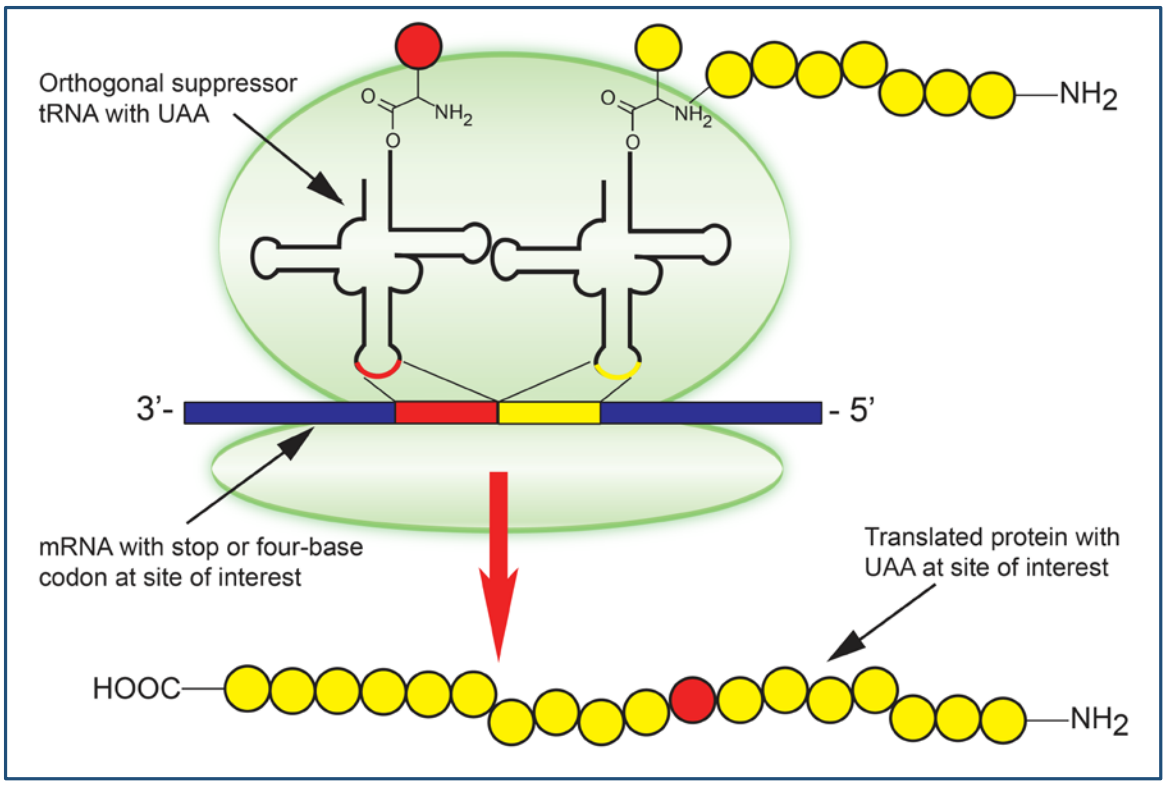

Figure 1.9 Hijacking the Ribosome. Schematic representation of the nonsense suppression methodology used for site-directed incorporation of unnatural amino acids (UAAs) into cells. Alternatively, a four-base codon instead of a stop codon can be used at the mutation site in which case the methodology is then termed frameshift suppression. The work portrayed in this thesis uses exclusively the nonsense suppression methodology.

Synthesis of the orthogonal suppressor tRNA involves first the transcription of a truncated suppressor tRNA lacking the last two bases in the acceptor stem (C and A). Next, a deoxy-C and A (dCA) dinucleotide and the desired unnatural amino acid is chemically synthesized and the unnatural amino acid is acylated onto the dCA. This complex is then enzymatically ligated onto the acceptor stem of the truncated suppressor tRNA to yield aminoacylated tRNA (Figure 1.10).

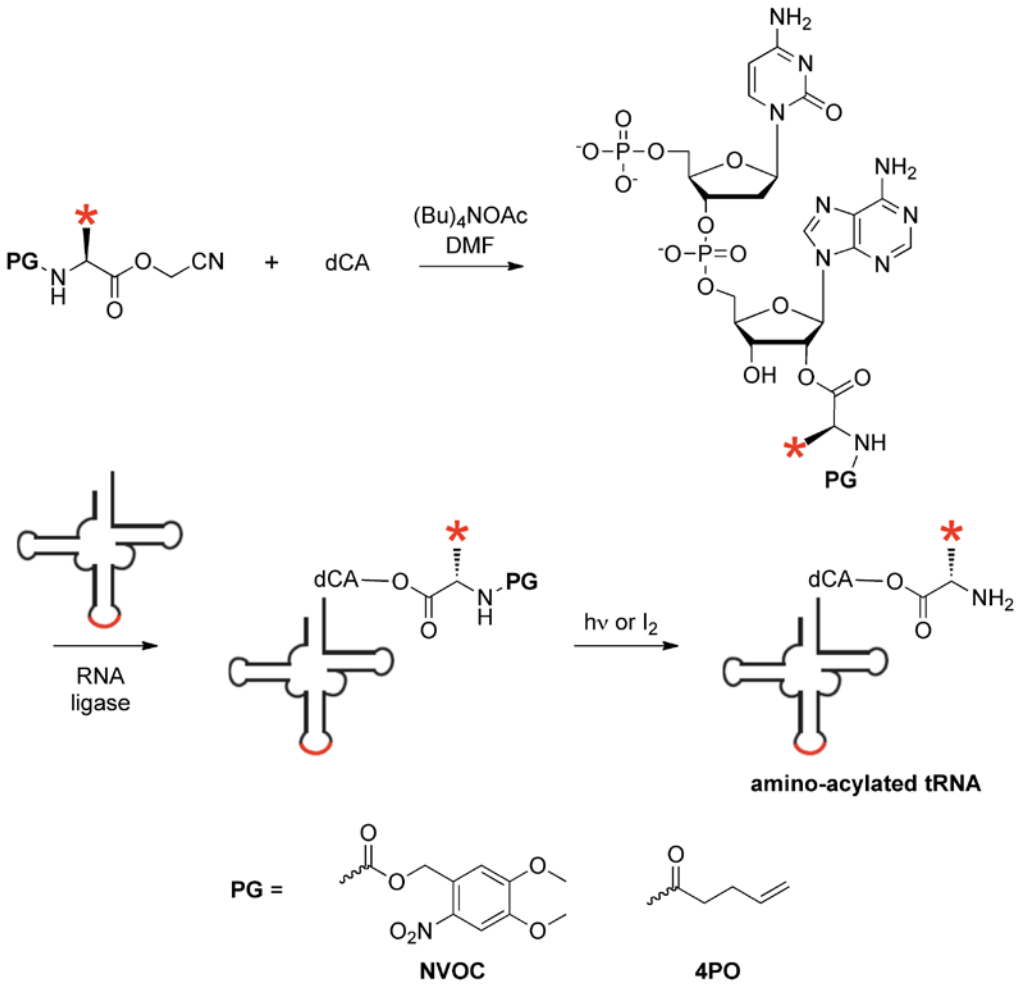

Figure 1.10 Synthesis of suppressor tRNA. Unnatural amino acids are chemically synthesized with a protected α-amino group and their carboxylate group is activated as a cyanomethyl ester to facilitate acylation onto dCA. This complex is then enzymatically ligated onto the acceptor stem of the truncated suppressor tRNA to yield aminoacylated tRNA. The nitroveratryloxycarbonyl (NVOC) protecting group (PG) is photolabile and the 4-PO protecting group is removable by treatment with I_2. α-hydroxy acids are not protected. The red asterisk denotes and unnatural amino acid side chain.

The orthogonal suppressor tRNA with the desired unnatural amino acid and the mRNA containing a stop codon at the site of interest are then coinjected into *Xenopus* oocytes. Following an incubation period of generally 24-48h the oocytes then express the protein containing the unnatural amino acid at the site of interest (Figure 1.11).

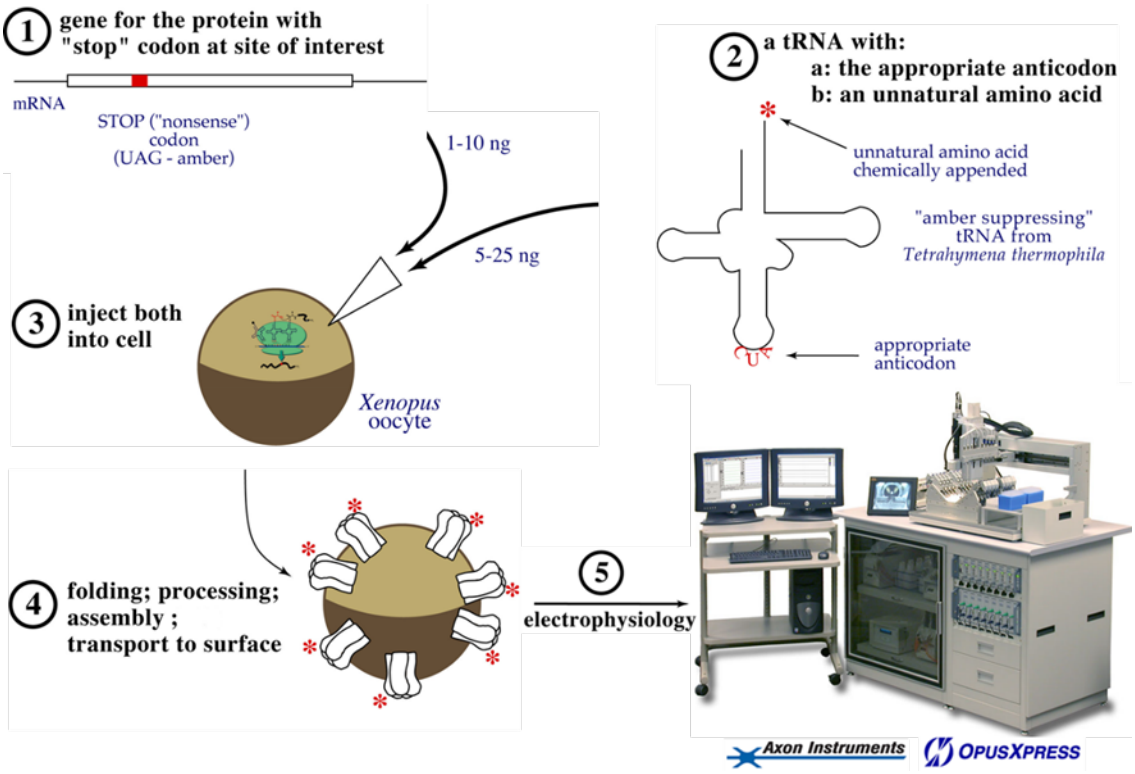

Figure 1.11 Schematic of the methodology for site-directed incorporation of unnatural amino acids into *Xenopus* oocytes by nonsense suppression.

1.3.2 Nonsense Suppression Methodology Controls

The Dougherty group uses mainly three controls to ensure that the nonsense suppression methodology is working as envisioned. Given the variability of biological systems, these controls essentially make sure that the protein we are actually expressing and the protein we intend to express are one and the same or at the very least that the readout in our functional assay corresponds overwhelmingly to the intended protein. The three controls we use are termed reaminoacylation, readthrough and wild type recovery (WTR) controls.

As previously mentioned, reaminoacylation occurs when endogenous aminoacyl-tRNA synthetases are able to “recharge” the suppressor tRNA after it

delivers its unnatural tRNA resulting a mixture of proteins. As a control, *Xenopus* oocytes are co-injected with mRNA containing the desired stop codon and suppressor tRNA lacking an amino acid, which is obtained by *in vitro* transcription of the tRNA with a complete acceptor stem containing the last C and A bases. This complete suppressor tRNA mimics the tRNA present in the cell after an aminoacylated suppressor tRNA delivers its unnatural amino acid to the ribosome. Control oocytes are then subjected to the same incubation conditions and functional assays and ideally no signal is detected for the control oocytes. In the case of nAChR expression, the Dougherty group has observed that reaminoacylation is site and tRNA dependent, meaning that some suppressor tRNAs will work for some sites but not others. In cases where reaminoacylation is a problem, using a different suppressor tRNA often solves the issue. Alternatively, a four-base codon and its corresponding tRNA can also be used (frameshift suppression methodology).

Readthrough occurs when an endogenous tRNA misreads the stop codon in the mRNA resulting in the incorporation of a natural amino acid at the site. In a readthrough control only the mRNA with the stop codon mutation is injected into the control oocyte and the oocyte is then subjected to the functional assay. Similarly to the reaminoacylation control, the readthrough control should yield no signal. In cases where there is significant readthrough the only option is to use the frameshift suppression methodology instead of the nonsense suppression methodology.

The fidelity of the nonsense suppression method for the incorporation of amino acids can be tested by the wild type recovery (WTR) control. In a WTR control the suppressor tRNA is chemically appended with the natural amino acid present at that site for the wild type receptor. For example, in the case of TrpB for the nAChR, the tRNA would be appended with a Trp residue. The tRNA is then co-injected with mRNA containing the stop codon into the oocyte and when nonsense suppression is working as intended the result should be the expression of wild type receptors yielding a signal indistinguishable from that of oocytes injected with wild type mRNA. The Dougherty group uses electrophysiology as the functional assay to study receptor function.

1.4 Electrophysiology

One limitation of the nonsense suppression methodology is that the suppressor tRNA used to deliver the unnatural amino acid is a stoichiometric reagent and as such limits the amount of protein that can be synthesized by the cell. Electrophysiological techniques are sensitive enough to detect the electrical signal resulting from the activity of a single ion channel and are thus suitable as a functional assay for ion channels expressing unnatural amino acids. Electrophysiology is the measurement of the electrical currents in living cells and tissues and electrophysiological techniques can be classified as whole-cell or singe-channel recording depending the source of the electrical signal being measured. In whole-cell recording electrodes are inserted into the cell to measure the change in voltage and/or current across the cell surface membrane. Thus, the electrical signal being measured arises from all of the receptors present in the cell

surface membrane. Section 1.4.1 describes the whole-cell recording method and data interpretation used within this thesis. As the name suggests, single-channel recording measures the electrical changes across a section of membrane containing a sole ion channel and is further detailed in Section 1.4.2.

1.4.1 Whole-Cell Recording

The whole-cell recording assays portrayed in this thesis were done using the two-electrode voltage clamp (TEVC) method. In TEVC the cell is injected with two electrodes, one electrode monitors the potential (voltage) relative to ground, while the other passes current in order to maintain the cell's membrane potential at a user-determined potential (voltage clamp) (Figure 1.12). Voltage clamp was developed in 1949 by Kenneth Cole to stabilize the membrane potential in neurons and was subsequently used by Hodgkin and Huxley in their renowned experiments that revealed the mechanism of the action potential.[28]

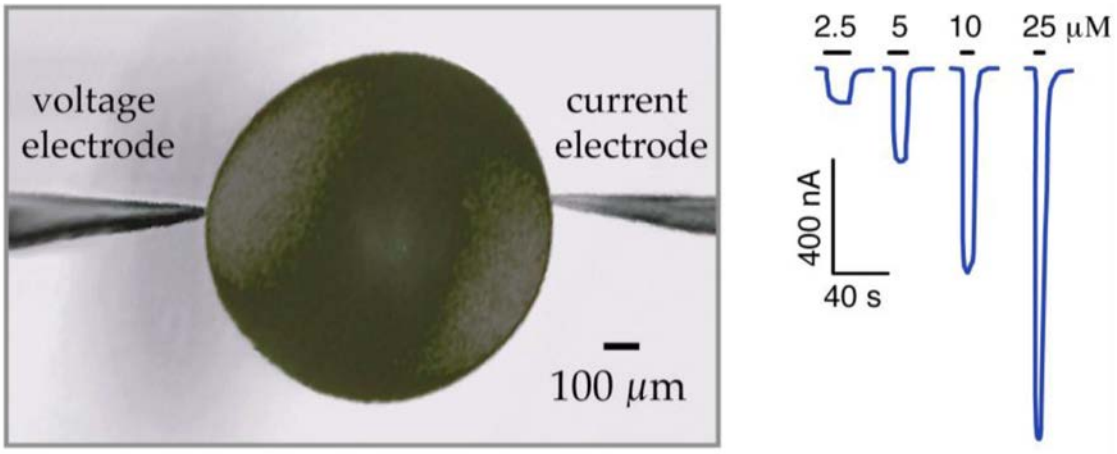

Figure 1.12. TEVC and sample current traces. Left: TEVC on a *Xenopus* oocyte. The scale bar represents ~ 1/10th of a typical stage V/VI oocyte's diameter (100 μm). **Right:** Sample traces from a TEVC experiment showing the current that must be injected into an oocyte in order to keep the oocyte at the preset potential (voltage clamp). Agonist is typically applied for 15 seconds, though longer drug applications may be required for low concentrations (nM range), when binding can become the rate-limiting activation step.

$$\frac{I}{I_{max}} = \frac{1}{1 + \left(\frac{EC_{50}}{[Agonist]}\right)^{n_H}}$$

Equation 1.1

In a typical TEVC whole-cell assay *Xenopus* oocytes expressing the LGIC of interest are subjected to increasing agonist concentrations until further increases to agonist concentration do not elicit increases in the whole-cell current (Figure 1.12). This maximal current value is termed I_{max}. The measured current (I) at each agonist concentration ([Agonist]) is normalized to the I_{max} value and this normalized current (I_{Norm}) is plotted against [Agonist]. The plot is fitted to the Hill equation (Equation 1.1) and is termed a dose-response curve (DRC, Figure 1.13).

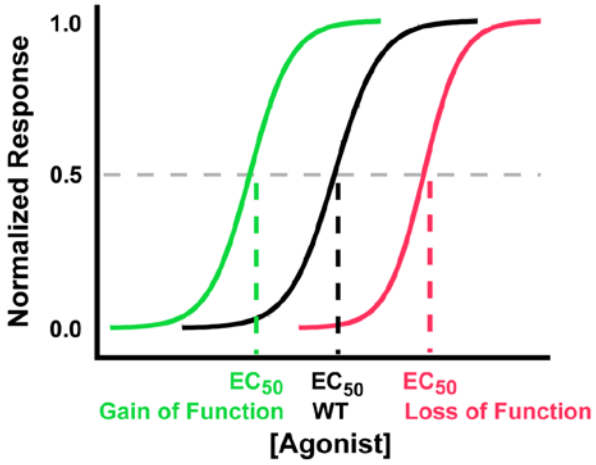

$$FoldShift(FS) = \frac{EC_{50}(mut)}{EC_{50}(WT)}$$

Figure 1.13 Left: Examples of dose-response curves (DRCs) in which the normalized current response (I/Imax) is plotted against the concentration of agonist applied. In each case, the concentration needed to reach the half-maximal response, EC_{50}, is denoted with a dotted line. The black DRC represents a wild type (WT) ion channel. The green DRC represents a mutation that caused less agonist to be needed to activate the channel. More commonly, a mutation produces a loss of function, represented by the pink DRC, and corresponding increase in EC_{50}. Fitting the dose-response curve to the Hill equation also produces n_H, which increases with increasing steepness of the DRC. **Right:** Definition of the fold-shift (FS) parameter.

The EC_{50} value and Hill coefficient (n_H) can be obtained from the DRC fit. The EC_{50} value is defined as the effective agonist concentration necessary to elicit a half-maximal response and our group as well as others use the EC_{50} value as a measure of receptor function. The relationship between the EC_{50} of the wild type receptor and the mutant receptor is presented throughout this thesis as a fold-shift value (FS, Figure 1.13) and is often our final measure of receptor function. When a mutation is introduced that is detrimental to receptor function, a higher concentration of agonist is needed to achieve half-maximal response. This translates as a higher EC_{50} value and FS>1 and is termed a loss of function mutation. The opposite is true for a gain of function mutation where receptor function is improved by mutation and less agonist is needed for half-maximal response, resulting in a lower EC_{50} value and FS<1 (Figure 1.13).

As suggested by the thesis title, this thesis focuses on binding studies at the nAChR and it is more often the case that the mutation introduced is designed to weaken or functionally eliminate a suspected binding interaction. Thus, the results of our whole-cell recording assays are often increased EC_{50} values (relative to wild type) and FS>1. Due to the inherent variability in biological systems such as the *Xenopus* oocyte expression system, our group does not typically consider FS<2 as meaningful for loss of function mutations. The work described in Chapters 2 and 3 of this thesis involves whole-cell recording in TEVC mode.

1.4.2 Single-Channel Recording

Single-channel recording offers a significant advantage over other electrophysiology measurements, such as TEVC used to determine EC_{50}, in that

more specific binding models and receptor activation kinetics can be obtained from single-channel data. Since EC_{50} is a measure of receptor activation, it is a composite of the rate at which the agonist associates with the receptor (binding) and that agonists' ability to induce the conformational change resulting in current flow through the ion channel (gating). Single-channel recording is achieved by use of the patch-clamp technique. The patch-clamp method was developed in the decades of 1970 and 1980 by Erwin Neher and Bert Sakmann for which they received the Nobel Prize in physiology or medicine in 1991.[29-31]

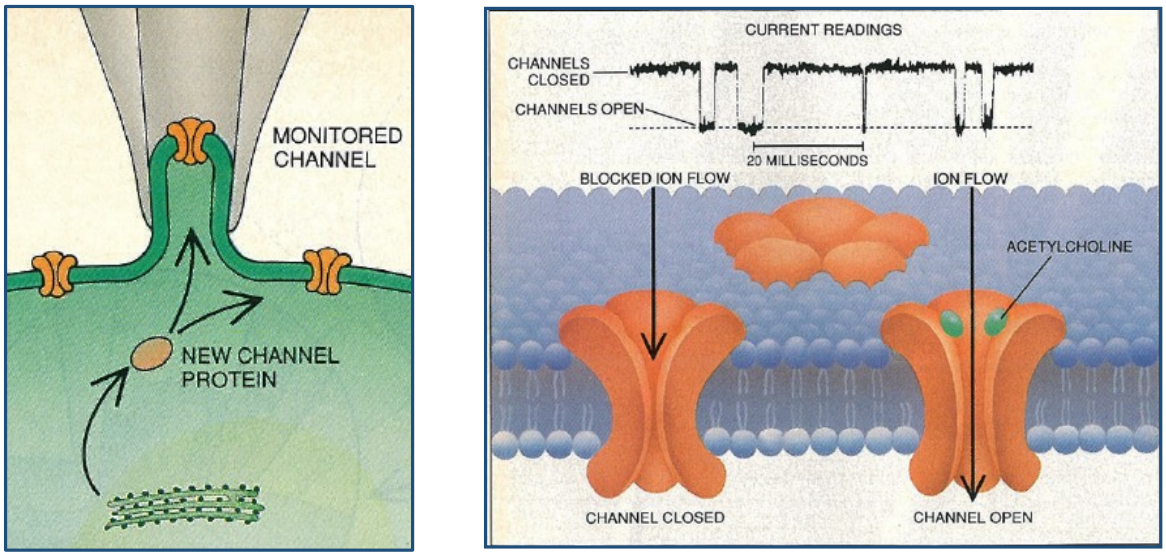

Figure 1.14 The patch-clamp technique. Left: Illustration of the patch-clamp technique where a micropipette containing an electrode and bath solution with a specific concentration of agonist is applied to the membrane forming a gigaohm seal and isolating the electrical signal from a single channel for electrophysiological recording. **Right:** Example of a single-channel recording trace (current readings) showing two discrete current levels corresponding to either the closed channel state (baseline current) or the open channel state. Adapted from [31].

The patch-clamp technique consists of applying a micropipette containing a chlorinated silver wire electrode and a solution of a receptor agonist to the cell membrane. Upon application of suction a high resistance seal termed the gigaohm seal is formed, effectively isolating the electrical signal from the channel trapped in

the sealed membrane patch (Figure 1.14). Note that, in contrast to whole-cell recording methods where the micropipette electrode pierces the cell membrane, in single-channel recording the micropipette adheres to the membrane to form the gigaohm seal. It is desirable then that the tip of the micropipette be smooth so as not to pierce the cell membrane and thus, a common practice for patch-clamping is to fire-polish the micropipette tip using a microforge. A more detailed description of single-channel recording parameters and data analysis is provided in Chapter 4 of this thesis as well as the results of single-channel experiments on A3B2 and A2B3 receptors.

1.5 The Cation-π Interaction

A common theme throughout this thesis is the study of binding interactions of agonists to the nAChR. An ubiquitous binding interaction observed in proteins is the cation-π interaction showing a wide-ranging biological significance.[32-34] There is one cation-π interaction for every 77 residues in the PDB, meaning that there are over 500,000 cation-π interactions in the PDB today.[35] One study showed that 25% of all tryptophan residues in the PDB participated in a cation-π interaction.[36] Research in our group has extensively validated the relevance of the cation-π interaction in receptor activation and function for a variety of receptors including nAChRs, G-protein coupled receptors (GPCRs), 5-HT3 receptors, GABA and glycine receptors.[23,37-47]

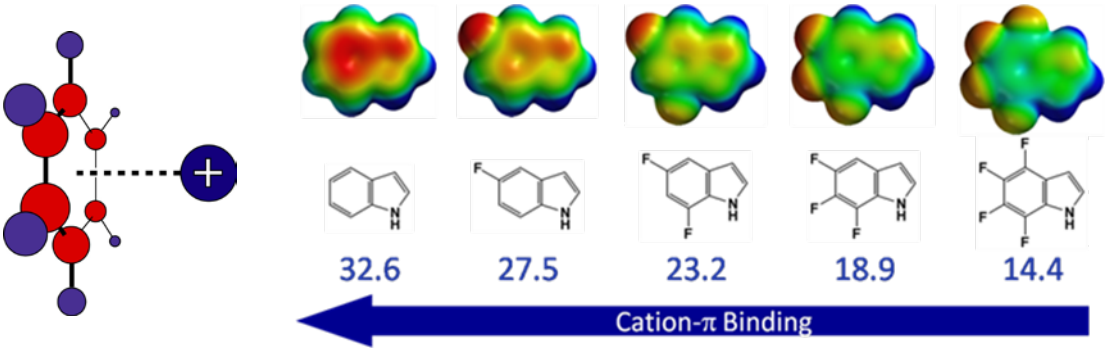

Figure 1.15 Left: Schematic of a cation-π interaction. **Right:** Potential energy surfaces, structures and cation-π binding energies (in kcal/mol) of the Trp fluorination series showing the progressive deactivation of the aromatic ring. Red denotes negative charge density and blue denotes positive charge density.

The cation-π interaction is defined as the stabilizing interaction between a cation and the face of a simple π-system such as the aromatic ring in tryptophan (Trp), tyrosine (Tyr) or phenylalanine (Phe) (Figure 1.15). It is comparable in strength to a hydrogen bond. The Dougherty group has developed a procedure for probing the functional significance of cation-π interactions by site-directed incorporation of unnatural amino acids into the receptor of study. The cation-π functional assay consists of systematically replacing the wild type amino acid of interest with the corresponding monofluoro-, difluoro-, trifluoro- etc derivative and measuring the EC_{50} value for each mutation (Figure 1.15). A cation-π interaction is established when a clear correlation between agonist affinity and degree of fluorination is observed by the linear fit of the “fluorination plot” shown in Figure 1.16.

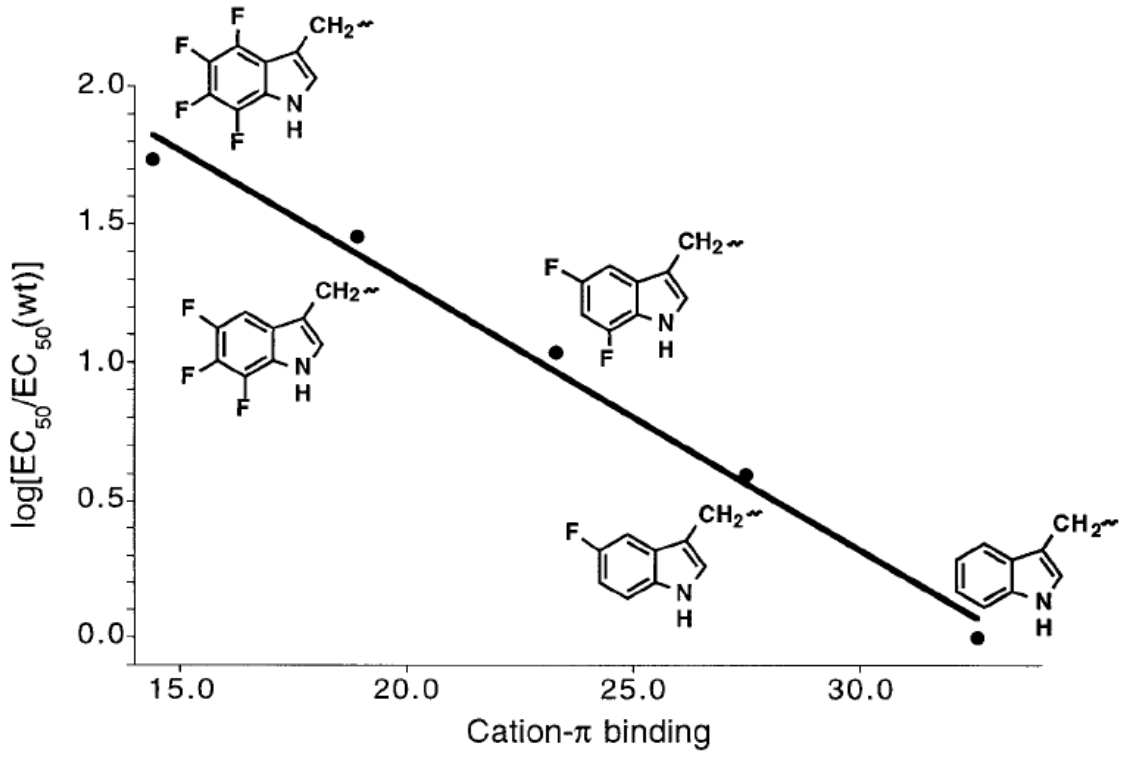

Figure 1.16 Fluorination plot at α1TrpB in the fetal, muscle-type nAChR with the agonist acetylcholine (ACh). The observed linear correlation establishes that there is a functionally significant cation-π interaction between ACh and TrpB. Binding of Na^+ to the aromatic ring was used as the quantitative measure of cation-π binding ability (in kcal/mol) denoted on the x-axis.[48]

1.6 Dissertation Work

To my knowledge, every pharmaceutical drug on the market works by acting on some type of receptor. Side-effects arise from the drug binding not only to the intended target receptor but to other non-intended and often related receptors. When we understand on a chemical scale how molecules bind to their target receptors and all the conformational changes giving rise to receptor activation we will then be able to design drugs that exclusively target the desired receptor and are essentially side-effect free. Today, we are far from attaining that level of insight into receptor structure and function, and much like understanding the complexity

of the human brain the task seems daunting and nigh unattainable in its immensity. However, every journey must start somewhere and every step forward no matter how small it might seem brings us one step closer to the end goal. The work presented in this thesis focuses on the study of two very closely related receptors, A3B2 and A2B3 α4β2 nicotinic receptors in hopes of bringing us one step closer to understanding the nuances of receptor selectivity.

Chapter 2 describes binding studies of select nicotinic agonists on A3B2 and A2B3 receptors determined by whole-cell recording. Three key binding interactions, a cation-π and two hydrogen bonds were probed for four nicotinic agonists, acetylcholine, nicotine, smoking cessation drug varenicline (Chantix®) and the related natural product cytisine.

Results from the binding studies presented in Chapter 2 show that the major difference in binding of these four agonists to A3B2 and A2B3 receptors lies in one of the two hydrogen bond interactions where the agonist acts as the hydrogen bond acceptor and the backbone NH of a conserved leucine residue in the receptor acts as the hydrogen bond donor. Chapter 3 focuses on studying the effect of modulating the hydrogen bond acceptor ability of nicotine and epibatidine on A3B2 receptor function determined by whole-cell recording.

Finally, Chapter 4 describes single-channel recording studies of varenicline binding to A2B3 and A3B2 receptors.

1.7 References

1 Green, T., Heinemann, S. F. & Gusella, J. F. Molecular neurobiology and genetics: Investigation of neural function and dysfunction. *Neuron* **20**, 427-444, doi:10.1016/s0896-6273(00)80986-1 (1998).

2 Kandel, E. R., Schwartz, J. H., and Jessell, T. M. *Principles of neural science*. 4th edn, (McGraw-Hill, 2000).

3 Wang, H. Y., Liu, T. & Malbon, C. C. Structure-function analysis of frizzleds. *Cell. Signal.* **18**, 934-941, doi:10.1016/j.cellsig.2005.12.008 (2006).

4 Dougherty, D. A. Cys-loop neuroreceptors: Structure to the rescue? *Chemical Reviews* **108**, 1642-1653, doi:10.1021/cr078207z (2008).

5 Karlin, A. Emerging structure of the nicotinic acetylcholine receptors. *Nature Reviews Neuroscience* **3**, 102-114 (2002).

6 Jensen, A. A., Frolund, B., Lijefors, T. & Krogsgaard-Larsen, P. Neuronal nicotinic acetylcholine receptors: Structural revelations, target identifications, and therapeutic inspirations. *Journal of Medicinal Chemistry* **48**, 4705-4745, doi:10.1021/jm040219e (2005).

7 Dougherty, D. A. Physical organic chemistry on the brain. *The Journal of organic chemistry* **73**, 3667-3673, doi:10.1021/jo8001722 (2008).

8 Brejc, K. *et al.* Crystal structure of an ACh-binding protein reveals the ligand-binding domain of nicotinic receptors. *Nature* **411**, 269-276 (2001).

9 Unwin, N. Refined structure of the nicotinic acetylcholine receptor at 4 angstrom resolution. *Journal of Molecular Biology* **346**, 967-989, doi:10.1016/j.jmb.2004.12.031 (2005).

10 Xiu, X. *Structure-function studies of nicotinic acetylcholine receptors using unnatural amino acids*, California Institute of Technology, (2008).

11 Millar, N. S. & Gotti, C. Diversity of vertebrate nicotinic acetylcholine receptors. *Neuropharmacology* **56**, 237-246, doi:10.1016/j.neuropharm.2008.07.041 (2009).

12 Nelson, M. E., Kuryatov, A., Choi, C. H., Zhou, Y. & Lindstrom, J. Alternate stoichiometries of alpha 4 beta 2 nicotinic acetylcholine receptors. *Mol. Pharmacol.* **63**, 332-341 (2003).

13 Grinevich, V. P. *et al.* Heterologous expression of human alpha 6 beta 4 beta 3 alpha 5 nicotinic acetylcholine receptors: Binding properties consistent with their natural expression require quaternary subunit assembly including the alpha 5 subunit. *Journal of Pharmacology and Experimental Therapeutics* **312**, 619-626, doi:DOI 10.1124/jpet.104.075069 (2005).

14 Laviolette, S. R. & van der Kooy, D. The neurobiology of nicotine addiction: Bridging the gap from molecules to behaviour. *Nature Reviews Neuroscience* **5**, 55-65, doi:Doi 10.1038/Nrn1298 (2004).

15 Mansvelder, H. D., Keath, J. R. & McGehee, D. S. Synaptic mechanisms underlie nicotine-induced excitability of brain reward areas. *Neuron* **33**, 905-919, doi:10.1016/s0896-6273(02)00625-6 (2002).

16 Mansvelder, H. D. & McGehee, D. S. Cellular and synaptic mechanisms of nicotine addiction. *Journal of Neurobiology* **53**, 606-617, doi:Doi 10.1002/Neu.10148 (2002).

17 Barrera, N. P. & Edwardson, J. M. The subunit arrangement and assembly of ionotropic receptors. *Trends in Neurosciences* **31**, 569-576, doi:DOI 10.1016/j.tins.2008.08.001 (2008).

18 Moroni, M., Zwart, R., Sher, E., Cassels, B. K. & Bermudez, I. alpha 4 beta 2 nicotinic receptors with high and low acetylcholine sensitivity: Pharmacology, stoichiometry, and sensitivity to long-term exposure to nicotine. *Molecular Pharmacology* **70**, 755-768, doi:10.1124/mol.106.023044 (2006).

19 Tapia, L., Kuryatov, A. & Lindstrom, J. Ca2+ permeability of the (alpha 4)(3)(beta 2)(2) stoichiometry greatly exceeds that of (alpha 4)(2)(beta 2)(3) human acetylcholine receptors. *Mol. Pharmacol.* **71**, 769-776, doi:DOI 10.1124/mol.106.030445 (2007).

20 Zwart, R. & Vijverberg, H. P. M. Four pharmacologically distinct subtypes of alpha 4 beta 2 nicotinic acetylcholine receptor expressed in Xenopus laevis oocytes. *Mol. Pharmacol.* **54**, 1124-1131 (1998).

21 Harpsoe, K. *et al.* Unraveling the high- and low-sensitivity agonist responses of nicotinic acetylcholine receptors. *The Journal of neuroscience : the official journal of the Society for Neuroscience* **31**, 10759-10766, doi:10.1523/JNEUROSCI.1509-11.2011 (2011).

22 Mazzaferro, S. *et al.* Additional acetylcholine (ACh) binding site at alpha4/alpha4 interface of (alpha4beta2)2alpha4 nicotinic receptor influences agonist sensitivity. *The Journal of biological chemistry* **286**, 31043-31054, doi:10.1074/jbc.M111.262014 (2011).

23 Xiu, X. A., Puskar, N. L., Shanata, J. A. P., Lester, H. A. & Dougherty, D. A. Nicotine binding to brain receptors requires a strong cation-pi interaction. *Nature* **458**, 534-U510, doi:10.1038/nature07768 (2009).

24 Sigel, E. Use of Xenopus Oocytes for the Functional Expression of Plasma-Membrane Proteins. *Journal of Membrane Biology* **117**, 201-221 (1990).

25 Noren, C. J., Anthonycahill, S. J., Griffith, M. C. & Schultz, P. G. A General-Method for Site-Specific Incorporation of Unnatural Amino-Acids into Proteins. *Science* **244**, 182-188 (1989).

26 Nowak, M. W. *et al.* Nicotinic Receptor-Binding Site Probed with Unnatural Amino-Acid-Incorporation in Intact-Cells. *Science* **268**, 439-442 (1995).

27 Nowak, M. W. *et al.* In vivo incorporation of unnatural amino acids into ion channels in Xenopus oocyte expression system. *Methods Enzymol.* **293**, 504-529 (1998).

28 Kandel, E. R., Schwartz, J. H. & Jessell, T. M. *Principles of neural science*. 4th edn, (McGraw-Hill, Health Professions Division, 2000).

29 Hamill, O. P., Marty, A., Neher, E., Sakmann, B. & Sigworth, F. J. Improved patch-clamp techniques for high-resolution current recording from cells and cell-free membrane patches. *Pflugers Arch.* **391**, 85-100, doi:10.1007/bf00656997 (1981).

30 Neher, E. & Sakmann, B. Single-channel currents recorded from membrane of denervated frog muscle-fibers. *Nature* **260**, 799-802, doi:10.1038/260799a0 (1976).

31 Neher, E. & Sakmann, B. The patch clamp technique. *Sci.Am.* **266**, 44-51 (1992).

32 Ma, J. C. & Dougherty, D. A. The cation-pi interaction. *Chem. Rev.* **97**, 1303-1324, doi:10.1021/cr9603744 (1997).

33 Zacharias, N. & Dougherty, D. A. Cation-pi interactions in ligand recognition and catalysis. *Trends Pharmacol. Sci.* **23**, 281-287, doi:10.1016/s0165-6147(02)02027-8 (2002).

34 Dougherty, D. A. Cation-pi interactions in chemistry and biology: A new view of benzene, Phe, Tyr, and Trp. *Science* **271**, 163-168, doi:10.1126/science.271.5246.163 (1996).

35 Dougherty, D. A. The Cation-pi Interaction. *Accounts Chem. Res.* **46**, 885-893, doi:10.1021/ar300265y (2013).

36 Gallivan, J. P. & Dougherty, D. A. Cation-pi interactions in structural biology. *Proc. Natl. Acad. Sci. U. S. A.* **96**, 9459-9464, doi:10.1073/pnas.96.17.9459 (1999).

37 Beene, D. L. *et al.* Cation-pi interactions in ligand recognition by serotonergic (5-HT3A) and nicotinic acetylcholine receptors: The anomalous binding properties of nicotine. *Biochemistry* **41**, 10262-10269, doi:10.1021/bi020266d (2002).

38 Duffy, N. H., Lester, H. A. & Dougherty, D. A. Ondansetron and Granisetron Binding Orientation in the 5-HT3 Receptor Determined by Unnatural Amino Acid Mutagenesis. *ACS Chem. Biol.* **7**, 1738-1745, doi:10.1021/cb300246j (2012).

39 Padgett, C. L., Hanek, A. P., Lester, H. A., Dougherty, D. A. & Lummis, S. C. R. Unnatural amino acid mutagenesis of the GABA(A) receptor binding site residues reveals a novel cation-pi interaction between GABA and beta(2)Tyr97. *J. Neurosci.* **27**, 886-892, doi:10.1523/jneurosci.4791-06.2007 (2007).

40 Pless, S. A. *et al.* A Cation-pi Interaction at a Phenylalanine Residue in the Glycine Receptor Binding Site Is Conserved for Different Agonists. *Mol. Pharmacol.* **79**, 742-748, doi:10.1124/mol.110.069583 (2011).

41 Pless, S. A. *et al.* A Cation-pi Interaction in the Binding Site of the Glycine Receptor Is Mediated by a Phenylalanine Residue. *J. Neurosci.* **28**, 10937-10942, doi:10.1523/jneurosci.2540-08.2008 (2008).

42 Puskar, N. L., Xiu, X. A., Lester, H. A. & Dougherty, D. A. Two Neuronal Nicotinic Acetylcholine Receptors, alpha 4 beta 4 and alpha 7, Show Differential Agonist Binding Modes. *J. Biol. Chem.* **286**, 14618-14627, doi:10.1074/jbc.M110.206565 (2011).

43 Santarelli, V. P., Eastwood, A. L., Dougherty, D. A., Horn, R. & Ahern, C. A. A cation-pi interaction discriminates among sodium channels that are either sensitive or resistant to tetrodotoxin block. *J. Biol. Chem.* **282**, 8044-8051, doi:10.1074/jbc.M611334200 (2007).

44 Tavares, X. D. S. *et al.* Variations in Binding Among Several Agonists at Two Stoichiometries of the Neuronal, alpha 4 beta 2 Nicotinic Receptor. *J. Am. Chem. Soc.* **134**, 11474-11480, doi:10.1021/ja3011379 (2012).

45 Torrice, M. M., Bower, K. S., Lester, H. A. & Dougherty, D. A. Probing the role of the cation-pi interaction in the binding sites of GPCRs using unnatural amino acids. *Proc. Natl. Acad. Sci. U. S. A.* **106**, 11919-11924, doi:10.1073/pnas.0903260106 (2009).

46 Van Arnam, E. B., Blythe, E. E., Lester, H. A. & Dougherty, D. A. An Unusual Pattern of Ligand-Receptor Interactions for the alpha 7 Nicotinic Acetylcholine Receptor, with Implications for the Binding of Varenicline. *Mol. Pharmacol.* **84**, 201-207, doi:10.1124/mol.113.085795 (2013).

47 Van Arnam, E. B. *et al.* Probing the Binding Sites and Transmembrane Prolines of GPCRs Using Unnatural Amino Acids. *Biophys. J.* **98**, 292A-292A (2010).

48 Zhong, W. G. *et al.* From ab initio quantum mechanics to molecular neurobiology: A cation-pi binding site in the nicotinic receptor. *Proc. Natl. Acad. Sci. U. S. A.* **95**, 12088-12093, doi:10.1073/pnas.95.21.12088 (1998).

Chapter 2:

Variations in Binding Among Several Agonists at Two Stoichiometries of the Neuronal, α4β2 Nicotinic Receptor

2.1 Introduction

This chapter details the study of three binding interactions, which are considered key to agonist binding and receptor activation, between four nicotinic agonists (Figure 2.1) and the A3B2 and A2B3 forms of the neuronal α4β2 receptor. Recall from Chapter 1 that A3B2 refers to the $(\alpha4)_3(\beta2)_2$ receptor stoichiometry and A2B3 to the $(\alpha4)_2(\beta2)_3$ stoichiometry.

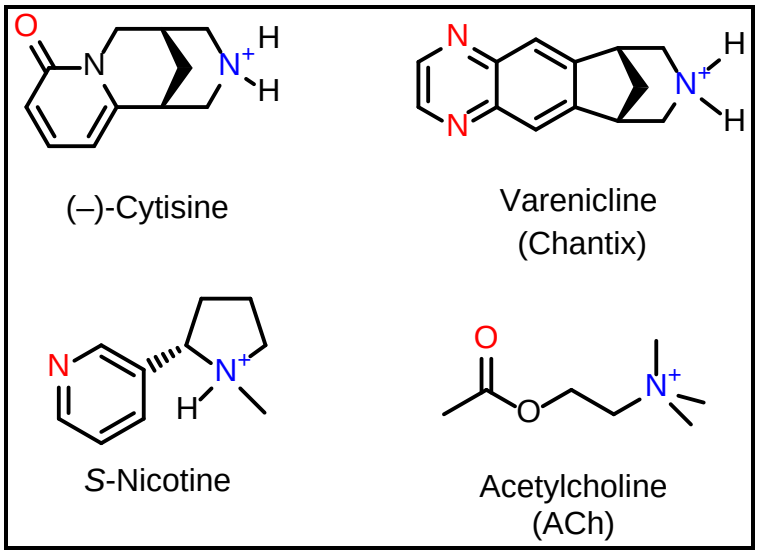

Figure 2.1 Nicotinic Agonists Studied. These four agonists share structural features consisting of a cationic nitrogen **(blue)** and a hydrogen bond acceptor moiety **(red)**.

2.1.1 α4β2, Nicotine Addiction and Smoking Cessation Therapies

The α4β2 receptor has been heavily implicated in nicotine addiction by a number of pharmacological studies and by extensive evaluations of knockout mice.[1-3] Nicotine addiction is the leading cause of mortality in the developed world, resulting in over 4,000,000 smoking-related deaths annually.[4] In the United States, the Centers for Disease Control and Prevention (CDC) report cigarette smoking as

the leading cause of preventable death, resulting in over 480,000 annual deaths.[5] To put this number in perspective, this is the equivalent of three jumbo jets crashing daily with no survivors every day of the year. Consequently, there is great interest in the development of pharmacotherapies to treat nicotine addiction. The highly addictive properties of nicotine arise from its ability to stimulate dopamine release in the mesolimbic pathway, the reward circuit of the brain. This leads to the feelings of pleasure, cognitive sensitization and alertness associated with smoking.[3,6,7]

Historically, smoking cessation therapies have primarily been based on some form of nicotine replacement, such as nicotine patches or gum.[8] An alternative strategy is to develop a nicotinic receptor partial agonist that is selective for the α4β2 receptor. Partial agonism is a relative term used to describe the relationship between the maximal responses (efficacy) elicited by two agonists for a certain receptor. The agonist with the highest efficacy is termed a full agonist, and the other a partial agonist. Acetylcholine (ACh) is considered the full agonist for the α4β2 receptor. In a generalized sense, partial agonism can be interpreted as the relative ability of a certain agonist to activate a receptor. In the development of novel non-nicotine based smoking cessation therapies, it was hypothesized that an effective agent would, through its intrinsic partial activation of the α4β2 receptor, elicit a moderate and sustained increase in mesolimbic dopamine levels, counteracting the low dopamine levels encountered in the absence of nicotine during smoking cessation attempts.[9] Low levels of dopamine have been associated with craving for and withdrawal from nicotine and are the key syndromes that precipitate relapse to smoking behavior.[10,11] Additionally, by

competitively binding to the α4β2 receptor, a partial agonist will shield the smoker from nicotine-induced dopaminergic activation in the event that they smoke.[12] In theory, without the nicotine-induced elevation in mesolimbic dopamine levels, tobacco will not produce a pharmacologic reward.[13] Thus, compounds that are selective partial agonists of the α4β2 receptor and that out-compete nicotine are suitable candidates as smoking cessation drugs.

2.1.2 Cytisine, Varenicline and Smoking Cessation

Cytisine is a pyridone alkaloid, which is extracted from the seeds of the tree *Cytisus laburnum*, exhibiting selectivity for α4β2 receptors over other common neuronal nAChRs, such as α4β4 and α7.[14] Cytisine, a partial agonist with low efficacy at α4β2 receptors, has been marketed (Tabex®) as a smoking cessation drug in Europe for the last five decades.[15-17] With cytisine and morphine as a structural starting point, Coe et al. developed the molecule varenicline seeking to improve efficacy and potency while maintaining partial agonism properties at α4β2 (Figure 2.2).[9] Varenicline was introduced by Pfizer as Chantix® in 2006 for smoking cessation treatment.[9,18-20] Clinical studies on over 1000 patients indicated that 44% of CHANTIX® users quit smoking versus 18% in the placebo group.[21]

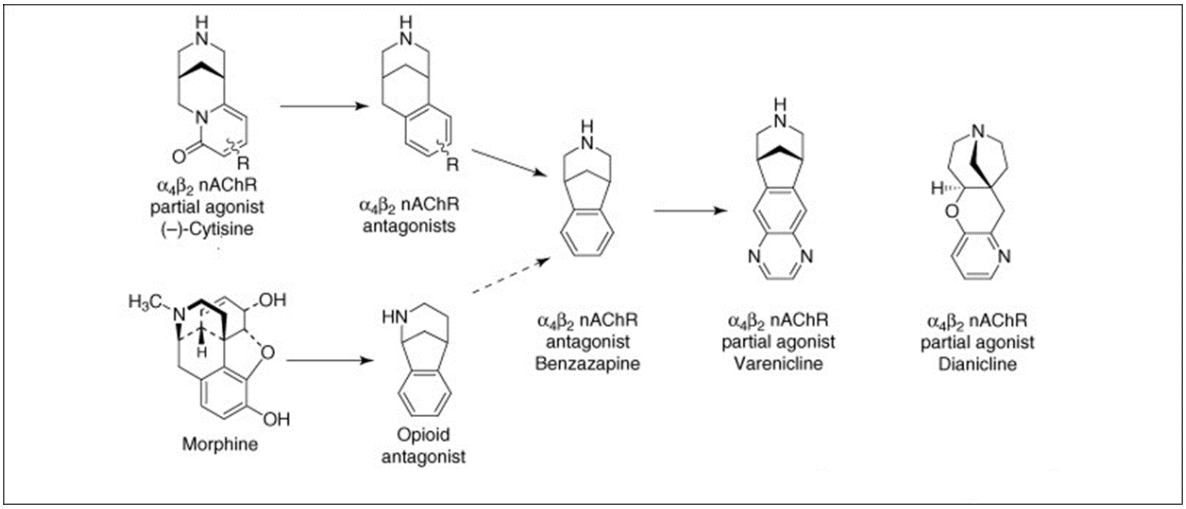

Figure 2.2 Pathway from cytisine (R=H) and morphine substructures to varenicline.[22]

The work detailed in this chapter addresses two key questions. First, we evaluated whether cytisine and varenicline fit the existing agonist binding model. Second, we probe the differential pharmacologies of the A2B3 and A3B2 stoichiometries of the α4β2 receptor, to determine whether the binding interactions of Figure 2.3 are responsible for the differences.

2.2 The Nicotinic Agonist Binding Model

Nicotine and related compounds adhere to what is termed the nicotinic pharmacophore. The essential nicotinic pharmacophore, a cationic N and a hydrogen bond acceptor separated by an appropriate distance, has been established for some time.[23-25] In recent years, the pharmacophore has been expanded to include the pyrrolidine N^+H of nicotine and similar structures as a hydrogen bond donor. Based on structural studies of the acetylcholine binding protein (AChBP)[26], a useful model for the agonist binding site of nAChRs, and

advanced structure-function studies, a binding model for nicotine has been developed (Figure 2.3).

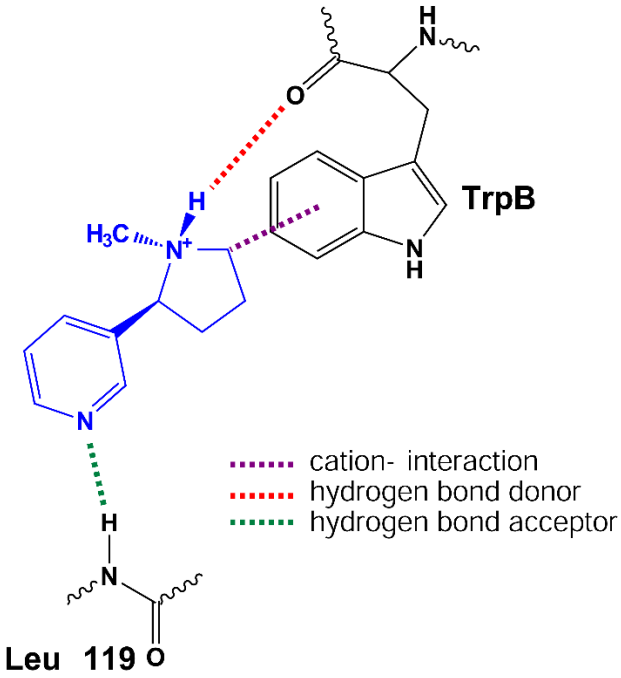

Figure 2.3 Binding model for nicotine at a nAChR

A cation-π interaction forms between the positive charge of the drug and the highly conserved Trp154 [27], termed TrpB in a standard model. In addition, the N^+H of the drug acts as a hydrogen bond donor to the backbone carbonyl of TrpB. Generally, drugs that have been developed to target the nAChRs have the potential to make this N^+H•••O=C hydrogen bond, but, of course, the endogenous agonist ACh cannot. The hydrogen bond acceptor component of the pharmacophore, the pyridine N of nicotine or the carbonyl O of ACh, makes a hydrogen bond to the backbone NH of Leu119 in the β2 subunit. This interaction was first revealed in a structure of AChBP with nicotine bound (Figure 2.4), where it is mediated by a water molecule.[26] In the actual nAChR, structure-function

studies of the type described in this chapter and previously by our group clearly established a hydrogen bonding interaction to the backbone NH in the α4β2 nAChR, but did not distinguish whether the water molecule is or is not present.[23]

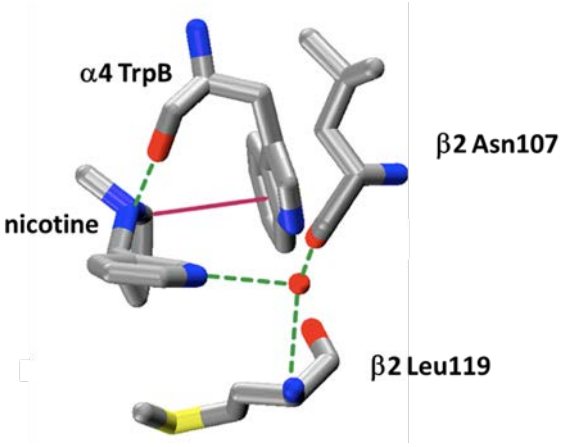

Figure 2.4 AChBP bound to nicotine. Red circle represents a water molecule. Adapted from [26].

In the binding model of Figure 2.3, the water molecule is not shown, with the understanding that it may be important in some or all nAChRs. An additional water-mediated hydrogen bonding interaction to the backbone carbonyl corresponding to Asn107 in the β2 subunit is also evident in the AChBP structure, but it has not been established to be important in nAChRs.[23] Note the interfacial nature of the agonist binding site: TrpB is in the α subunit while the Leu119 backbone NH comes from the β subunit.

2.2.1 Methodology for Probing Hydrogen Bonds

In the Dougherty lab, we regularly use unnatural amino acid mutagenesis to probe for functionally significant hydrogen bonds.[23,27-33] To probe hydrogen bonding interactions to the protein backbone, we replace the appropriate amino

acid with its α-hydroxy analogue (Figure 2.5). This converts the backbone amide to an ester, with predictable consequences. In the case of the hydrogen bond donor interaction to the carbonyl of TrpB, we replace the i+1 residue, Thr155, with its α-hydroxy analogue, Tah (threonine, α-hydroxy).[27,34] This attenuates the hydrogen bond-accepting ability of the backbone carbonyl, as it is an ester carbonyl rather than an amide carbonyl. To probe the hydrogen bond acceptor interaction, Leu119 of the β2 subunit is replaced by Lah (leucine, α-hydroxy).[23] This removes the backbone NH that participates in the hydrogen bond. For both strategies, we and others have seen significant impacts for mutations of this sort when a functionally significant hydrogen bond is involved. [25,35]

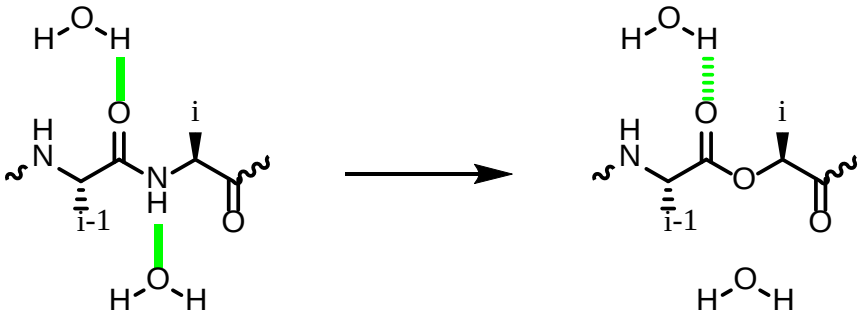

Figure 2.5 Backbone ester strategy for modulating hydrogen bonds.

For both hydrogen bonding interactions, simply seeing an impact on receptor function from α-hydroxy acid incorporation does not establish the existence of the hydrogen bond; some other aspect of receptor function could be perturbed by the mutation. At both sites, however, we have control experiments that strongly support the hydrogen bonding model. For the hydrogen bond donor interaction, we have shown that activation by ACh is not perturbed by the backbone mutation in the A2B3 receptor. This establishes that the backbone mutation has

not generically altered receptor function, and that it is indeed the $N^{+}H$ of the agonist that is responding to the mutation. For the hydrogen bond acceptor interaction, previous studies of nicotine at the A2B3 receptor used a pharmacological approach to probe the hydrogen bonding interaction. The nicotine analogue S-MPP lacks the pyridine N of nicotine and so cannot participate in the backbone hydrogen bond. It responded to the backbone mutation in the A2B3 receptor very differently from nicotine, and mutant cycle analysis clearly linked the backbone NH of Leu119 to the pyridine N of nicotine.[23] The same strategy was applied to the A3B2 form here with similar results.

2.3 The L9'A Mutation

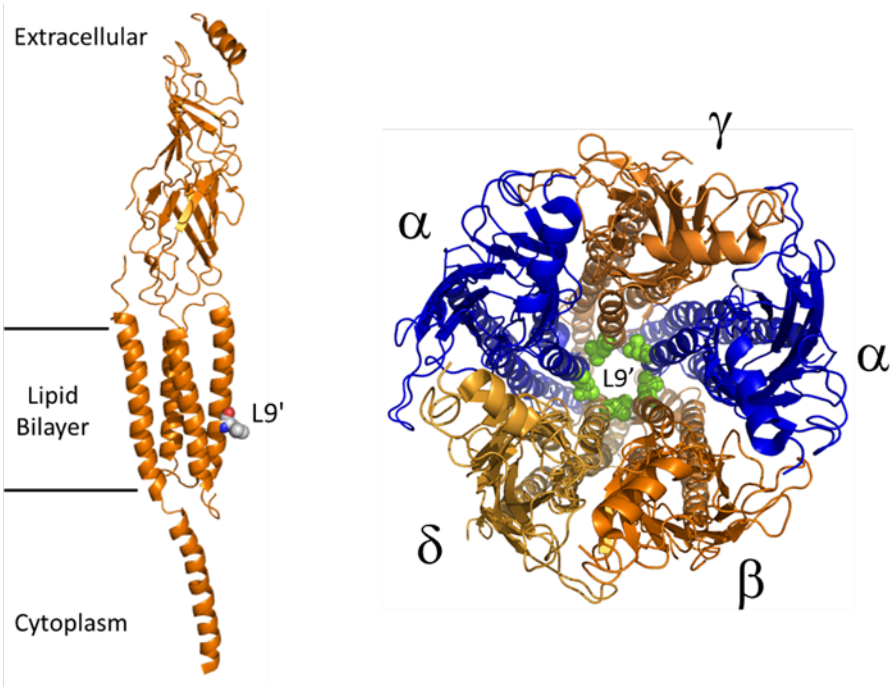

Figure 2.6 Location of the L9' Residue shown for the Muscle-type nAChR based on Unwin's model of the Torpedo receptor (pdb file 2BG9). Note that the L9' residue is in close prximity to the channel gate.

In the work presented herein, a known Leu to Ala mutation in the M2 transmembrane helix of the α4 subunit (shown in Figure 2.6 and referred to as L9'A, where 9' denotes the ninth amino acid from the cytoplasmic end of the transmembrane helix) was introduced to improve receptor expression, while maintaining pharmacological selectivity of the receptor. [27,36] Mutations of this type also increase receptor sensitivity to agonists, and they do so in an additive manner. Thus, in the present study, agonists acting at A3B2 receptors, with three L9'A mutations, generally show greater potency than at A2B3 receptors, which have two L9'A mutations, even though the A2B3 stoichiometry is intrinsically the high potency form. Moroni et al. provide a correction factor for this effect allowing for direct EC_{50} value comparison to receptors lacking this mutation.[37]

Additionally, the introduction of the L9'A mutation allowed for the studies of cytisine at A2B3 presented in this chapter. Absent the L9'A mutation, cytisine is generally found to be inactive at the A2B3, essentially acting as a competitive antagonist.[37] Upon introduction of the L9'A mutation, cytisine does activate the A2B3 receptor albeit with very low efficacy (~3% relative to acetylcholine), compared to the 50% relative efficacy seen for the A3B2 receptor. Throughout this thesis, the term "wild type" applied to either A2B3 or A3B2 receptors denotes receptors containing the L9'A mutation. When necessary, receptors lacking the L9'A mutation (or any other mutation) will be referred to as "true wild type".

2.4 α4β2 Receptor Stoichiometry Control and Characterization

The Dougherty lab has established a method for the control and characterization of α4β2 receptor stoichiometry.[27] As in the case of previous studies, we find that the stoichiometry of α4β2 receptors can be controlled by altering the ratio of the subunits of mRNA during injection (Table 2.1).[27,37,38]

	mRNA ratio	ACh EC_{50} (μM)	nH	Stoichiometry
α4L9'Aβ2	100:1	0.02 ± 0	1.47 ± 0.18	A3B2
	10:1	0.02 ± 0	1.33 ± 0.14	
	6:1	0.15 ± 0.02	0.67 ± 0.04	mixture
	3:1	0.44 ± 0.03	1.24 ± 0.07	A2B3
	1:1	0.4 ± 0.01	1.22 ± 0.02	
	1:10	0.43 ± 0.02	1.17 ± 0.06	

Table 2.1 Relationship between mRNA α4L9'A to β2 injection ratios and receptor stoichiometry as evidenced by EC_{50} values and hill coefficients (n_H).

We use three criteria for defining pure populations of either A2B3 or A3B2. First, the observed whole-cell dose-response curves must fit to a single component and second, we use the fact that A2B3 and A3B2 show markedly different rectification behaviors (Figure 2.7). The third criterion only applies to wild type receptors and, as shown in Table 2.1, is that a mixed population of receptors produces an intermediate EC_{50} value as well as a lower hill coefficient (n_H). Thus, observing EC_{50} values matching the known values for that stoichiometry confirms that the desired receptor is expressed. This third criterion was useful in determining α4:β2 injection ratios for wild type recovery experiments. All α4:β2 injection ratios used for work presented herein are detailed in the materials and methods section (see Section 2.8.3)

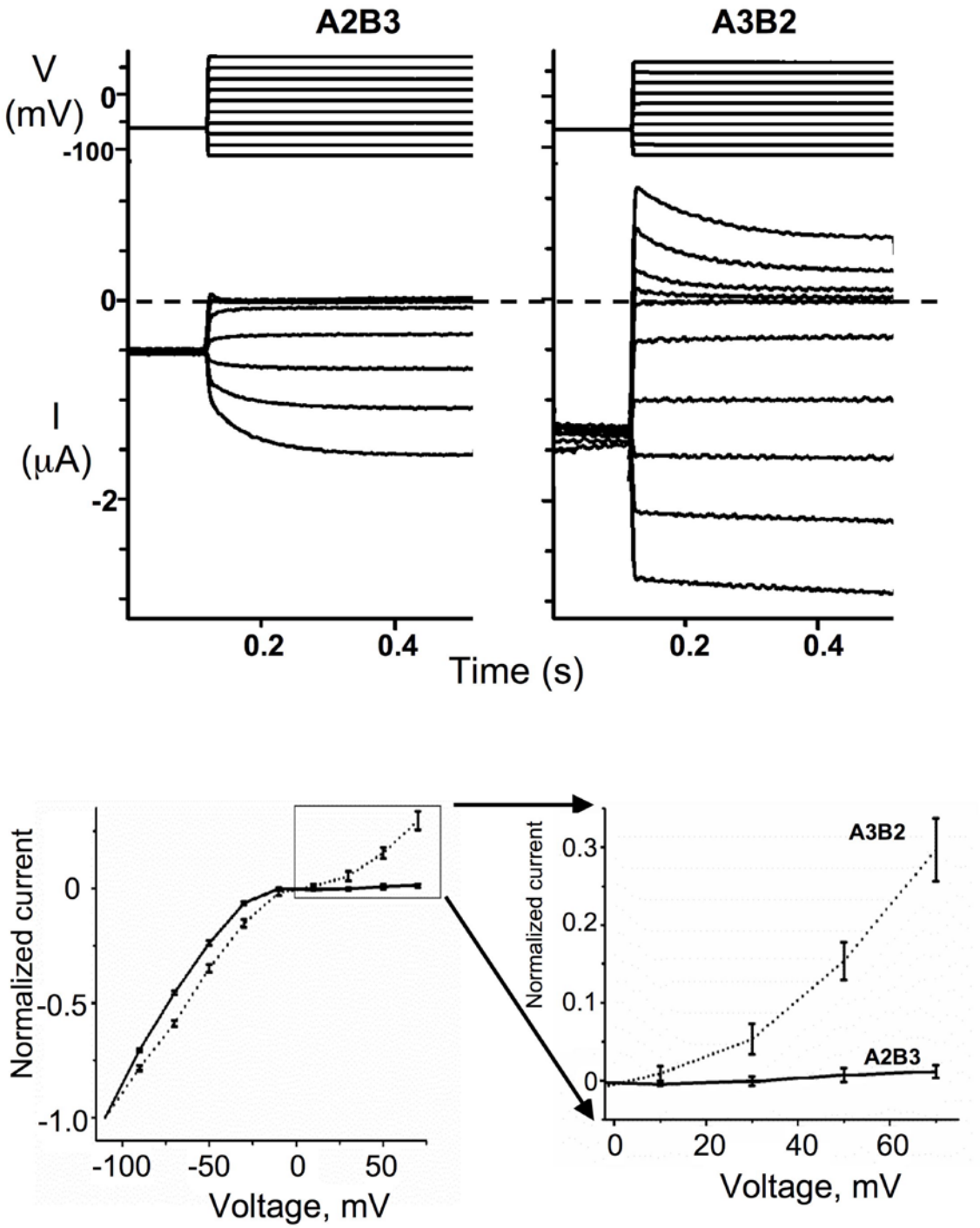

Figure 2.7 Rectification behaviors of A2B3 and A3B2 receptors. **Upper:** Representative voltage traces and current responses for voltage jump experiments. **Lower:** I-V curves for A2B3 (solid line) and A3B2 (dotted line). The inset shows positive voltages, where A2B3 and A3B2 exhibit markedly different rectification behavior.[27]

The rectification behavior of either A3B2 or A2B3 receptors was assessed through voltage jump whole-cell electrophysiology assays. In a voltage jump experiment, a non-saturating agonist concentration (usually close to the EC_{50} value) is applied and the resulting current is measured at a series of incremental voltage values, hence the term voltage “jump”. A3B2 and A2B3 receptors respond differentially to voltage jump experiments, thus providing a measure of subunit composition. A2B3 is significantly more inward rectifying than A3B2 meaning that, at positive voltages, A2B3 passes much less outward current than A3B2. This effect is evidenced in the shape of the IV relationship curves (Figure 2.7). The current value at +70mV is normalized to the measured current at -110mV and used as a measure of receptor stoichiometry, a parameter we call I_{norm}(+70mV). Cells exhibiting I_{norm}(+70mV) values lower than 0.1 are considered to express A2B3, whereas cells displaying I_{norm}(+70mV) values higher than 0.2 are considered to express A3B2.[27]

2.5 Challenges in working with A3B2

There were three main issues that arose when working with A3B2. First, we found that protein expression was lower for A3B2 than A2B3. Second, we observed that varenicline and ACh showed a biphasic behavior not seen for A2B3 and third, possibly due to the very low concentrations (pM and low nM range) of agonists used such that binding events becoming rate limiting, A3B2 shows markedly slower activation kinetics. The following sections describe how we addressed these challenges.

2.5.1 Improving A3B2 Receptor Expression

Nonsense suppression at A3B2 receptors was challenging, due to the fact that expression of α4β2 in *Xenopus* oocytes is inherently biased toward A2B3 receptors. For example, a 1:1 α4 to β2 mRNA injection ratio produces exclusively A2B3 receptors (Table 2.1). The challenge of expressing A3B2 receptors was amplified when unnatural amino acids were incorporated into the α4 subunit, because of the consistently lower expression levels seen for subunits incorporating unnatural amino acids by nonsense suppression. Several strategies were employed to overcome these difficulties. In order to obtain an essentially pure population of A3B2, an α4:β2 mRNA injection ratio at or above 100:1 was necessary. We also injected larger than usual amounts of mRNA (~100-150ng total per oocyte, compared to the ~25 ng used in typical sup-pression experiments) and aminoacylated tRNA (up to 125ng total per oocyte), and employed longer incubation times (48–72h) as necessary. In especially challenging cases, we included a second injection of mRNA and tRNA 24h after the initial injection, and allowed the injected oocytes to incubate at room temperature for 2-3h prior to electrophysiological recording.

2.5.2 Biphasic Behavior of Varenicline and ACh at A3B2

Biphasic behaviors for varenicline and, to a lesser extent, ACh were observed at injection ratios that were expected to produce pure populations of A3B2. For varenicline, the second component of the dose-response curve shows markedly lower binding affinity but does not correspond to the EC_{50} value of A2B3 (Figure 2.8). Thus, the second component was not believed to be contamination

by the A2B3 receptor. Additionally, very high α4:β2 mRNA injection ratios of 150:1 and 200:1 for wild type A3B2 (recall that 10:1 is sufficient to express A3B2) failed to eliminate the biphasic behavior, further supporting that A2B3 contamination was not the problem. In the time since these studies were performed, it has been shown that the A3B2 receptor possesses a third binding site at an α/α interface in addition to the two equivalent α/β binding sites shared by A2B3 and A3B2.[39,40] Thus, it is highly likely that the low affinity component corresponds to binding to the α/α site of A3B2 and not to contamination by a different receptor stoichiometry.

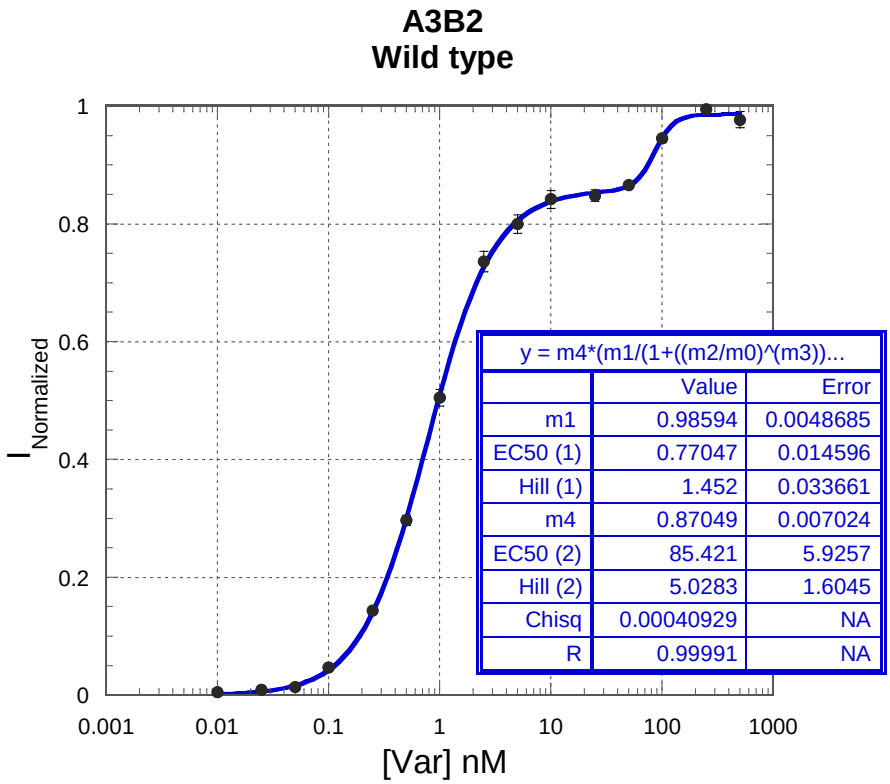

Figure 2.8 Sample dose-response curve showing the biphasic behavior of varenicline (Var) at A3B2 wild type. $I_{Normalized}$ corresponds to current values normalized to the current response at 500nM Var. The high affinity component (1) showed an EC_{50} = 0.77 ± 0.01nM and nH = 1.45 ± 0.03, whereas the low affinity component (2) exhibits an EC_{50} = 85 ± 6nM and nH = 5 ± 2. This last EC_{50} value is markedly different from the EC_{50} = 2.9 ± 0.1nM of Var at A2B3.

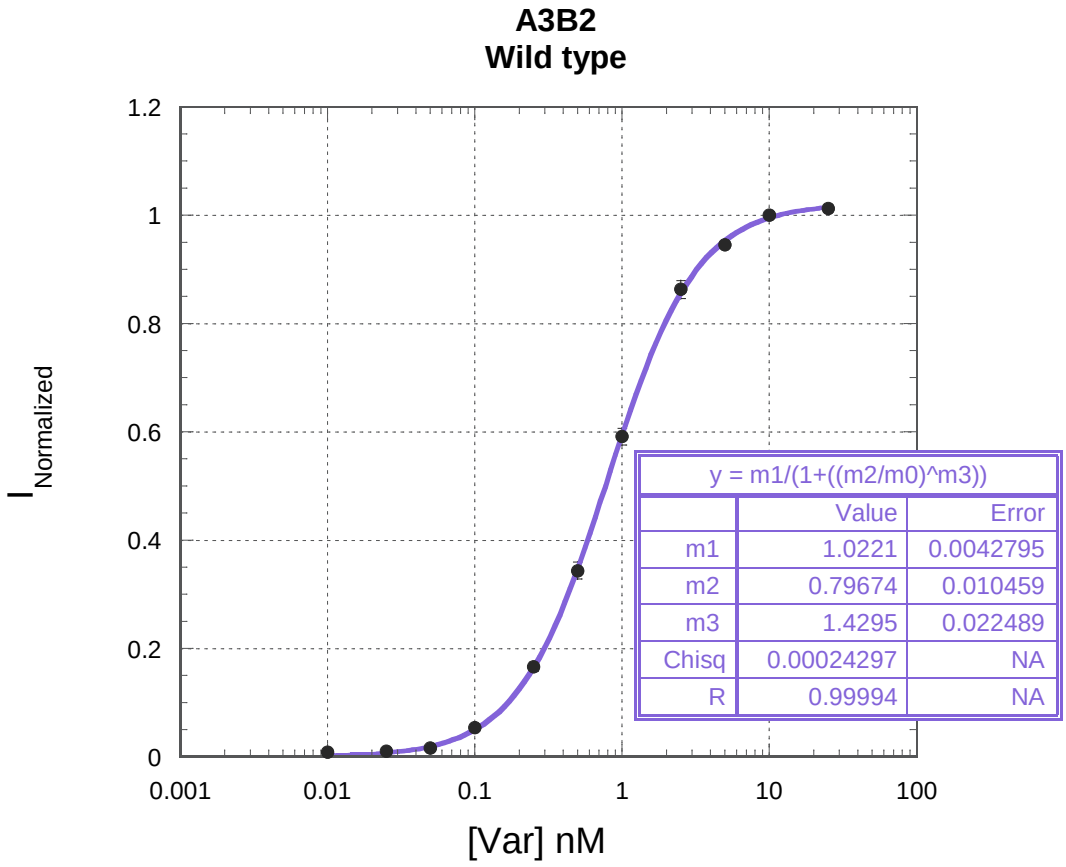

Figure 2.9 High affinity component isolated from the dose-response curve in Figure 2.8. $I_{Normalized}$ corresponds to current values normalized to the current response at 25nM Var (instead of 500nM as in Figure 2.8). The resulting EC_{50} = 0.80 ± 0.01nM (m2) and nH = 1.43 ± 0.02 (m3) values are essentially indistinguishable from the values for the biphasic fit of EC_{50} = 0.77 ± 0.01nM and nH = 1.45 ± 0.03 shown in Figure 2.8.

We decided to isolate the high affinity component corresponding to the α/β binding site to allow for equivalent comparison between A3B2 and A2B3. As evidenced by the clear plateau in the dose-response curve in Figure 2.8, the EC_{50} values of the two components were sufficiently different to allow the response of the high affinity component to reach a maximum before the low affinity component began to respond. We therefore processed the data from the high affinity component as for a monophasic dose response curve by fitting it to the Hill equation according to our standard protocol without any loss in accuracy (Figure

2.9). It is noted that this biphasic behavior was not observed for either nicotine or cytisine, which could be attributed to nicotine and cytisine causing desensitization at high agonist concentrations such that the low affinity component is “masked”.

2.5.3 Overcoming Slow Activation Kinetics at A3B2

For A2B3 receptors, a 15s drug application time is sufficient for the various agonists tested to activate all the possible receptor molecules at that specific agonist concentration. In other words, at 15s the observed current for that agonist concentration has reached its maximum because all the available agonist molecules are bound to a receptor and those receptors are in the open state. A saturating agonist concentration is one that causes maximal activation of the available receptors on the membrane. At non-saturating drug concentrations, the amount of receptors in the active state is dependent on the number of ligand molecules available, and once all the ligand molecules are bound, the maximal response for that agonist concentration can be attained. However, a 15 sec drug application time was not sufficient for the all available agonist to bind and activate the A3B2 receptor (Figure 2.10), meaning that the overall activation rate is slower for the A3B2 receptor. This could happen for several reasons; first, at very low agonist concentrations (pM or low nM range) agonist binding can become diffusion limited. We believe that this is the cause of this effect as, due to the additive nature of the L9’A mutation, A3B2 shows higher affinity than A2B3. Other possible, but less likely, causes are either a slower on-rate of the ligand or a slower activation rate (the receptor requiring a longer time to enter the active, open state once the ligand is bound) of the A3B2 receptor related to the A2B3 receptor.

We modified our standard 15s drug application time at a rate of 4mL/min protocol to allow for the slower activation kinetics at A3B2. As shown in Figure 2.10, several variations on drug application time and rate were pursued. A drug application time of 60s at two different rates, 4mL/min for the initial 15s and 1.25mL/min for the subsequent 45s, produced the desired response where the current signal is saturated within the drug application time.

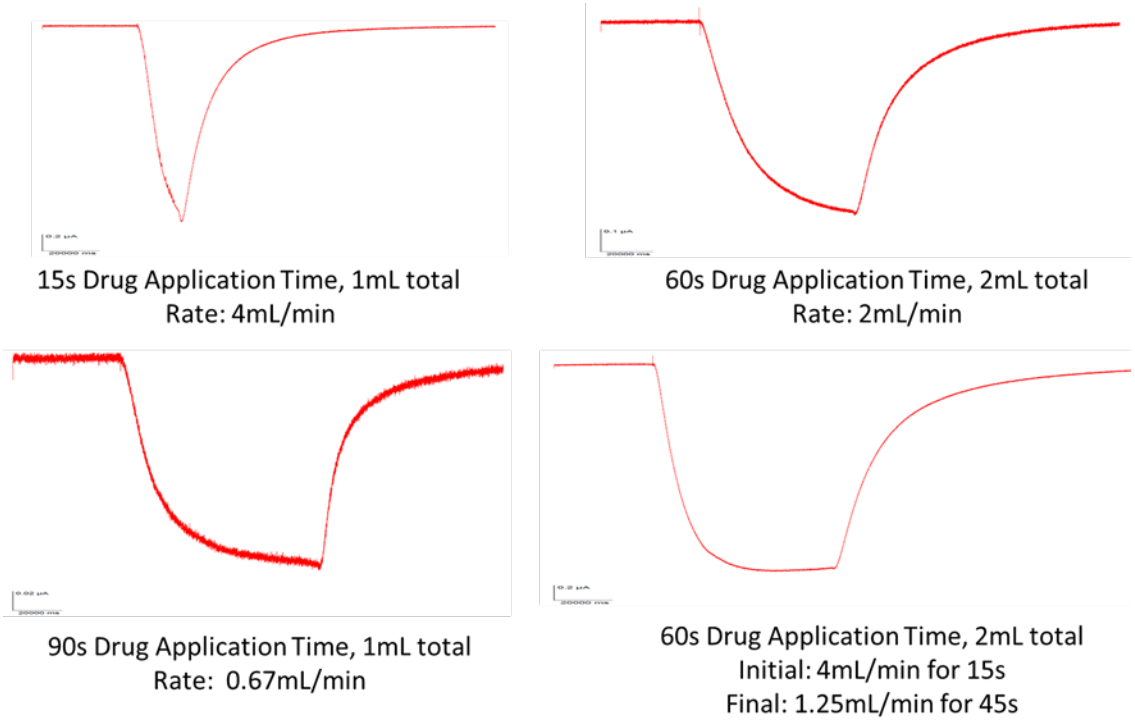

Figure 2.10 Sample traces from A3B2 in response to 0.562nM cytisine at several different drug application time intervals and different drug delivery rates. Whereas a drug application time of 60s at 4mL/min delivery rate would have been the ideal setup, this would require a total of 4 mL of drug solution and the instrument being used was limited to 2mL of drug solution. A 60s drug application time at two different rates proved to be the best setup allowing for saturation of the current signal.

2.6 Results

Unnatural amino acid mutagenesis was applied to evaluate four compounds, ACh, nicotine, varenicline, and cytisine, at both the A2B3 and A3B2 receptors. We find many similarities, and some key differences, in the binding behaviors of these prototype drugs. Results are summarized below in Table 2.2 and all measured EC_{50} values are given in Tables 2.3 – 2.7. Dose-response curves for the fluorination series of α4W154 at A3B2 for cytisine and varenicline are shown in Figure 2.11.

		wild type EC_{50} (μM)[a]	relative efficacy[b]	Cation-π interaction[c]	N^+–H•••O=C (donor)[d]	N–H•••N(O) (acceptor)[e]
ACh	A2B3	4.0	[1.0]	69[f]	1.1[f]	6.8[g]
	A3B2	87	[1.0]	540	1.1	8.5
Nicotine	A2B3	0.76	0.3 (0.3)	53[f]	19[f]	6.7[g]
	A3B2	38	0.6 (0.6)	130	19	5.6
Varenicline	A2B3	0.027	0.1	20	14	1.8
	A3B2	3.6	0.3	16	19	1.1
Cytisine	A2B3	0.066	0.03 (0)	31	8.8	62
	A3B2	15	0.5 (0.2)	30	27	14

Table 2.2 Evaluation of Binding Interactions in the α4β2 A3B2 and A2B3 receptors. a. Values are corrected for the effects of α4L9'A mutation according to the procedure of Moroni et al. (EC_{50} value was multiplied by a factor of 456 for A3B2 and 4.18 for A2B3). [37] As such, these are EC_{50} for true wild type receptors. Measured EC_{50} values are provided in Tables 2.3 to 2.7. b. Defined as the ratio I_{max} of agonist/ I_{max} of ACh. Numbers in parentheses represent efficacies for receptors that do not contain the L9'A mutation, as reported by Moroni, et al. [37] c. Ratio of EC_{50} values for F_4-Trp/Trp at position 154 in α4. d. Ratio of EC_{50} values for Tah/Thr at position 155 in α4. e. Ratio of EC_{50} values for Lah/Leu at position 119 in β2. f. Previously reported in [27]. g. Previously reported in [23].

A2B3 Receptor					
Agonist	**Mutation**	**EC_{50} (nM)**	**Fold Shift**	**n_H**	**I_{norm} (+70mV)**
ACh[a]	Wild type	420 ± 10	-	1.2 ± 0.1	0.041 ± 0.005
	α4W154 Trp	440 ± 30	1.0	1.3 ± 0.1	0.006 ± 0.014
	α4W154 F-Trp	1900 ± 100	4.5	1.2 ± 0.1	-0.065 ± 0.047
	α4W154 F_2-Trp	2000 ± 100	4.8	1.3 ± 0.1	0.032 ± 0.025
	α4W154 F_3-Trp	13000 ± 1000	31	1.3 ± 0.1	-0.073 ± 0.029
	α4W154 F_4-Trp	29000 ± 2000	69	1.1 ± 0.1	-0.027 ± 0.023
Nic[a]	Wild type	80 ± 10	-	1.2 ± 0.1	0.041 ± 0.005
	α4W154 Trp	90 ± 10	1.1	1.5 ± 0.1	0.006 ± 0.014
	α4W154 F-Trp	260 ± 20	3.3	1.3 ± 0.1	-0.065 ± 0.047
	α4W154 F_2-Trp	320 ± 40	4.0	1.3 ± 0.1	0.032 ± 0.025
	α4W154 F_3-Trp	1200 ± 100	15	1.4 ± 0.2	-0.073 ± 0.029
	α4W154 F_4-Trp	4200 ± 400	53	1.3 ± 0.2	-0.027 ± 0.023
Cy	Wild type	6.9 ± 0.3	-	1.4 ± 0.1	0.05 ± 0.01
	α4W154 Trp	11 ± 1	1.6	1.1 ± 0.1	0.03 ± 0.01
	α4W154 F-Trp	22 ± 1	3.2	1.1 ± 0.1	0.05 ± 0.01
	α4W154 F_2-Trp	21 ± 1	3.0	1.1 ± 0.1	0.08 ± 0.01
	α4W154 F_3-Trp	180 ± 7	26	1.3 ± 0.1	0.05 ± 0.03
	α4W154 F_4-Trp	212 ± 60	31	0.62 ± 0.08	0.04 ± 0.01
Var	Wild type	2.9 ± 0.1	-	1.4 ± 0.1	0.037 ± 0.007
	α4W154 Trp	2.4 ± 0.2	0.8	1.2 ± 0.1	0.043 ± 0.005
	α4W154 F-Trp	5.7 ± 0.2	2.0	1.2 ± 0.1	0.040 ± 0.007
	α4W154 F_2-Trp	9.0 ± 0.4	3.1	1.2 ± 0.1	0.05 ± 0.011
	α4W154 F_3-Trp	27 ± 1	9.5	1.3 ± 0.1	0.044 ± 0.009
	α4W154 F_4-Trp	56 ± 5	20	1.1 ± 0.1	0.033 ± 0.008

Table 2.3 Cation-π at A2B3 EC_{50} values (nM), fold shift values, Hill coefficients (n_H) and current size at +70mV (normalized to current size at -110mV). Errors are SEM (standard error from the mean). a. Previously reported in [27].

A3B2 Receptor					
Agonist	**Mutation**	**EC_{50} (nM)**	**Fold Shift**	**n_H**	**I_{norm} (+70mV)**
ACh	Wild type	23 ± 1	-	1.3 ± 0.1	0.30 ± 0.04
	α4W154 Trp	24 ± 1	1.0	1.6 ± 0.1	0.27 ± 0.01
	α4W154 F-Trp	260 ± 8	11	1.2 ± 0.1	0.19 ± 0.01
	α4W154 F_2-Trp	290 ± 10	13	1.5 ± 0.1	0.26 ± 0.06
	α4W154 F_3-Trp	8200 ± 100	357	0.63 ± 0.03	0.19 ± 0.01
	α4W154 F_4-Trp	12400 ± 2000	539	0.63 ± 0.04	0.23 ± 0.02
Nic	Wild type	10 ± 1	-	1.7 ± 0.2	0.30 ± 0.04
	α4W154 Trp	8.0 ± 1.0	0.80	1.5 ± 0.3	0.27 ± 0.01
	α4W154 F-Trp	49 ± 2	4.9	1.5 ± 0.1	0.19 ± 0.01
	α4W154 F_2-Trp	110 ± 10	11	1.5 ± 0.2	0.26 ± 0.06
	α4W154 F_3-Trp	510 ± 60	51	1.1 ± 0.1	0.19 ± 0.01
	α4W154 F_4-Trp	1300 ± 100	130	1.1 ± 0.1	0.23 ± 0.02
Cy	Wild type	3.9 ± 0.1	-	2.0 ± 0.1	0.24 ± 0.03
	α4W154 Trp	3.8 ± 0.1	1.0	2.1 ± 0.1	0.17 ± 0.02
	α4W154 F-Trp	15 ± 1	3.9	1.3 ± 0.1	0.19 ± 0.02
	α4W154 F_2-Trp	35 ± 2	9.0	1.1 ± 0.1	0.19 ± 0.02
	α4W154 F_3-Trp	78 ± 5	20	0.95 ± 0.04	0.20 ± 0.02
	α4W154 F_4-Trp	120 ± 10	31	0.88 ± 0.05	0.18 ± 0.02
Var	Wild type	0.95 ± 0.02	-	1.7 ± 0.05	0.22 ± 0.03
	α4W154 Trp	0.73 ± 0.02	0.77	1.4 ± 0.1	0.30 ± 0.03
	α4W154 F-Trp	2.0 ± 0.2	2.1	1.1 ± 0.1	0.24 ± 0.01
	α4W154 F_2-Trp	2.4 ± 0.1	2.5	1.2 ± 0.1	0.21 ± 0.01
	α4W154 F_3-Trp	11 ± 1	12	1.0 ± 0.1	0.20 ± 0.02
	α4W154 F_4-Trp	15 ± 2	16	0.64 ± 0.04	0.18 ± 0.02

Table 2.4 Cation-π at A3B2 EC_{50} values (nM), fold shift values, Hill coefficients (n_H) and current size at +70mV (normalized to current size at -110mV). Errors are SEM (standard error from the mean).

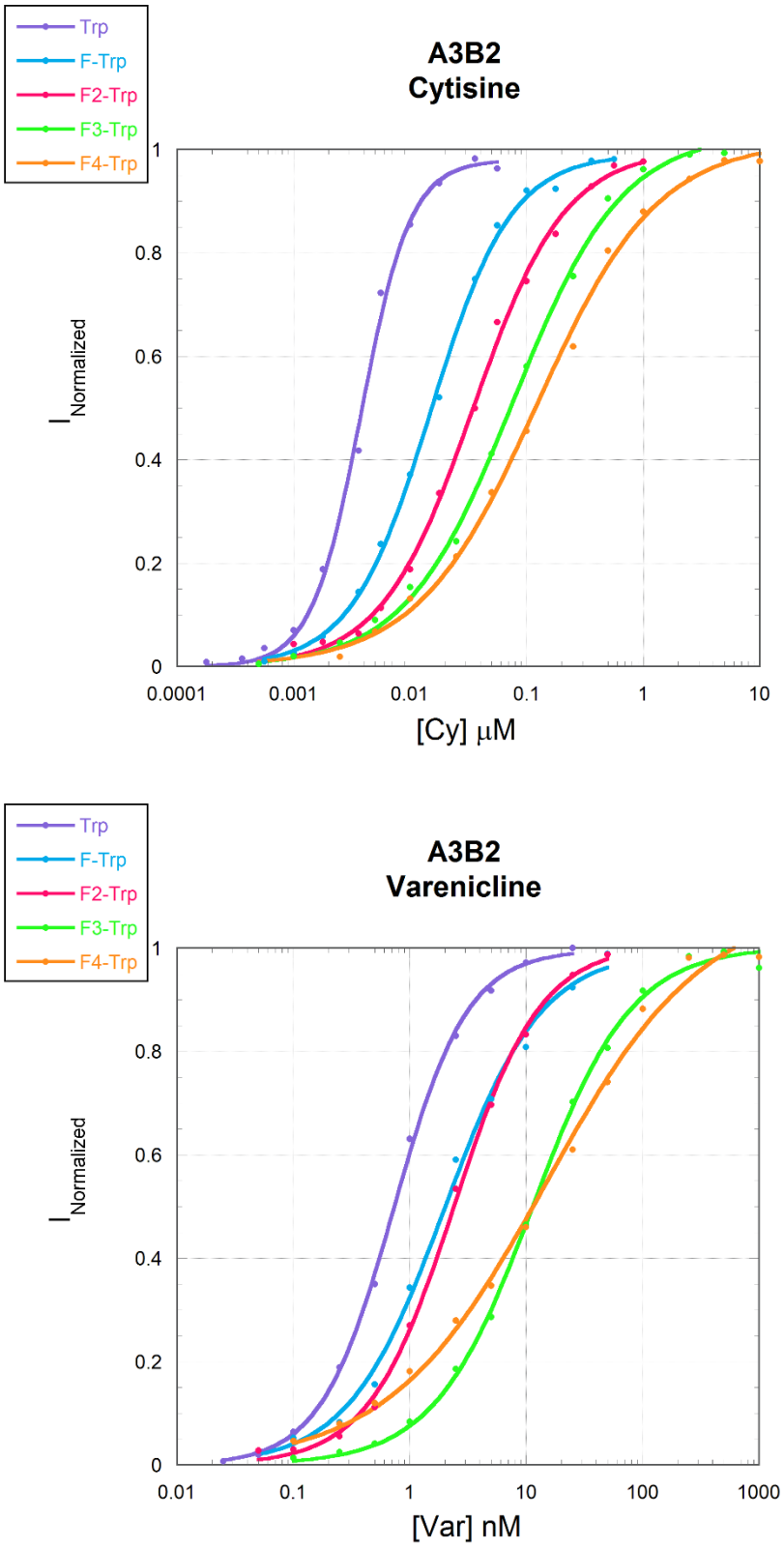

Figure 2.11 Dose-response curves for the fluorination series of α4W154 at A3B2 for cytisine (upper) and varenicline (lower).

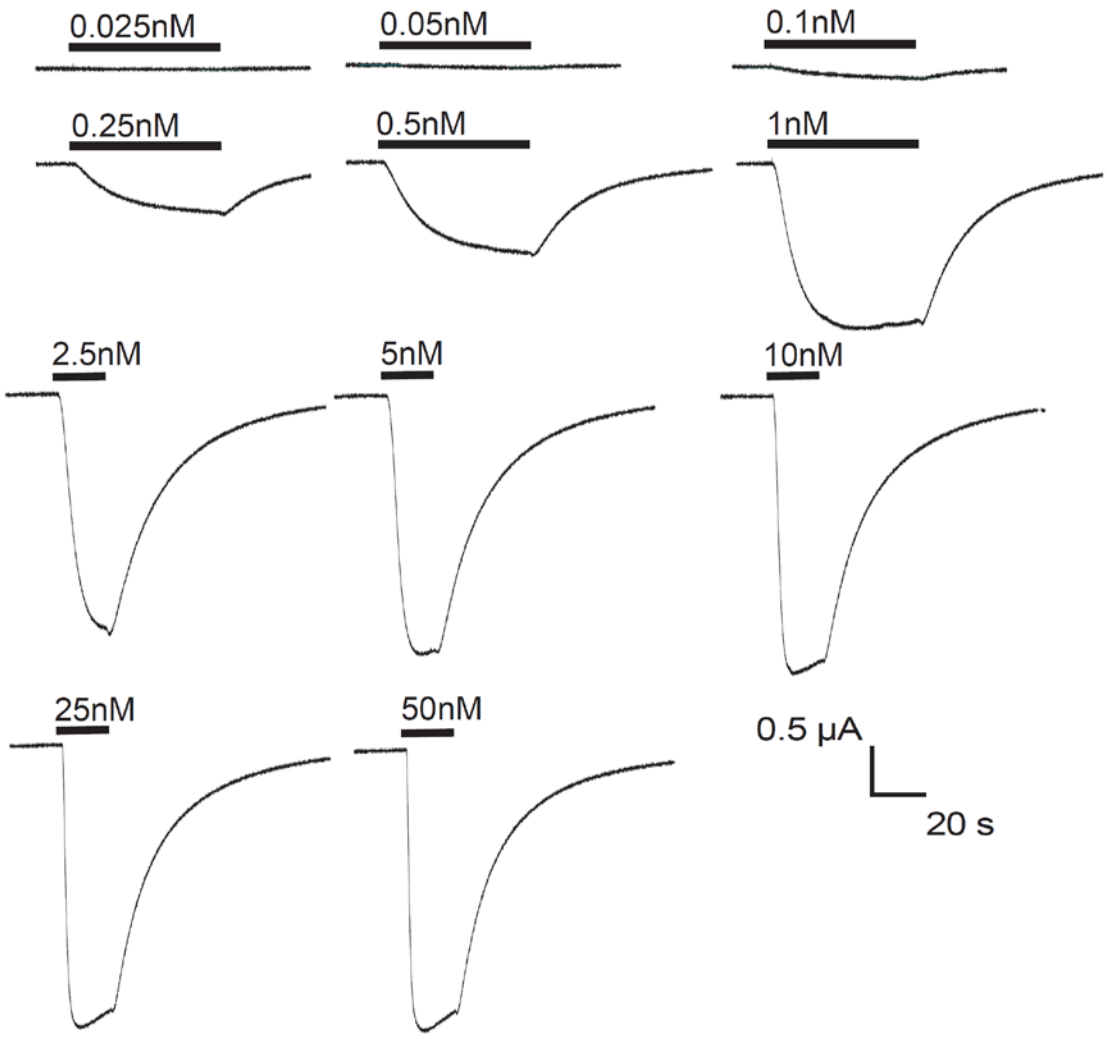

Figure 2.12 Representative traces of voltage-clamp current for a wild type recovery experiment at αW154 of the A3B2 receptor. Bars show application of varenicline at concentrations noted.

2.6.1 The Cation-π Interaction

Previous work in the group has shown that both ACh and nicotine make a cation-π interaction to TrpB (Trp154) in the A2B3 $\alpha 4\beta 2$ receptor. [27] In the present work, we establish comparable cation-π interactions for varenicline and cytisine at A2B3 and for all four agonists at the A3B2 receptor. Plots of cation-π binding ability (which correlates with the degree of fluorination) vs. log EC_{50} are linear in all cases (Figure 2.13).

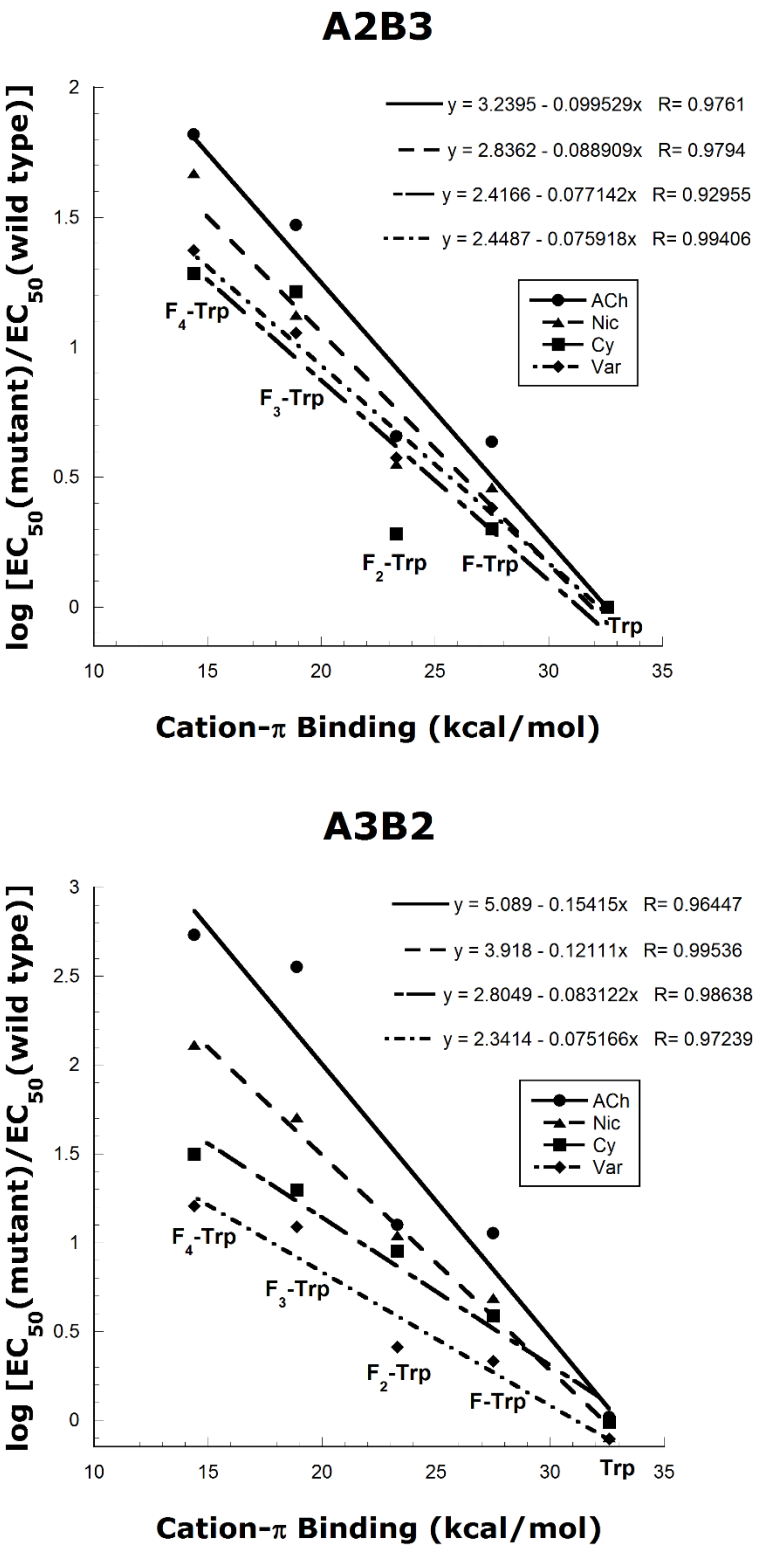

Figure 2.13 Fluorination plots for the agonists studied at A2B3 (upper) and A3B2 (lower). Data for nicotine and ACh at A2B3 were previously published by Xiu et al. and are reproduced here for comparison purposes.[27] Nic = nicotine; Cy = cytisine; Var = varenicline.

We have previously argued that the magnitude of the perturbation to EC_{50} induced by fluorination can be taken as an indicator of the relative strength of a cation-π interaction.[41] In Table 2.2 we characterize the strength of a cation-π interaction by the ratio of EC_{50} values for the F_4-Trp mutant vs. the wild type. The F_4-Trp residue represents a side chain in which the electrostatic component of the cation-π interaction has been completely removed, but other features of the residue are essentially intact (Figure 2.14). As shown in Table 2,2, all drug-receptor pairings reported here show a significant "cation-π ratio", thus establishing a common anchor point for the binding of all drugs considered here to both receptors.

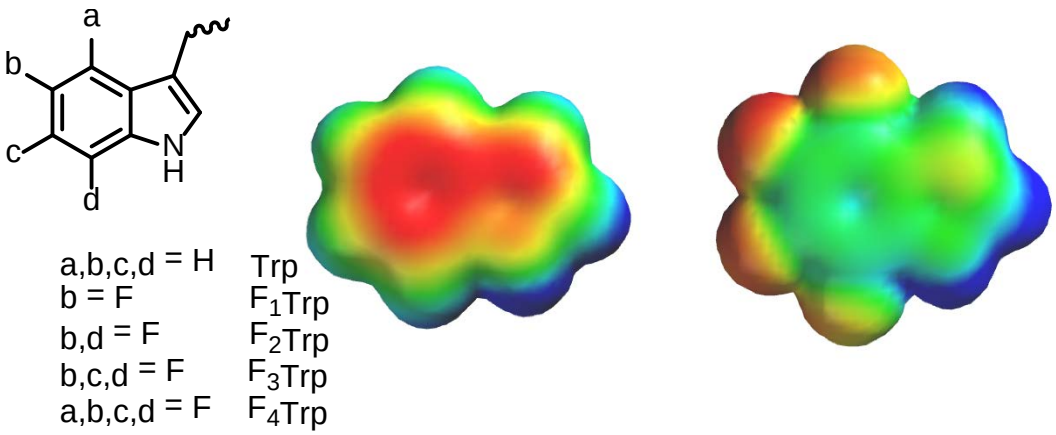

Figure 2.14 Left: Structure of unnatural amino acids in the Trp fluorination series studied herein. **Middle/Right:** Electrostatic potential surfaces of indole (middle) and F_4-indole (right), corresponding to the aromatic portions of the side chains of Trp and F_4-Trp, respectively. Results are from HF-6-31G** calculations. Electrostatic potential ranges from -25kcal/mol (**red**) to +25kcal/mol (**blue**), so that **green** represents ~0 electrostatic potential.

2.6.2 The Hydrogen Bond Donor

All the agonists that possess an N^+H moiety are significantly impacted by the Thr155Tah mutation in both stoichiometries, suggesting the hydrogen bond donor interaction to the backbone carbonyl of TrpB is significant. ACh is not impacted by this mutation, as expected. To facilitate comparison, we have expressed variations as a ratio of EC_{50} values, comparing the receptor with Tah at residue 155 to the wild type Thr (Table 2.2). All agonists except ACh show an EC_{50} ratio significantly greater than 1, with only modest variations in magnitude.

2.6.3 The Hydrogen Bond Acceptor

In previous studies of the A2B3 receptor, Blum et al. showed that ACh and nicotine respond equivalently to the β2 Leu119Lah mutation, with a moderate rise in EC_{50}.[23] Importantly, it was observed that analogs lacking the hydrogen bond acceptor moiety, S-MPP for nicotine and choline for ACh, responded quite differently to the β2 Leu119Lah mutation. This established that it is, indeed, the pyridine N of nicotine and the carbonyl O of ACh that interact with the backbone NH. We now report parallel results for ACh and nicotine in the A3B2 receptor. Again, expressing our results as a ratio of EC_{50} values for backbone mutant vs. wild type receptors, both compounds show moderate increases in EC_{50} in response to the backbone ester in both receptor stoichiometries (Table 2.2). However, choline is not impacted by the mutation, and S-MPP is actually *gain of function* in response to the backbone mutation in the A3B2 receptor (Table 2.5). A similar result was seen for S-MPP in the A2B3 receptor.[23]

S-MPP				
Receptor	**Mutation**	**EC_{50} (nM)**	**Fold Shift**	**n_H**
A2B3	Wild type[a]	11000 ± 400	-	1.7 ± 0.1
	β2L119 Leu[a]	14000 ± 900	1.3	1.5 ± 0.1
	β2L119 Lah[a]	1100 ± 40	0.08	1.5 ± 0.1
A3B2	Wild type	4500 ± 100	-	1.1 ± 0.1
	β2L119 Leu	4200 ± 300	0.93	1.6 ± 0.1
	β2L119 Lah	130 ± 10	0.03	1.2 ± 0.1

Table 2.5 EC_{50} values (nM), fold shift values and Hill coefficients (n_H) for S-MPP. a. Previously reported [23]. Errors are SEM.

The results for varenicline are surprising and stand in contrast to those for ACh and nicotine. With only a 2-fold shift in A2B3 and no meaningful shift in A3B2, it would appear that there is no functionally significant hydrogen bond acceptor interaction between a quinoxaline N of varenicline and the backbone NH of β2 Leu119 in the α4β2 receptor.

Cytisine also produces intriguing results for the hydrogen bond acceptor interaction. A remarkable 62-fold shift is seen for this subtle mutation in the A2B3 receptor. A much smaller effect is seen in the A3B2 receptor, although it is still larger than seen for any other drug-receptor combination.

A2B3 Receptor					
Agonist	**Mutation**	**EC_{50} (nM)**	**Fold Shift**	**n_H**	**I_{norm} (+70mV)**
ACh	α4T155 Thr[a]	410 ± 20	-	1.4 ± 0.1	0.044 ± 0.007
	α4T155 Tah[a]	370 ± 20	0.90	1.3 ± 0.1	0.02 ± 0.01
	β2L119 Leu[b]	440 ± 20	-	1.3 ± 0.1	0.04 ± 0.01
	β2L119 Lah[b]	3000 ± 100	6.8	1.2 ± 0.1	0.04 ± 0.01
Nic	α4T155 Thr[a]	90 ± 10	-	1.6 ± 0.1	0.044 ± 0.007
	α4T155 Tah[a]	1700 ± 140	19	1.2 ± 0.2	0.02 ± 0.01
	β2L119 Leu[b]	120 ± 3	-	1.5 ± 0.1	0.05 ± 0.01
	β2L119 Lah[b]	800 ± 30	6.7	1.3 ± 0.1	0.06 ± 0.01
Cy	α4T155 Thr	15 ± 0.7	-	1.2 ± 0.1	0.026 ± 0.009
	α4T155 Tah	130 ± 9	8.7	1.2 ± 0.1	0.03 ± 0.01
	β2L119 Leu	8.7 ± 0.5	-	1.2 ± 0.1	0.06 ± 0.02
	β2L119 Lah	540 ± 30	62	1.0 ± 0.1	0.06 ± 0.01
Var	α4T155 Thr	2.2 ± 0.1	-	1.3 ± 0.1	0.020 ± 0.002
	α4T155 Tah	30 ± 2	14	1.2 ± 0.1	0.029 ± 0.006
	β2L119 Leu	2.6 ± 0.2	-	1.3 ± 0.1	0.06 ± 0.01
	β2L119 Lah	4.7 ± 0.2	1.8	1.3 ± 0.1	0.05 ± 0.01

Table 2.6 Hydrogen bonds at A2B3. EC_{50} values (nM), fold shift values, Hill coefficients (n_H) and current size at +70mV (normalized to current size at -110mV). a. Previously reported [27]. b. Previously reported [23]. Errors are SEM.

A3B2 Receptor					
Agonist	**Mutation**	**EC_{50} (nM)**	**Fold Shift**	**n_H**	**I_{norm} (+70mV)**
ACh	α4T155 Thr	20 ± 1	-	1.4 ± 0.1	0.20 ± 0.02
	α4T155 Tah	25 ± 2	1.3	1.2 ± 0.1	0.22 ± 0.01
	β2L119 Leu	26 ± 1	-	1.6 ± 0.1	0.23 ± 0.02
	β2L119 Lah	220 ± 10	8.5	1.2 ± 0.1	0.24 ± 0.03
Nic	α4T155 Thr	9.9 ± 0.5	-	1.7 ± 0.1	0.20 ± 0.02
	α4T155 Tah	210 ± 20	21	1.6 ± 0.2	0.22 ± 0.01
	β2L119 Leu	12 ± 0.5	-	1.6 ± 0.1	0.23 ± 0.02
	β2L119 Lah	67 ± 3	5.6	1.4 ± 0.1	0.20 ± 0.03
Cy	α4T155 Thr	3.6 ± 0.4	-	1.4 ± 0.1	0.20 ± 0.04
	α4T155 Tah	96 ± 6	27	1.1 ± 0.1	0.19 ± 0.02
	β2L119 Leu	3.6 ± 0.1	-	1.9 ± 0.1	0.32 ± 0.03
	β2L119 Lah	51 ± 2	14	1.4 ± 0.1	0.24 ± 0.02
Var	α4T155 Thr	0.47 ± 0.03	-	1.5 ± 0.1	0.27 ± 0.02
	α4T155 Tah	8.9 ± 0.3	19	1.2 ± 0.1	0.23 ± 0.04
	β2L119 Leu	1.0 ± 0.1	-	1.5 ± 0.1	0.23 ± 0.03
	β2L119 Lah	1.1 ± 0.05	1.1	1.2 ± 0.1	0.22 ± 0.01

Table 2.7 Hydrogen bonds at A3B2. EC_{50} values (nM), fold shift values, Hill coefficients (n_H) and current size at +70mV (normalized to current size at -110mV). Errors are SEM.

2.7 Discussion

From a combination of structural and functional studies, strong evidence has emerged for an agonist binding model at the nAChR that consists of three distinct binding interactions: a cation-π interaction, a hydrogen bond donor interaction to a backbone carbonyl, and a hydrogen bond acceptor interaction to a backbone NH. In the present work we have evaluated these three interactions for four different agonists at two stoichiometries of the $\alpha4\beta2$ receptor A2B3 and A3B2.

A cation-π interaction to TrpB (Trp154) has been found in both stoichiometries of the $\alpha4\beta2$ receptor for all compounds studied here: ACh, nicotine, varenicline, and cytisine. The data of Table 2.2 suggest mostly modest variations, with perhaps two meaningful differences. At both stoichiometries, ACh shows the strongest cation-π interaction of the four drugs. Note that intrinsically (i.e., in the gas phase) a quaternary ammonium cation as in ACh makes a weaker cation-π interaction than a protonated amine.[42,43] It would appear that the nAChR evolved to optimize this interaction for its natural agonist, ACh. Also, for both ACh and nicotine, the A3B2 stoichiometry produces a stronger cation-π interaction than the A2B3. No meaningful differences are seen for varenicline or cytisine.

We have argued that F_4-Trp represents a side chain for which the electrostatic component of the cation-π interaction has been completely removed, while other secondary effects such as dispersion forces and induced dipole interactions remain. The EC_{50} ratios of Table 2.2 thus provide an estimate of the magnitude of this effect. For the largest interaction, ACh in A3B2, the ratio of 540

corresponds to a $\Delta G°$ value of 3.7 kcal/mol. This is consistent with other estimations of the cation-π interaction in protein systems.[44-46]

The cation-π interaction is a universal feature of ACh binding sites, but some variations have been seen. For example, a cation-π interaction is seen for ACh but *not* for nicotine in the muscle-type nAChR ($(\alpha 1)_2\beta 1\gamma\delta$), a key feature in distinguishing peripheral vs. central nervous system effects of nicotine.[27,41] In the muscle-type nAChR, the much more potent nicotine analogue epibatidine does show a cation-π interaction to TrpB.[34] In the $\alpha 4\beta 4$ nAChR (A2B3 stoichiometry), both ACh and nicotine make a cation-π interaction to TrpB.[32] However, in the homopentameric $\alpha 7$ nAChR, the cation-π site moves to an alternative aromatic residue in the agonist binding site.[32] Similar results are seen for other members of Cys-loop (pentameric) superfamily of neurotransmitter-gated ion channels. In the 5-HT_3 (serotonin) receptor [41], the glycine receptor [47], and the $GABA_A$ and $GABA_C$ receptors [48,49], the agonist makes a cation-π interaction to an aromatic residue at the agonist binding site. The analogue to TrpB is the most common cation-π site, but some variation is seen across the family.[50] For the drug-receptor combinations probed here, however, all cation-π interactions are to TrpB.

Two hydrogen bonding interactions contribute to agonist binding, and we have referred to them as the hydrogen bond donor and the hydrogen bond acceptor of the drug (Figure 2.3). Of course, ACh cannot participate in the hydrogen bond donor interaction, but nicotine shows a strong interaction with the backbone carbonyl of TrpB. For ACh and nicotine, both stoichiometries show similar behaviors for the hydrogen bond acceptor interaction.

The two smoking cessation compounds, varenicline and cytisine, show interesting variations with regard to hydrogen bonding interactions. In discussing these compounds, we will refer to Figure 2.15, which shows structures and electrostatic potential surfaces for ACh, nicotine, cytisine, and varenicline.

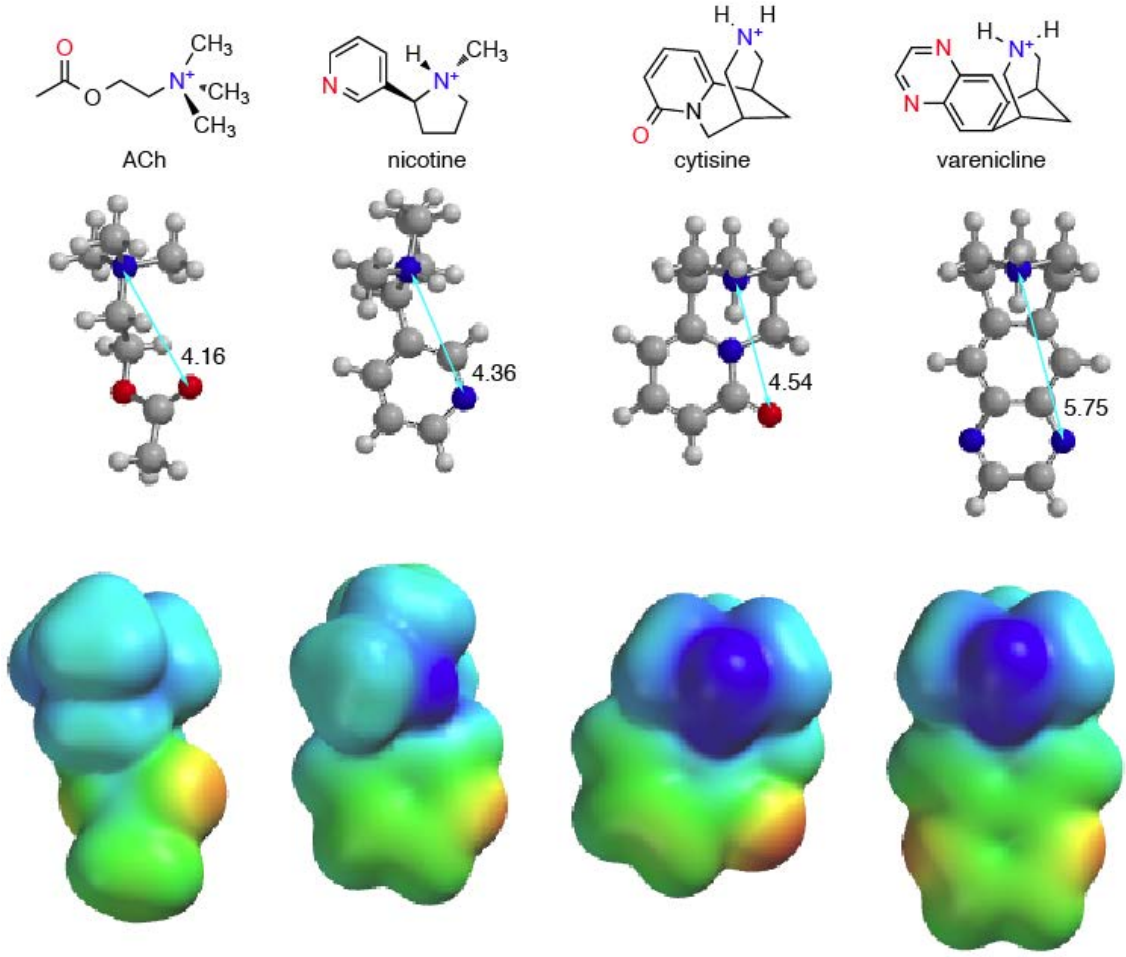

Figure 2.15 Structures and electrostatic potential surfaces for the agonists considered here. Results are from HF-3-21G* calcula-tions. Electrostatic potential ranges from -4.8 kcal/mol (red) to +143 kcal/mol (blue). As such, unlike in Figure 2.14, **green** does not represent ~0 electrostatic potential. As all these molecules are cations, the surfaces are positive over their entirety, except for a small negative electrostatic potential at the carbonyl oxygen of cytisine. The **light blue** line represents the "internitrogen distance" for each agonist, the number is that distance in Å.

Varenicline is similar to nicotine in its participation in the hydrogen bond donor interaction. However, varenicline is qualitatively different from all the other

compounds considered with regard to the hydrogen bond acceptor interaction. With less than a 2-fold effect at the A2B3 stoichiometry and no meaningful effect at the A3B2 stoichiometry, we conclude that varenicline does not make a functionally important hydrogen bond to the backbone NH of Leu119 in the β2 subunit. Figure 2.15 provides a rationalization. By visual inspection, and from the distances shown, is it clear that the quinoxaline nitrogens of varenicline are not well aligned with the hydrogen bond acceptor moieties of the other compounds. Thus, it may be that the geometry of varenicline makes formation of the hydrogen bond impossible. Alternatively, the quinoxaline N is a much poorer hydrogen bond acceptor than the pyridine N of nicotine (pK_a values for pyridine and quinoxaline are 5.2 and 0.8, respectively). It may be that the protein can adjust to the geometry of varenicline, but the hydrogen bonding interaction is so weak that it does not show up in our assay.

Cytisine shows an intriguing hydrogen bonding pattern, distinct from the other agonists considered here. Recall that, more so than the other drugs, cytisine shows a strong distinction between the two stoichiometries of the α4β2 receptor. Generally, cytisine is considered to be inactive (an antagonist) at the A2B3 form; we are able to record EC_{50} values because of the L9'A mutations present in our system. Cytisine is however efficacious at the A3B2 form. Interestingly, cytisine also shows the greatest stoichiometry differences for both hydrogen bonding interactions (Table 2.2). Concerning the hydrogen bond donor interaction, cytisine shows a stronger than usual hydrogen bond in the A3B2 stoichiometry, but a weaker than usual interaction in the A2B3 stoichiometry. The effects are not large,

but we feel the systems being compared are similar enough that the differences are meaningful. The pattern is reversed in the hydrogen bond acceptor site. The A2B3 stoichiometry shows a remarkable 62-fold rise in EC_{50} in response to the backbone mutation, much larger than anything we have seen previously. The A3B2 stoichiometry now shows the smaller effect, although it is still larger than what is seen with nicotine or ACh.

We propose a speculative model to rationalize these results. Recall that cytisine is efficacious at A3B2 but not at A2B3. Also, A3B2 shows a strong hydrogen bond donor interaction and a relatively weaker hydrogen bond acceptor interaction, while the reverse pattern holds for A2B3. We propose that cytisine is positioned closer to TrpB in the efficacious A3B2 stoichiometry than in the A2B3, and that a strong interaction with TrpB is required for receptor gating. By moving closer to TrpB in the A3B2 receptor, cytisine is moving further from Leu119, thus explaining the pattern of hydrogen bond strengths. Hydrogen bonding shows a fairly steep distance dependence, and so only a slight shift would be required to meaningfully strengthen/weaken a hydrogen bond. In contrast, the cation-π interaction is much less sensitive to the distance separation between the charge and the π-system [44], and so there is no stoichiometry distinction for this interaction. As previously noted, for some indications a partial agonist could be preferable to a full agonist. If validated by further studies, the present findings could suggest a strategy for tuning agonist efficacy. Maximizing the interaction with TrpB, through both the cation-π interaction and the hydrogen bond donor interaction, should

maximize efficacy, while biasing the system toward the hydrogen bond acceptor interaction could diminish efficacy.

Another aspect of cytisine's pharmacology is that the hydrogen bond acceptor interaction is stronger for *both* stoichiometries than for the any of the other drug-receptor pairs. We can rationalize this general effect with reference to the electrostatic potential plots of Figure 2.15. Visually, the carbonyl oxygen of cytisine presents a much stronger negative electrostatic potential than the corresponding nitrogen of nicotine. Quantitative evaluation of the electrostatic potentials at these atoms confirms the visual impression. Thus, the amide carbonyl oxygen of cytisine should be a better hydrogen bond acceptor than the pyridine nitrogen of nicotine or the ester carbonyl of ACh, completely consistent with expectations based on known hydrogen bonding propensities.

In studies such as these, it is typical to acknowledge the ambiguity that a change in EC_{50} could reflect a change in "binding" or a change in "gating". In the present study, we are probing a cation-π interaction and two hydrogen bonds; these are unambiguously binding interactions. Structural models and the very subtle nature of the mutations we introduce make it clear that we are perturbing a binding interaction between the drug and the receptor. A shift in EC_{50} indicates that the interaction probed is strengthened (or weakened) in one or more of the equilibria that contribute to EC_{50}. A simple case would be the formation of a key hydrogen bond in the drug binding step. However, it could be that the gating equilibrium is perturbed, even if the mutation is quite remote to the region of the receptor thought to contain the channel gate. This would mean that the drug binds

more tightly to the open state than to the closed (or vice versa). Either way, we are probing a binding interaction between the drug and the receptor. Certainly, there is value in knowing which step of the overall equilibrium is most sensitive to the interaction being probed. Single-channel studies with the patch clamp technique can provide such information, and we have used this approach in the past to further characterize unnatural amino acid mutations we have made (Chapter 4 and [27]). In the present work we present over 60 EC_{50} values obtained from multiple dose-response curves (Tables 2.3 to 2.7). It is not feasible to perform single-channel studies on every combination of drug and mutation considered here. More importantly, for studies of comparative pharmacology, EC_{50} is arguably the most appropriate measure of receptor function.

In conclusion, we have evaluated a binding model for ACh, nicotine, and two smoking cessation drugs, varenicline and cytisine, at both stoichiometries, A2B3 and A3B2, of the $\alpha4\beta2$ nAChR, the receptor most associated with nicotine addiction. We find a universal cation-π interaction, and a hydrogen bond donor interaction to a backbone carbonyl. However, we find that varenicline violates the nicotinic binding model and does not make a functionally significant hydrogen bond acceptor interaction seen with other agonists. In addition, the differential hydrogen bonding interactions for cytisine suggest a structural model to explain the variation in efficacy seen for the two receptor stoichiometries.

2.8 Materials and Methods

2.8.1 Mutagenesis and mRNA synthesis

Rat α4L9'A and β2 subunits were expressed in pAMV vectors. The mutations for each subunit were introduced according to the QuikChange mutagenesis protocol (Stratagene) and sequencing verified the incorporation of desired mutations. Rat α4L9'A and β2 mRNA were prepared from NotI linearizations of the circular expression vector pAMV, followed by in vitro transcription using the mMessage mMachine T7 kit (Ambion, Austin, TX).

2.8.2 Ion channel expression

To express the ion channels with a wild type ligand binding site, α4L9'A mRNA was co-injected with β2 mRNA at various ratios to obtain desired receptor stoichiometry. Specifically, 20:1 α4L9'A:β2 ratio for A3B2 and 1:3 for A2B3. Total mRNA amount for microinjection was 10-50ng/cell in a total volume of 75nL. Stage V-VI *Xenopus* oocytes were microinjected and incubated at 18˚C for 24-48h in ND96 buffer (96mM NaCl, 2mM KCl, 1mM MgCl2, 2mM CaCl2, and 5mM HEPES, pH 7.5) with 0.005% (w/v) gentamycin and 2% (v/v) horse serum.

2.8.3 Unnatural amino acid incorporation

Nitroveratryloxycarbonyl (NVOC) protected cyanomethyl ester forms of unnatural amino acids and α-hydroxythreonine cyanomethyl ester were synthesized, coupled to the dinucleotide dCA, and enzymatically ligated to either 74-nucleotide THG73 tRNA (for α4W154 and α4T155 experiments) or 74-nucleotide TQOpS' tRNA (for β2L119 experiments) as described previously. [25,27] The unnatural amino acid-conjugated tRNA was deprotected by photolysis and

then immediately co-injected with mRNA containing the UAG mutation (for THG73 tRNA) or the UGA mutation (TQOpS' tRNA) at the site of interest. Stage V–VI oocytes were injected with ~10-150ng mRNA and 25-125ng tRNA-amino acid or tRNA-hydroxy acid in a total volume of 75nL. For unnatural amino acid incorporation into the α4 subunit, a 3:1 α4L9'A:β2 mRNA injection ratio yielded A2B3 receptors and 100:1 to 150:1 ratios yielded A3B2 receptors. For unnatural amino acid incorporation into the β2 subunit, a 1:20 α4L9'A:β2 mRNA injection ratio yielded A2B3 receptors and a 10:1 ratio yielded A3B2 receptors. In cases where receptor expression needed to be increased, a second microinjection (double injection) of the same concentration and volume of α4L9'A:β2 mRNA and tRNA was performed after 24h incubation at 18°C. Double injected oocytes were incubated for an additional 24-48h for a total of 48-72h. Cells were incubated in ND96 buffer, 0.005% (w/v) gentamycin and 2% (v/v) horse serum, and the solution was changed at least daily and up to every 6h. The fidelity of unnatural amino acid incorporation was confirmed at each site with a "wild type recovery" experiment and "readthrough/reaminoacylation" tests (see Section 1.3.2). In the "wild type recovery" experiment, UAG mutant mRNA was co-injected with tRNA charged with the amino acid that was present at this residue in the wild type protein. Generation of receptors that were indistinguishable from the wild type protein indicated that the residue carried by the suppressor tRNA was successfully and exclusively integrated into the protein. In a "readthrough/reaminoacylation" test, the UAG mutant mRNA was introduced with (1) no tRNA, (2)76-nucleotide THG73 tRNA that was not charged with any amino acid or (3) tRNA THG73 enzymatically ligated

to the dinucleotide dCA. A lack of current in these experiments validated the reliability of the nonsense suppression experiments.

2.8.4 Whole-cell electrophysiological characterizations of the channels

Oocyte recordings were performed 24h after microinjection for wild type receptors and 48 to 72h after microinjection for unnatural amino acids. Agonist-induced currents were recorded in two-electrode voltage clamp mode using the OpusXpress 6000A (Axon Instruments, Union City, CA) at a holding potential of −60mV. Oocytes were superfused with Ca^{2+}-free ND96 solution (96mM NaCl, 2mM KCl, 1mM MgCl2, and 5mM HEPES, pH 7.5) at flow rates of either 1.25 or 4mL/min during drug application and 3mL/min during wash. For A2B3 experiments, drug application was 15s in duration at 4mL/min rate (1mL total drug volume), while wash duration between each concentration was 116s. For A3B2 experiments, drug application was 15s in duration at 4mL/min rate immediately followed by 45s at 1.25mL/min rate (2mL total drug volume), while wash duration between each concentration was 116s. Data were sampled at 50Hz and filtered at 20Hz. Acetylcholine chloride, (−)-nicotine tartrate, and (−)-cytisine were purchased from Sigma/Aldrich/RBI (St. Louis, MO). Varenicline tartrate was a generous gift from Targacept company. Agonists were prepared in sterile, distilled, deionized water for dilution in Ca^{2+}-free ND96 solution. Dose-response data were obtained for at least 6 concentrations of agonist and for a minimum of 5 oocytes originating from at least two different donor frogs. Mutants with I_{max} of at least 80nA of current were defined as functional. EC_{50} and Hill coefficients were calculated by fitting the dose-response relation to the Hill equation (see Section 1.4.1). The dose-

responses of individual oocytes were examined to identify outliers. All data are reported as mean ± standard error (SE). Voltage jump experiments were used to verify the stoichiometry of the mutant and wild type receptors, as described previously.[27]

2.9 Note on Project Contributions

The work presented in this chapter was a collaborative effort between myself and four other members of the Dougherty group, Dr. Angela P. Blum, Dr. Nyssa L. Puskar, Dr. Jai A. P. Shanata and Darren T. Nakamura.[51] Angela performed all the functional assays pertaining to the β2L119 H-bond for both A3B2 and A2B3. Nyssa was responsible for probing the cation-π interaction and the H-bond to the backbone CO of TrpB (α4T155 data) for all agonists at the A2B3 receptor. I was responsible for probing those last two binding interactions at the A3B2 receptor in collaboration with Darren, from whom I took over the project early on. Finally, Jai and I performed all the single-channel recording assays and data analysis related to this project presented in Chapter 4.

2.10 References

1 Mansvelder, H. D., Keath, J. R. & McGehee, D. S. Synaptic mechanisms underlie nicotine-induced excitability of brain reward areas. *Neuron* **33**, 905-919, doi:10.1016/s0896-6273(02)00625-6 (2002).

2 Nashmi, R. *et al.* Chronic nicotine cell specifically upregulates functional alpha 4*nicotinic receptors: Basis for both tolerance in midbrain and enhanced long-term potentiation in perforant path. *Journal of Neuroscience* **27**, 8202-8218, doi:10.1523/jneurosci.2199-07.2007 (2007).

3 Tapper, A. R. *et al.* Nicotine activation of alpha 4*receptors: Sufficient for reward, tolerance, and sensitization. *Science* **306**, 1029-1032, doi:10.1126/science.1099420 (2004).

4 Ezzati, M. & Lopez, A. D. Estimates of global mortality attributable to smoking in 2000. *Lancet* **362**, 847-852, doi:10.1016/s0140-6736(03)14338-3 (2003).

5 CDC. *Tobacco-Related Mortality*, <http://www.cdc.gov/tobacco/data_statistics/fact_sheets/health_effects/tobacco_related_mortality/> (2014).

6 Dani, J. A. & Heinemann, S. Molecular and cellular aspects of nicotine abuse. *Neuron* **16**, 905-908, doi:10.1016/s0896-6273(00)80112-9 (1996).

7 Picciotto, M. R. *et al.* Acetylcholine receptors containing the beta 2 subunit are involved in the reinforcing properties of nicotine. *Nature* **391**, 173-177 (1998).

8 Henningfield, J. E., Fant, R. V., Buchhalter, A. R. & Stitzer, A. L. Pharmacotherapy for nicotine dependence. *CA-Cancer J. Clin.* **55**, 281-299 (2005).

9 Coe, J. W. *et al.* Varenicline: An alpha 4 beta 2 nicotinic receptor partial agonist for smoking cessation. *Journal of Medicinal Chemistry* **48**, 3474-3477, doi:10.1021/jm050069n (2005).

10 Hughes, J. R., Higgins, S. T. & Bickel, W. K. NICOTINE WITHDRAWAL VERSUS OTHER DRUG-WITHDRAWAL SYNDROMES - SIMILARITIES AND DISSIMILARITIES. *Addiction* **89**, 1461-1470, doi:10.1111/j.1360-0443.1994.tb03744.x (1994).

11 Malin, D. H. Nicotine dependence - Studies with a laboratory model. *Pharmacol. Biochem. Behav.* **70**, 551-559, doi:10.1016/s0091-3057(01)00699-2 (2001).

12 Zhu, B. T. Rational design of receptor partial agonists and possible mechanisms of receptor partial activation: A theory. *J. Theor. Biol.* **181**, 273-291, doi:10.1006/jtbi.1996.0130 (1996).

13 Fagerstrom, K. & Balfour, D. J. Neuropharmacology and potential efficacy of new treatments for tobacco dependence. *Expert Opin. Investig. Drugs* **15**, 107-116, doi:10.1517/13543784.15.2.107 (2006).

14 Houlihan, L. M. *et al.* Activity of cytisine and its brominated isosteres on recombinant human alpha 7, alpha 4 beta 2 and alpha 4 beta 4 nicotinic acetylcholine receptors. *J. Neurochem.* **78**, 1029-1043, doi:10.1046/j.1471-4159.2001.00481.x (2001).

15 Etter, J. F., Lukas, R. J., Benowitz, N. L., West, R. & Dresler, C. M. Cytisine for smoking cessation: A research agenda. *Drug Alcohol Depend.* **92**, 3-8, doi:10.1016/j.drugalcdep.2007.06.017 (2008).

16 Papke, R. L. & Heinemann, S. F. Partial Agonist Properties of Cytisine on Neuronal Nicotinic Receptors Containing the Beta-2 Subunit. *Mol. Pharmacol.* **45**, 142-149 (1994).

17 Tutka, P. & Zatonski, W. Cytisine for the treatment of nicotine addiction: from a molecule to therapeutic efficacy. *Pharmacol. Rep.* **58**, 777-798 (2006).

18 Hays, J. T., Ebbert, J. O. & Sood, A. Efficacy and safety of varenicline for smoking cessation. *American Journal of Medicine* **121**, S32-S42, doi:10.1016/j.amjmed.2008.01.017 (2008).

19 Niaura, R., Jones, C. & Kirkpatrick, P. Varenicline. *Nat. Rev. Drug Discov.* **5**, 537-538, doi:10.1038/nrd2088 (2006).

20 Rollema, H. *et al.* Preclinical properties of the alpha 4 beta 2 nAChR partial agonists varenicline, cytisine and dianicline translate to clinical efficacy for nicotine dependence. *Biochemical Pharmacology* **78**, 918-919, doi:10.1016/j.bcp.2009.06.077 (2009).

21 http://www.chantix.com/about-chantix.aspx.

22 Rollema, H. *et al.* Rationale, pharmacology and clinical efficacy of partial agonists of alpha(4)beta(2) nACh receptors for smoking cessation. *Trends Pharmacol. Sci.* **28**, 316-325, doi:10.1016/j.tips.2007.05.003 (2007).

23 Blum, A. P., Lester, H. A. & Dougherty, D. A. Nicotinic pharmacophore: The pyridine N of nicotine and carbonyl of acetylcholine hydrogen bond across a subunit interface to a backbone NH. *Proc. Natl. Acad. Sci. U. S. A.* **107**, 13206-13211, doi:10.1073/pnas.1007140107 (2010).

24 Glennon, R. A., Dukat, M. & Liao, L. Musings on alpha 4 beta 2 nicotinic acetylcholine (nACh) receptor pharmacophore models. *Curr. Top. Med. Chem.* **4**, 631-644, doi:10.2174/1568026043451122 (2004).

25 Nowak, M. W. *et al.* In vivo incorporation of unnatural amino acids into ion channels in Xenopus oocyte expression system. *Methods Enzymol.* **293**, 504-529 (1998).

26 Celie, P. H. N. *et al.* Nicotine and carbamylcholine binding to nicotinic acetylcholine receptors as studied in AChBP crystal structures. *Neuron* **41**, 907-914, doi:10.1016/s0896-6273(04)00115-1 (2004).

27 Xiu, X. A., Puskar, N. L., Shanata, J. A. P., Lester, H. A. & Dougherty, D. A. Nicotine binding to brain receptors requires a strong cation-pi interaction. *Nature* **458**, 534-U510, doi:10.1038/nature07768 (2009).

28 Blum, A. P., Gleitsman, K. R., Lester, H. A. & Dougherty, D. A. Evidence for an Extended Hydrogen Bond Network in the Binding Site of the Nicotinic Receptor ROLE OF THE VICINAL DISULFIDE OF THE alpha 1 SUBUNIT. *J. Biol. Chem.* **286**, 32251-32258, doi:10.1074/jbc.M111.254235 (2011).

29 Blum, A. P., Van Arnam, E. B., German, L. A., Lester, H. A. & Dougherty, D. A. Binding Interactions with the Complementary Subunit of Nicotinic Receptors. *J. Biol. Chem.* **288**, 6991-6997, doi:10.1074/jbc.M112.439968 (2013).

30 Gleitsman, K. R., Kedrowski, S. M. A., Lester, H. A. & Dougherty, D. A. An Intersubunit Hydrogen Bond in the Nicotinic Acetylcholine Receptor That Contributes to Channel Gating. *J. Biol. Chem.* **283**, 35638-35643, doi:10.1074/jbc.M807226200 (2008).

31 Gleitsman, K. R., Lester, H. A. & Dougherty, D. A. Probing the Role of Backbone Hydrogen Bonding in a Critical beta Sheet of the Extracellular Domain of a Cys-Loop Receptor. *ChemBioChem* **10**, 1385-1391, doi:10.1002/cbic.200900092 (2009).

32 Puskar, N. L., Xiu, X. A., Lester, H. A. & Dougherty, D. A. Two Neuronal Nicotinic Acetylcholine Receptors, alpha 4 beta 4 and alpha 7, Show Differential Agonist Binding Modes. *J. Biol. Chem.* **286**, 14618-14627, doi:10.1074/jbc.M110.206565 (2011).

33 Van Arnam, E. B., Blythe, E. E., Lester, H. A. & Dougherty, D. A. An Unusual Pattern of Ligand-Receptor Interactions for the alpha 7 Nicotinic Acetylcholine Receptor, with Implications for the Binding of Varenicline. *Mol. Pharmacol.* **84**, 201-207, doi:10.1124/mol.113.085795 (2013).

34 Cashin, A. L., Petersson, E. J., Lester, H. A. & Dougherty, D. A. Using physical chemistry to differentiate nicotinic from cholinergic agonists at the nicotinic acetylcholine receptor. *J. Am. Chem. Soc.* **127**, 350-356, doi:10.1021/ja0461771 (2005).

35 England, P. M., Zhang, Y. N., Dougherty, D. A. & Lester, H. A. Backbone mutations in transmembrane domains of a ligand-gated ion channel: Implications for the mechanism of gating. *Cell* **96**, 89-98, doi:10.1016/s0092-8674(00)80962-9 (1999).

36 Fonck, C. *et al.* Novel seizure phenotype and sleep disruptions in knock-in mice with hypersensitive alpha 4*nicotinic receptors. *Journal of Neuroscience* **25**, 11396-11411, doi:10.1523/jneurosci.3597-05.2005 (2005).

37 Moroni, M., Zwart, R., Sher, E., Cassels, B. K. & Bermudez, I. alpha 4 beta 2 nicotinic receptors with high and low acetylcholine sensitivity: Pharmacology, stoichiometry, and sensitivity to long-term exposure to nicotine. *Molecular Pharmacology* **70**, 755-768, doi:10.1124/mol.106.023044 (2006).

38 Nelson, M. E., Kuryatov, A., Choi, C. H., Zhou, Y. & Lindstrom, J. Alternate stoichiometries of alpha 4 beta 2 nicotinic acetylcholine receptors. *Mol. Pharmacol.* **63**, 332-341, doi:10.1124/mol.63.2.332 (2003).

39 Harpsoe, K. *et al.* Unraveling the high- and low-sensitivity agonist responses of nicotinic acetylcholine receptors. *The Journal of neuroscience : the official journal of the Society for Neuroscience* **31**, 10759-10766, doi:10.1523/JNEUROSCI.1509-11.2011 (2011).

40 Mazzaferro, S. *et al.* Additional acetylcholine (ACh) binding site at alpha4/alpha4 interface of (alpha4beta2)2alpha4 nicotinic receptor influences agonist sensitivity. *The Journal of biological chemistry* **286**, 31043-31054, doi:10.1074/jbc.M111.262014 (2011).

41 Beene, D. L. *et al.* Cation-pi interactions in ligand recognition by serotonergic (5-HT3A) and nicotinic acetylcholine receptors: The anomalous binding properties of nicotine. *Biochemistry* **41**, 10262-10269, doi:10.1021/bi020266d (2002).

42 Deakyne, C. A. & Meotner, M. UNCONVENTIONAL IONIC HYDROGEN-BONDS .2. NH+...PI - COMPLEXES OF ONIUM IONS WITH OLEFINS AND BENZENE-DERIVATIVES. *J. Am. Chem. Soc.* **107**, 474-479 (1985).

43 Meotner, M. & Deakyne, C. A. UNCONVENTIONAL IONIC HYDROGEN-BONDS .1. CH-DELTA+...X - COMPLEXES OF QUATERNARY IONS WITH NORMAL-DONORS AND PI-DONORS. *J. Am. Chem. Soc.* **107**, 469-474, doi:10.1021/ja00288a033 (1985).

44 Dougherty, D. A. Cation-pi interactions in chemistry and biology: A new view of benzene, Phe, Tyr, and Trp. *Science* **271**, 163-168, doi:10.1126/science.271.5246.163 (1996).

45 Ma, J. C. & Dougherty, D. A. The cation-pi interaction. *Chem. Rev.* **97**, 1303-1324, doi:10.1021/cr9603744 (1997).

46 Ting, A. Y., Shin, I., Lucero, C. & Schultz, P. G. Energetic analysis of an engineered cation-pi interaction in staphylococcal nuclease. *J. Am. Chem. Soc.* **120**, 7135-7136, doi:10.1021/ja981520l (1998).

47 Pless, S. A. *et al.* A Cation-pi Interaction at a Phenylalanine Residue in the Glycine Receptor Binding Site Is Conserved for Different Agonists. *Mol. Pharmacol.* **79**, 742-748, doi:10.1124/mol.110.069583 (2011).

48 Lummis, S. C. R., Beene, D. L., Harrison, N. J., Lester, H. A. & Dougherty, D. A. A cation-pi binding interaction with a tyrosine in the binding site of the GABA(C) receptor. *Chem. Biol.* **12**, 993-997, doi:10.1016/j.chembiol.2005.06.012 (2005).

49 Padgett, C. L., Hanek, A. P., Lester, H. A., Dougherty, D. A. & Lummis, S. C. R. Unnatural amino acid mutagenesis of the GABA(A) receptor binding site residues reveals a novel cation-pi interaction between GABA and beta(2)Tyr97. *J. Neurosci.* **27**, 886-892, doi:10.1523/jneurosci.4791-06.2007 (2007).

50 Dougherty, D. A. Cys-loop neuroreceptors: Structure to the rescue? *Chem. Rev.* **108**, 1642-1653, doi:10.1021/cr078207z (2008).

51 Tavares, X. D. S. *et al.* Variations in Binding Among Several Agonists at Two Stoichiometries of the Neuronal, alpha 4 beta 2 Nicotinic Receptor. *J. Am. Chem. Soc.* **134**, 11474-11480, doi:10.1021/ja3011379 (2012).

Chapter 3:

Investigating the Effect of Modulating the Hydrogen Bond Acceptor of the Nicotinic Pharmacophore on the β2L119 Hydrogen Bond of the A3B2 α4β2 Receptor

3.1 Introduction

The essential nicotinic pharmacophore, a cationic N and a hydrogen bond acceptor separated by an appropriate distance, has been established for some time.[1-3] The Dougherty group has identified the binding partners for these moieties, as well as the nature of the binding interactions, and expanded the nicotinic pharmacophore to include an additional hydrogen bond between the cationic N and the backbone CO of the receptor (see Section 2.2).[1,4-8] The cationic N participates in a cation-π interaction to an aromatic residue in the agonist binding site (TrpB for α4β2), while the hydrogen bond acceptor engages in a hydrogen bond to the backbone NH of a conserved leucine residue (β2L119 for α4β2).

3.1.1 Hydrogen Bond at β2L119

Hydrogen Bond to Backbone NH				
Agonist	**α4β2 A2B3**	**α4β2 A3B2**	**Muscle $(\alpha1)_2\beta1\delta\gamma$**	**$(\alpha4)_2(\beta4)_3$**
ACh	6.8[a]	8.5[b]	29[c]	2.9[c]
Nicotine	6.7[a]	5.6[b]	10[c]	2.8[c]
Cytisine	62[b]	14[b]	ND	14[c]
Varenicline	1.8[b]	1.1[b]	ND	0.38[c]
Epibatidine	5.0[a]	1.8	1.3[c]	1.9[c]

Table 3.1 Hydrogen bonding of several nicotinic agonists to the backbone NH of a conserved leucine residue in the complementary subunit of various types of nicotinic receptors. An amide-to-ester strategy was used to evaluate the functional significance of the hydrogen bond and the numbers represent the ratio of Lah/Leu EC_{50} values. The higher the ratio, the stronger the hydrogen bond. a. Previously reported in [1]. b. Previously reported in [6]. c. Previously reported in [4]. ND: Not Determined.

Of the three binding interactions composing the expanded nicotinic pharmacophore, we have observed the most variation at the β2L119 hydrogen bond. As described in Section 2.5 of this thesis, we use a backbone amide-to-ester

mutation strategy to probe for hydrogen bonds. In this context, we use the α-hydroxy EC_{50}/wild type EC_{50} ratio as a metric to evaluate the functional impact of the hydrogen bond on receptor activation; the higher the ratio, the more significant the hydrogen bond. Typically, we see loss of function for these mutations, and we do not interpret ratios of <2 and >1 as significant (for gain of function mutations the cut-off is <1 and >0.5).

As shown in Table 3.1, the agonists showing the weakest hydrogen bonding at the β2L119 (or equivalent leucine position for non-β2 receptors) are varenicline and epibatidine with the exception being epibatidine at A2B3. We have hypothesized that this is due to the relatively weaker hydrogen bond acceptor components present for varenicline and epibatidine. The work presented in this chapter aims to test this hypothesis by using a pharmacological approach to modulate the hydrogen bond acceptor ability of two agonist pairs: epibatidine/deschloroepibatidine and nicotine/chloronicotine (Figure 3.1)

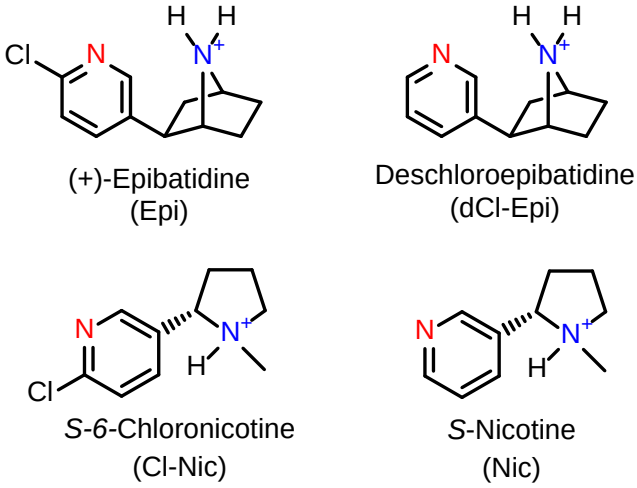

Figure 3.1 Agonists studied in this chapter. A single enantiomer of each, Epi and dCl-Epi is shown but the respective racemates were used. Cl-Nic and Nic were enantiomerically pure.

3.2 Double Mutant Cycle Analysis

Double mutant cycle analysis is the standard method used to measure the strength of intramolecular or intermolecular interactions in proteins or in protein-ligand complexes.[9] EC_{50}-based mutant cycle analyses have been applied by our group[1,10-13] and others[14-16] to investigate several interactions in Cys-loop receptors. Herein, double mutant cycle analysis is applied to study protein-agonist type interactions involving mutation of an amino acid of the protein and, also, “mutation” of the agonist by classical pharmacological strategies. Specifically, we use double mutant cycle analysis of protein-agonist interactions to understand the energetic effect of modulating the hydrogen bond acceptor component of the β2L119 hydrogen bond.

For residues (or residue/agonist pairs) that are considered non-interacting, mutation of one site should have no energetic impact on the second site, and so the effect of simultaneous mutation at both sites is expected to be multiplicative.[9] In a double mutant cycle analysis, this is evidenced by in a coupling coefficient, Ω of 1 (Figure 3.2). If, on the other hand, the two residues (or residue/agonist pairs) do interact, then the effect of simultaneous mutation will be greater or less than the product of the individual effects. Typically, we consider an interaction significant when having an Ω of <0.2 or >5. The coupling coefficient, Ω can be converted into a free energy value, $\Delta\Delta G^{\circ}$ (Figure 3.2), a metric that we consider to be approximately equivalent to the strength of the interaction being studied. A coupling energy of >1kcal/mol is generally considered indicative of a strong noncovalent interaction.

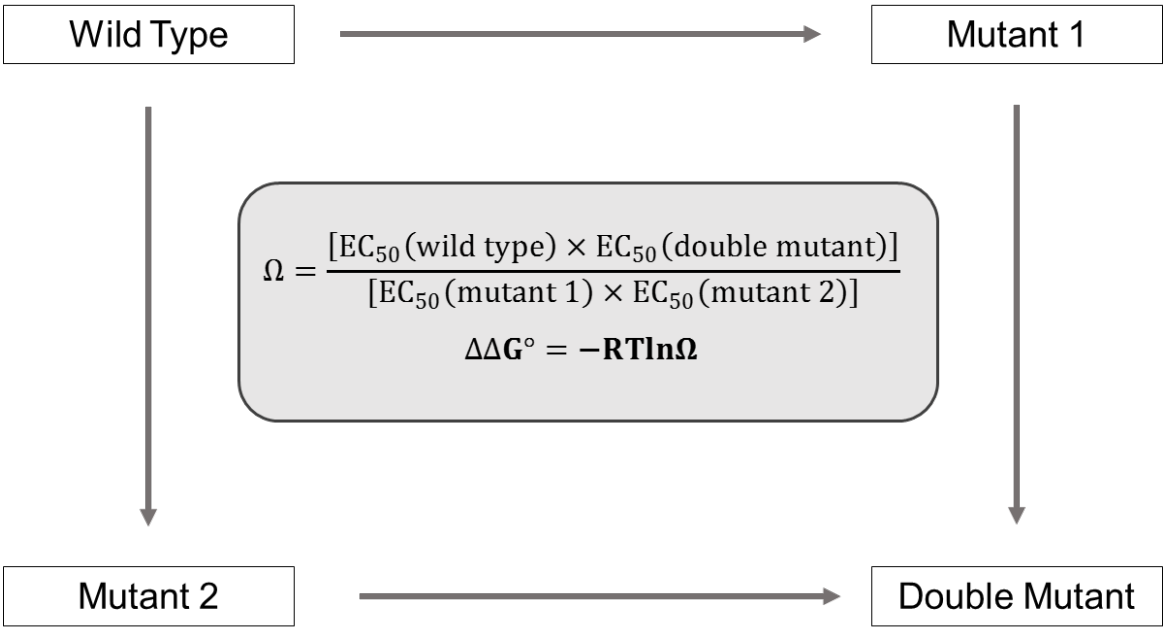

Figure 3.2 Schematic of a double mutant cycle analysis showing equations for calculating the coupling coefficient, Ω and associated free energy, ΔΔG˚.

3.3 Incremental Dose-Response Protocol

We found that epibatidine is a very tight binder (slow off rate). This presented a problem in that, for the higher doses needed for the dose-response curve to turn over (reach its maximum), epibatidine would not wash off and thus we were not able to obtain a good turn over using our regular recording protocol (Figure 3.3). Longer washes of up to 10 minutes (compared to a 2 minute regular wash), not only failed to completely wash off epibatidine but also significantly impacted the number of living cells at the end of a run due to the total recording time of 1.5 to 2h becoming too long for oocyte viability.

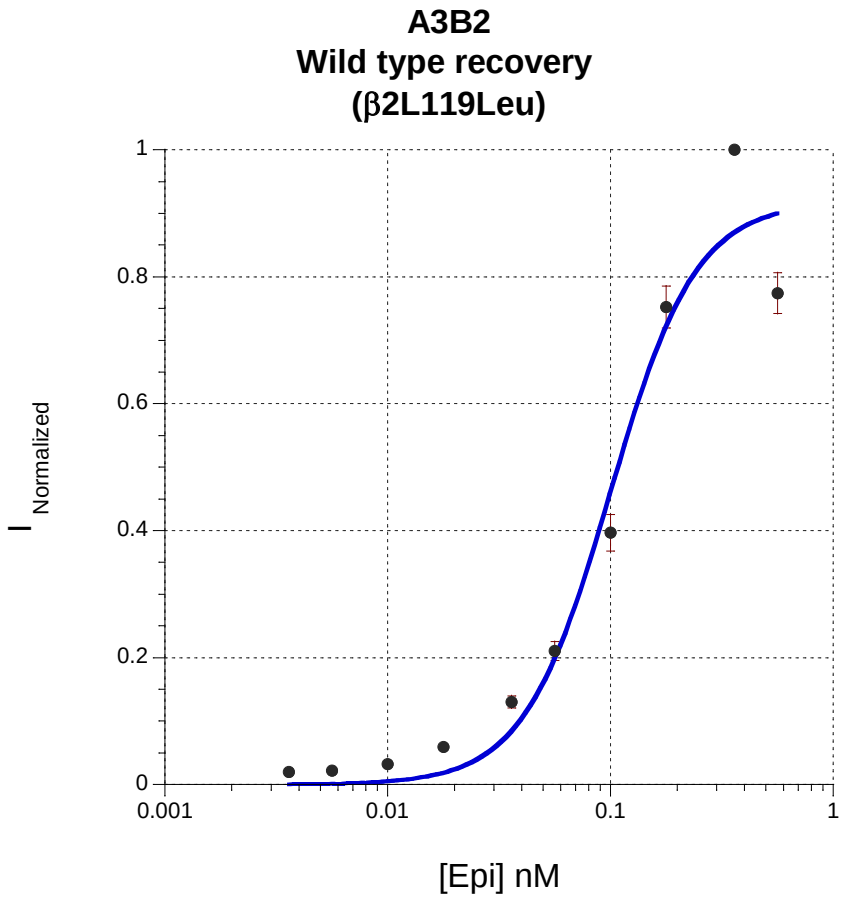

Figure 3.3 Sample wild type recovery dose-response curve for epibatidine showing poor turn over. EC50 was 0.10 ± 0.02nM and hill coefficient, n_H = 2.3 ± 0.6.

The solution was to implement what we termed an "incremental dose-response" protocol where no wash was applied between subsequent drug applications, while a final wash of 2 minutes was applied after the last drug application. The rationale behind this protocol is that, at non-saturating agonist concentrations, not all available receptor sites are occupied and thus, increasing agonist concentration with subsequent doses would occupy more receptor sites until all available receptors are activated (saturating agonist concentration) (Figure 3.4). The downside of this protocol is a time constraint of approximately 15 minutes (for the α4β2 receptor) of total drug application time to avoid severe desensitization

that would interfere with our measurements. Naturally, this protocol is not viable for receptors, such as α7, exhibiting fast desensitization behavior. While some desensitization is observed, we tested the accuracy of the protocol by comparing EC_{50} values obtained with this protocol to EC_{50} values obtained with our regular protocol with no significant loss in accuracy. Interestingly, epibatidine did wash off under our regular protocol conditions (2 minute wash between drug applications) for the β2L119Lah mutant. We hypothesize that this is due to both the agonist on and off rates being similarly affected (impacts binding affinity but not EC_{50}).

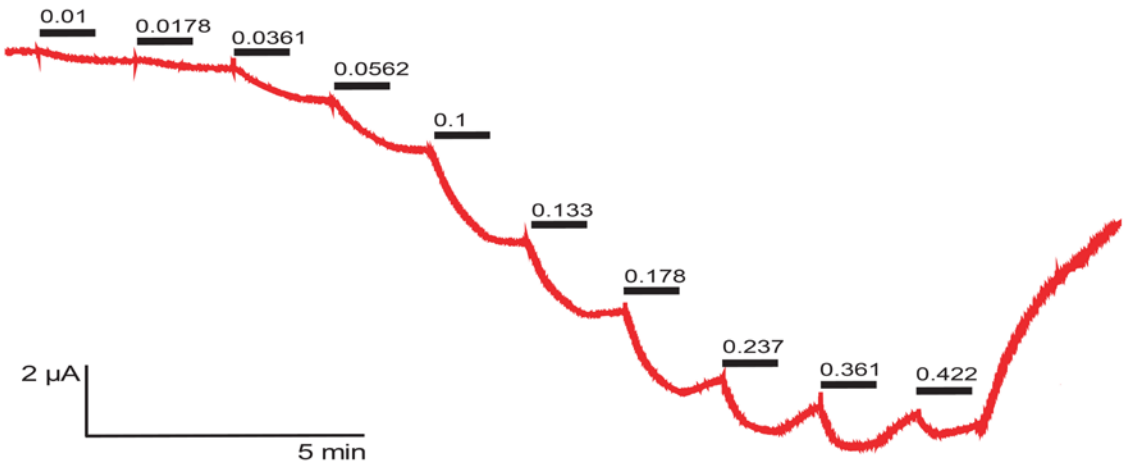

Figure 3.4 Sample trace of an incremental dose-response run for wild type recovery (β2L119Leu) at A3B2 with the agonist (±)-epibatidine. Bars represent drug application time and concentration is given in nM.

3.4 Results

A backbone amide to ester mutation strategy was applied to probe the β2L119 hydrogen bond for epibatidine, deschloroepibatidine, chloronicotine and nicotine at the A3B2 receptor. Results are summarized below in Table 3.2. Double mutant cycle analysis was performed to evaluate the energetic effect of modulating the hydrogen bond acceptor component for the relevant agonist pairs, nicotine/chloronicotine and epibatidine/deschloroepibatidine (Figures 3.5 and 3.6, respectively). Table 3.3 summarizes the results of the double mutant cycle analyses.

A3B2 Receptor					
Agonist	**Mutation**	**EC_{50} (nM)**	**Fold Shift (Lah/Leu)**	**n_H**	**I_{norm} (+70mV)**
Cl-Nic	Wild type	7.1 ± 0.8	-	1.5 ± 0.2	0.09 ± 0.03
	β2L119 Leu	7.2 ± 0.7	-	1.4 ± 0.1	0.08 ± 0.01
	β2L119 Lah	11.8 ± 0.3	**1.6**	1.6 ± 0.1	0.12 ± 0.05
Nic[a]	Wild type	10 ± 1	-	1.7 ± 0.2	0.30 ± 0.04
	β2L119 Leu	12 ± 0.5	-	1.6 ± 0.1	0.23 ± 0.02
	β2L119 Lah	67 ± 3	**5.6**	1.4 ± 0.1	0.20 ± 0.03
Epi	Wild type	0.10 ± 0.01	-	1.9 ± 0.2	0.23 ± 0.03
	β2L119 Leu	0.094 ± 0.007	-	1.9 ± 0.2	0.18 ± 0.02
	β2L119 Lah	0.17 ± 0.01	**1.8**	2.1 ± 0.2	0.18 ± 0.03
dCl-Epi	Wild type	0.074 ± 0.005	-	1.6 ± 0.2	0.09 ± 0.03
	β2L119 Leu	0.061 ± 0.007	-	1.8 ± 0.2	0.08 ± 0.01
	β2L119 Lah	0.29 ± 0.01	**4.8**	1.9 ± 0.1	0.12 ± 0.05

Table 3.2 β2L119 Hydrogen Bond at A3B2 EC_{50} values (nM), fold shift values calculated as Lah/Leu EC_{50} ratios, Hill coefficients (n_H) and current size at +70mV (normalized to current size at -110mV). Errors are SEM (standard error from the mean). a. Previously reported in [6]. Abbreviations are Cl-Nic for S-6-chloronicotine, Nic for S-nicotine, Epi for (±)-epibatidine and dCl-Epi for (±)-deschloroepibatidine.

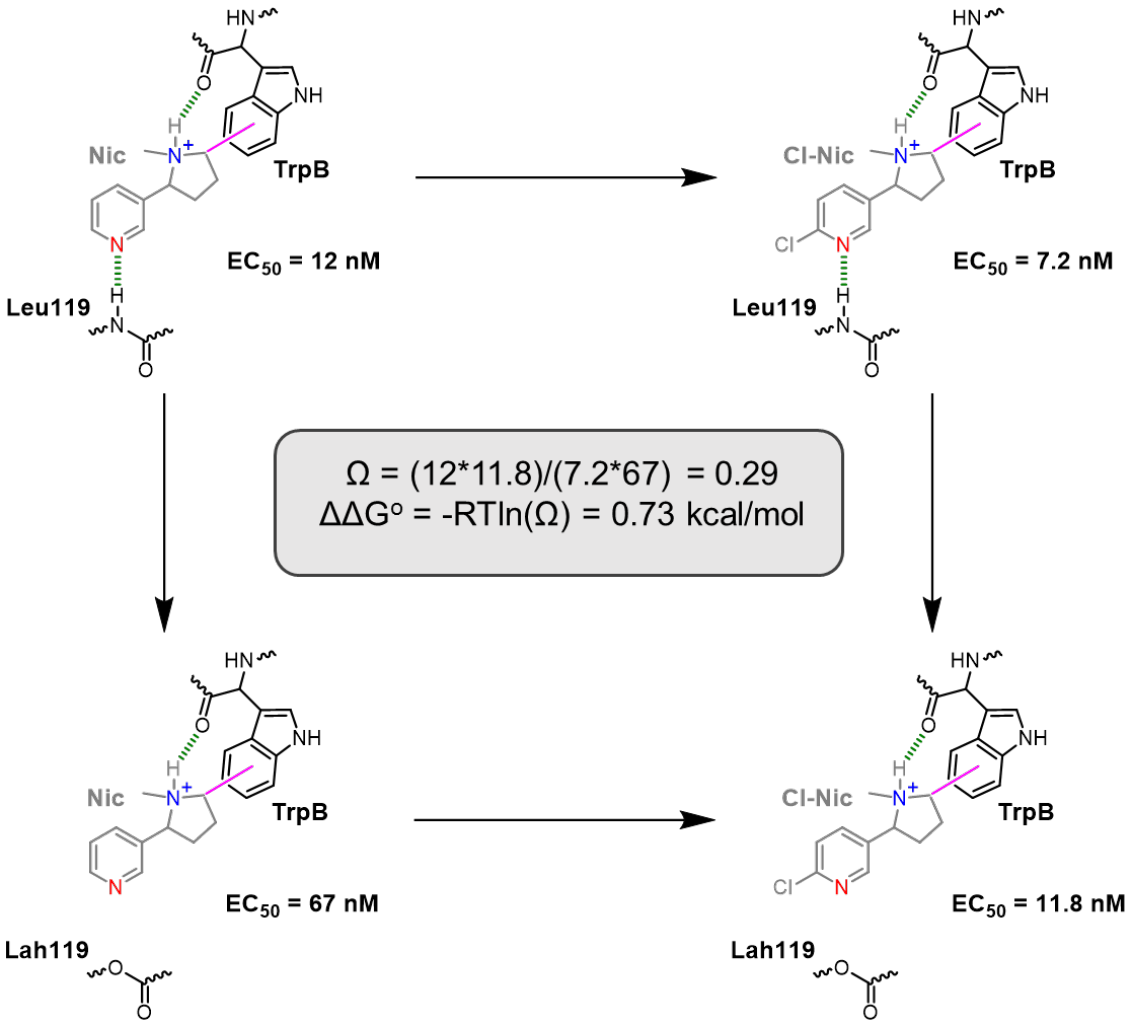

Figure 3.5 Double mutant cycle analysis for nicotine (Nic) and chloronicotine (Cl-Nic) at Leu119 (wild type recovery at the β2119 position) and Lah119 of the A3B2 stoichiometry of the α4β2 receptor.

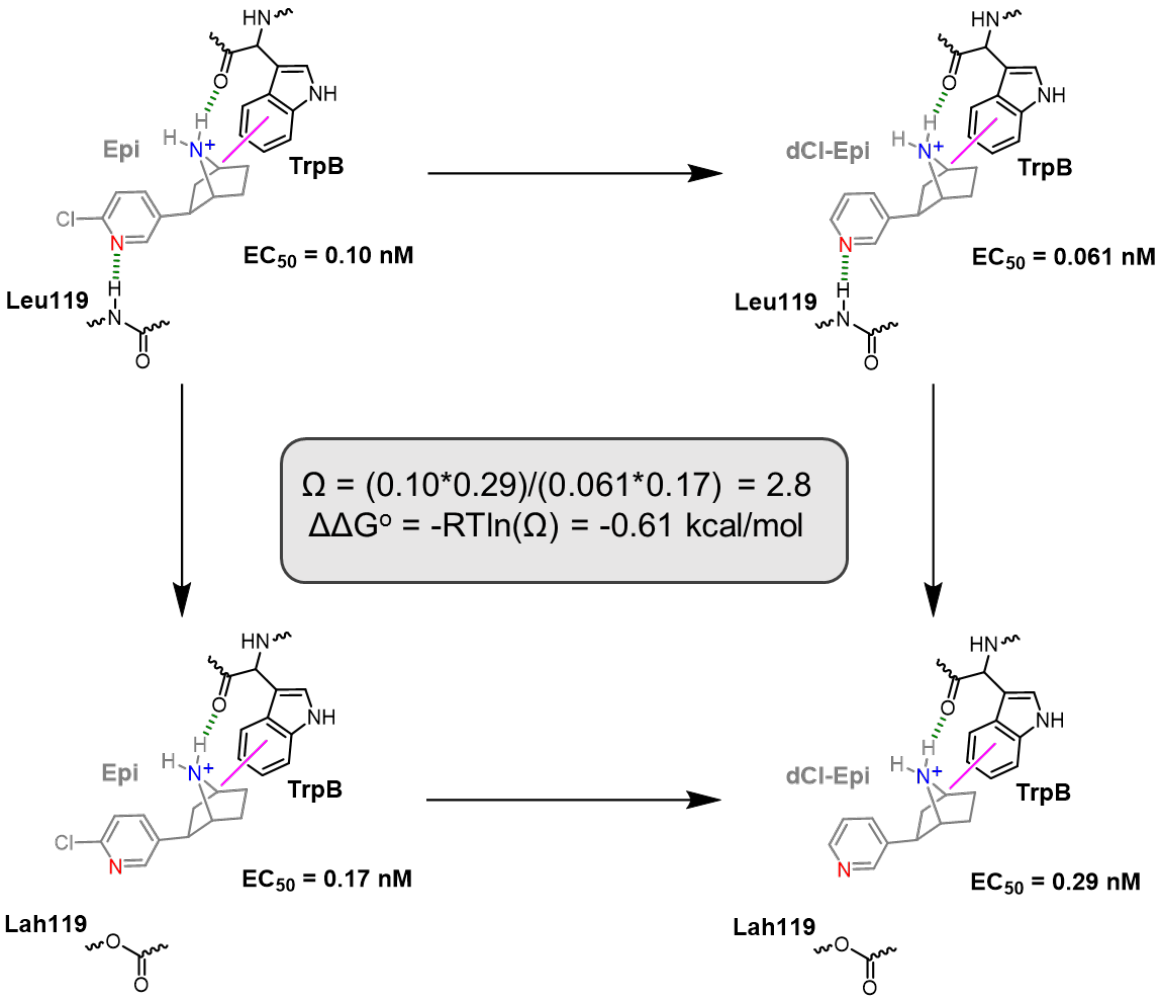

Figure 3.6 Double mutant cycle analysis for epibatidine (Epi) and deschloroepibatidine (dCl-Epi) at Leu119 (wild type recovery at the β2119 position) and Lah119 of the A3B2 stoichiometry of the α4β2 receptor.

Agonist Pair	Ω	ΔΔG° (kcal/mol)
Nic/*S*-MPP[a]	0.0055	3.1
Nic/Cl-Nic	0.29	0.73
Epi/dCl-Epi	2.8	-0.61

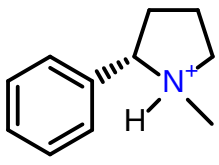

S-MPP

Table 3.3 Coupling coefficients (Ω) and ΔΔG° values for mutant cycle analyses at A3B2. a. Is included for comparison purposes and was previously reported in [17]. **Right**: structure of *S*-MPP.

3.5 Discussion

Previously, we hypothesized that varenicline, in lacking a functionally significant hydrogen bond at the β2L119 position, violated the nicotinic pharmacophore model by having a much poorer hydrogen bond acceptor component than other nicotinic agonists (see Chapter 2).[6] We see a similar effect for epibatidine at A3B2 and other nicotinic receptors.[4] Given the similar pK_a values of the hydrogen bond acceptor components of varenicline and epibatidine (0.8 for quinoaxiline and 0.5 for 2-chloropyridine versus 5.2 for pyridine), we sought to test the weaker hydrogen bond acceptor hypothesis via a pharmacological approach with two agonist pairs: epibatidine with deschloroepibatidine and chloronicotine with nicotine.

We use the Lah to Leu fold shift as a metric to evaluate the functional significance of the β2L119 hydrogen bond, as previously described.[1,6] As shown in Table 3.2, we observe that the fold shift value goes from 1.8 to 4.8 for epibatidine and deschloroepibatidine, respectively. Similarly, we see the fold shift value goes from 1.6 to 5.6 for chloronicotine and nicotine, respectively. In structural terms, going from epibatidine to deschloroepibatidine and chloronicotine to nicotine represents “removal” of the 2-chloropyridine chlorine. As expected, this improves the hydrogen bond acceptor ability of the pyridine N, thereby strengthening the hydrogen bond to β2L119, an effect which is evidenced by the higher fold shift of the deschloro analogues. The double mutant cycle analyses shown in Figures 3.5 and 3.6 were used to evaluate the energetic impact of either introducing the chlorine for nicotine/chloronicotine or removing the chlorine for

epibatidine/deschloroepibatidine. As anticipated, we observed that the energetic impact is opposite in sign, 0.73kcal/mol for nicotine/chloronicotine and -0.61kcal/mol for epibatidine/deschloroepibatidine. Also as expected, introducing a chlorine, or weakening the β2L119 hydrogen bond was energetically unfavorable ($\Delta\Delta G^\circ>0$) whereas strengthening the hydrogen bond by removing the chlorine was energetically favorable ($\Delta\Delta G^\circ<0$). It is worth noting that, while these effects are modest in value (we typically consider $|\Delta\Delta G^\circ|>1$ as indicative of a strong interaction), it is not surprising given the subtle nature of the modification introduced, we are not eliminating the hydrogen bond, but attenuating it by introduction of the 2-chloropyridine chlorine. In contrast, eliminating the hydrogen bond altogether, as is the case for the nicotine/*S*-MPP pair (Table 3.3), produces a strong coupling energy of 3.1kcal/mol, within the expected energy value for a hydrogen bond.

As previously reported in the literature[18], we observe that epibatidine and deschloroepibatidine are similarly potent. Furthermore, we find that chloronicotine and nicotine also exhibit similar potencies. It is possible that this is due to a hydrophobic effect of the chlorine substituent, in other words, that the benefit of strengthening the hydrogen bond is off-set by the loss of hydrophobicity. Thus, removal of the chlorine substituent has competing effects on the resulting EC_{50} values (for deschloroepibatine and nicotine); on one hand, it lowers the EC_{50} by strengthening the pyridine hydrogen bond and on the other hand, the EC_{50} value is increased by loss of the hydrophobic effect of chlorine. Since, $\Delta\Delta G^\circ$ values are calculated based on the coupling coefficient, Ω which is in turn defined based on

EC_{50} values, loss the hydrophobic effect granted by chlorine also explains why the observed ΔΔG˚ values are small.

In conclusion, we have demonstrated that for agonists nicotine, epibatidine and by association, varenicline, hydrogen bond acceptor strength has a meaningful functional impact on receptor activation for the A3B2 receptor. Epibatidine shows a stronger β2L119 hydrogen bond for A2B3 (Lah/Leu fold shift of 5.0) than for other receptors (Table 3.1). Further work with the epibatidine/deschloroepibatidine and nicotine/chloronicotine pairs on the A2B3 receptor would therefore be of interest.

3.6 Materials and Methods

3.6.1 Mutagenesis and mRNA synthesis

Rat α4L9'A and β2 subunits were expressed in pAMV vectors. The mutations for each subunit were introduced according to the QuikChange mutagenesis protocol (Stratagene) and sequencing verified the incorporation of desired mutations. Rat α4L9'A and β2 mRNA were prepared from NotI linearizations of the circular expression vector pAMV, followed by in vitro transcription using the mMessage mMachine T7 kit (Ambion, Austin, TX).

3.6.2 Ion channel expression

To express the ion channels with a wild type ligand binding site, α4L9'A mRNA was co-injected with β2 mRNA at a ratio of 20:1 α4L9'A:β2 to obtain the A3B2 receptor. Total mRNA amount for microinjection was 5-10ng/cell in a total volume of 75nL. Stage V-VI *Xenopus* oocytes were microinjected and incubated

at 18˚C for 24h in ND96 buffer (96mM NaCl, 2mM KCl, 1mM MgCl2, 2mM CaCl2, and 5mM HEPES, pH 7.5) with 0.005% (w/v) gentamycin and 2% (v/v) horse serum.

3.6.3 Unnatural amino acid incorporation

Nitroveratryloxycarbonyl (NVOC) protected cyanomethyl ester forms of unnatural amino acids and α-hydroxythreonine cyanomethyl ester were synthesized, coupled to the dinucleotide dCA, and enzymatically ligated to 74-nucleotide TQOpS' tRNA (for β2L119 experiments) as described previously. [3,8] The unnatural amino acid-conjugated tRNA was deprotected by photolysis and then immediately co-injected with mRNA containing the UGA mutation at the site of interest. For both α4L9'A and β2 mRNA, the actual stop codon is also UGA. Thus, to avoid unwanted incorporation of unnatural aminoacylated tRNA, both subunits were mutated at the stop codon from UGA to UAA, a mutation we called "opal masking". Stage V–VI oocytes were injected with ~10-150ng mRNA and 25-125ng tRNA-amino acid or tRNA-hydroxy acid in a total volume of 75nL at a ratio of 10:1 to yield A3B2 receptors. In cases where receptor expression needed to be increased, a second microinjection (double injection) of the same concentration and volume of α4L9'A:β2 mRNA and tRNA was performed after 24h incubation at 18°C. Double injected oocytes were incubated for an additional 24-48h for a total of 48-72h. Cells were incubated in ND96 buffer, 0.005% (w/v) gentamycin and 2% (v/v) horse serum, and the solution was changed at least daily and up to every 6h. The fidelity of unnatural amino acid incorporation was confirmed at each site with

a “wild type recovery” experiment and “readthrough/reaminoacylation” tests (see Section 1.3.2) as described previously.[1]

3.6.4 Whole-cell electrophysiological characterizations of the channels

Oocyte recordings were performed 24h after microinjection for wild type receptors and 48 to 72h after microinjection for unnatural amino acids. Agonist-induced currents were recorded in two-electrode voltage clamp mode using the OpusXpress 6000A (Axon Instruments, Union City, CA) at a holding potential of −60mV. Oocytes were superfused with Ca^{2+}-free ND96 solution (96mM NaCl, 2mM KCl, 1mM MgCl2, and 5mM HEPES, pH 7.5) at flow rates of either 1.25 or 4mL/min during drug application and 3mL/min during wash. For deschloroepibatidine experiments, drug application was 15s in duration at 4mL/min rate immediately followed by 45s at 1.25mL/min rate (2mL total drug volume), while wash duration between each concentration was 116s. For chloronicotine and (±)-epibatidine at β2L119Lah experiments, drug application was 15s in duration at 4mL/min rate immediately followed by 45s at 1.25mL/min rate (2mL total drug volume), while wash duration between each concentration was 116s for the initial 5 agonist doses and drug application was 15s in duration at 4mL/min rate (1mL total drug volume); wash duration between each concentration was 116s for the following agonist doses. For (±)-epibatidine wild type and wild type recovery (β2L119Leu) experiments, the incremental dose response protocol (see Section 3.3) was used where drug application was 30s at 4mL/min rate followed by a 30s pause with no wash between subsequent drug applications but a final wash time (after last drug application) of 120s at 3mL/min.

Data were sampled at 50Hz and filtered at 20Hz. (±)-Epibatidine was purchased from Tocris Bioscience (Minneapolis, MN), (*S)*-6-chloronicotine was purchased from Toronto Research Chemicals (Toronto, ON, Canada) and (±)-deschloroepibatidine was synthesized from (±)-epibatidine as described in Section 3.6.5. Stock solutions of 25mM (±)-epibatidine and 383mM (*S)*-6-chloronicotine were prepared in a 50:50 solution of sterile, distilled, deionized water and ethanol for dilution in Ca^{2+}-free ND96 solution. (±)-Deschloroepibatidine was dissolved in 8% DMSO/water (sterile, distilled and deionized) to a concentration of 0.92mM. Dilutions in Ca^{2+}-free ND96 solution were at least 10^4 fold, so amounts of ethanol and DMSO in the final solutions were negligible and did not impact cell health. Dose-response data were obtained for at least 8 concentrations of agonist and for a minimum of 5 oocytes. Mutants with I_{max} of at least 200nA of current were defined as functional. EC_{50} and Hill coefficients were calculated by fitting the dose-response relation to the Hill equation (see Section 1.4.1). The dose-responses of individual oocytes were examined to identify outliers. All data are reported as mean ± standard error. Voltage jump experiments were used to verify the stoichiometry of the mutant and wild type receptors, as described previously.[8]

3.6.5 Synthesis of Deschloroepibatidine

(±)-Deschloroepibatidine was synthesized from (±)-epibatidine as described in the literature.[19] (±)-Epibatidine was dissolved in 1M KOH in methanol followed by addition of 10% Pd/C catalyst and exposure to H_2 gas at atmospheric pressure and RT for 90 min. Catalyst was removed by filtration and product was extracted in 2:3 water/chloroform (10mL water and 3x 15mL chloroform extracts) and

protonated with 1eq of HCl. Yield was 19%. Product was purified by HPLC and verified by LCMS and ^{1}H-NMR in CD_3OD.[18]

3.7 Acknowledgements

I would like to thank Professor Henry A. Lester for the suggestion of using the incremental dose-response protocol and my fellow Dougherty lab member, Matt Rienzo, for the synthesis and characterization of deschloroepibatidine.

3.8 References

1 Blum, A. P., Lester, H. A. & Dougherty, D. A. Nicotinic pharmacophore: The pyridine N of nicotine and carbonyl of acetylcholine hydrogen bond across a subunit interface to a backbone NH. *Proceedings of the National Academy of Sciences of the United States of America* **107**, 13206-13211, doi:10.1073/pnas.1007140107 (2010).

2 Glennon, R. A., Dukat, M. & Liao, L. Musings on alpha 4 beta 2 nicotinic acetylcholine (nACh) receptor pharmacophore models. *Curr. Top. Med. Chem.* **4**, 631-644, doi:10.2174/1568026043451122 (2004).

3 Nowak, M. W. *et al.* In vivo incorporation of unnatural amino acids into ion channels in Xenopus oocyte expression system. *Methods Enzymol.* **293**, 504-529 (1998).

4 Blum, A. P., Van Arnam, E. B., German, L. A., Lester, H. A. & Dougherty, D. A. Binding Interactions with the Complementary Subunit of Nicotinic Receptors. *J. Biol. Chem.* **288**, 6991-6997, doi:10.1074/jbc.M112.439968 (2013).

5 Puskar, N. L., Xiu, X. A., Lester, H. A. & Dougherty, D. A. Two Neuronal Nicotinic Acetylcholine Receptors, alpha 4 beta 4 and alpha 7, Show Differential Agonist Binding Modes. *J. Biol. Chem.* **286**, 14618-14627, doi:10.1074/jbc.M110.206565 (2011).

6 Tavares, X. D. S. *et al.* Variations in Binding Among Several Agonists at Two Stoichiometries of the Neuronal, alpha 4 beta 2 Nicotinic Receptor. *J. Am. Chem. Soc.* **134**, 11474-11480, doi:10.1021/ja3011379 (2012).

7 Van Arnam, E. B., Blythe, E. E., Lester, H. A. & Dougherty, D. A. An Unusual Pattern of Ligand-Receptor Interactions for the alpha 7 Nicotinic Acetylcholine Receptor, with Implications for the Binding of Varenicline. *Mol. Pharmacol.* **84**, 201-207, doi:10.1124/mol.113.085795 (2013).

8 Xiu, X. A., Puskar, N. L., Shanata, J. A. P., Lester, H. A. & Dougherty, D. A. Nicotine binding to brain receptors requires a strong cation-pi interaction. *Nature* **458**, 534-U510, doi:10.1038/nature07768 (2009).

9 Horovitz, A. Double-mutant cycles: A powerful tool for analyzing protein structure and function. *Fold. Des.* **1**, R121-R126, doi:10.1016/s1359-0278(96)00056-9 (1996).

10 Blum, A. P., Gleitsman, K. R., Lester, H. A. & Dougherty, D. A. Evidence for an Extended Hydrogen Bond Network in the Binding Site of the Nicotinic Receptor ROLE OF THE VICINAL DISULFIDE OF THE alpha 1 SUBUNIT. *J. Biol. Chem.* **286**, 32251-32258, doi:10.1074/jbc.M111.254235 (2011).

11 Gleitsman, K. R., Kedrowski, S. M. A., Lester, H. A. & Dougherty, D. A. An Intersubunit Hydrogen Bond in the Nicotinic Acetylcholine Receptor That Contributes to Channel Gating. *J. Biol. Chem.* **283**, 35638-35643, doi:10.1074/jbc.M807226200 (2008).

12 Kedrowski, S. M. A., Bower, K. S. & Dougherty, D. A. 1-oxo-5-hydroxytryptamine: A surprisingly potent agonist of the 5-HT3 (serotonin) receptor. *Org. Lett.* **9**, 3205-3207, doi:10.1021/ol071083s (2007).

13 Miles, T. F., Bower, K. S., Lester, H. A. & Dougherty, D. A. A Coupled Array of Noncovalent Interactions Impacts the Function of the 5-HT(3)A Serotonin Receptor in an Agonist-Specific Way. *ACS Chem. Neurosci.* **3**, 753-760, doi:10.1021/cn3000586 (2012).

14 Kash, T. L., Jenkins, A., Kelley, J. C., Trudell, J. R. & Harrison, N. L. Coupling of agonist binding to channel gating in the GABA(A) receptor. *Nature* **421**, 272-275, doi:10.1038/nature01280 (2003).

15 Price, K. L., Millen, K. S. & Lummis, S. C. R. Transducing agonist binding to channel gating involves different interactions in 5-HT3 and GABA(C) receptors. *J. Biol. Chem.* **282**, 25623-25630, doi:10.1074/jbc.M702524200 (2007).

16 Venkatachalan, S. P. & Czajkowski, C. A conserved salt bridge critical for GABA(A) receptor function and loop C dynamics. *Proc. Natl. Acad. Sci. U. S. A.* **105**, 13604-13609, doi:10.1073/pnas.0801854105 (2008).

17 Blum, A. P. *StructureFunction Studies of Nicotinic Acetylcholine Receptors Using Unnatural Amino Acids and Synthetic Agonist Analogs* Ph. D. thesis, California Institute of Technology, (2012).

18 Carroll, F. I. *et al.* Synthesis, nicotinic acetylcholine receptor binding, and antinociceptive properties of 2-exo-2-(2 '-substituted 5 '-pyridinyl)-7-azabicyclo 2.2.1 heptanes. Epibatidine analogues. *J. Med. Chem.* **44**, 2229-2237, doi:10.1021/jm0100178 (2001).

19 Scheffel, U., Taylor, G. F., Kepler, J. A., Carroll, F. I. & Kuhar, M. J. In vivo labeling of neuronal nicotinic acetylcholine receptors with radiolabeled isomers of norchloroepibatidine. *Neuroreport* **6**, 2483-2488, doi:10.1097/00001756-199512150-00011 (1995).

Chapter 4:

Single-Channel Studies of Varenicline at A3B2 and A2B3 α4β2 Receptors

4.1 Introduction

We have found that the smoking cessation drug, varenicline, acts on its target receptor, α4β2, via two binding interactions. First, a cation-π interaction to a conserved tryptophan residue (TrpB, Trp154 in rat α4) and second, a hydrogen bond to the backbone CO of TrpB.[1] As described in Chapter 2, we established that this binding pattern holds for both stoichiometries of the α4β2 receptor, A3B2 and A2B3. We also find that varenicline appears to violate the nicotinic pharmacophore by failing to make a functionally significant additional hydrogen bond to the backbone NH of a conserved leucine residue (L119 in rat β2). We have proposed that this is due to varenicline having a weaker hydrogen bond acceptor moiety than the other nicotinic agonists studied (acetylcholine, nicotine and cytisine). Studies described in Chapter 3 support this claim. The work presented in this chapter is aimed at further studying activation by varenicline of wild type and unnatural amino acid-expressing forms of A2B3 and A3B2 receptors. Specifically, we used single-channel recording with varenicline to determine if the gating properties of the receptor change upon fluorination of TrpB. Ideally, the best fluorinated TrpB mutant to study would be F_4W. However, we find that F_4W does not incorporate efficiently enough to provide the level of expression necessary for single-channel recording. Thus, the F_3W mutant was studied in single-channel experiments using the cell-attached configuration as reported in this chapter.

4.2 Patch-Clamp: Types of Patches

The patch-clamp technique allows for single-molecule studies of LGICs (Ligand-Gated Ion Channels). There are four types of patches that can be used for

electrophysiological recording: cell-attached, whole-cell, outside-out and inside-out (Figure 4.1). Each has its unique advantages and disadvantages, as has been summarized previously.[2,3]

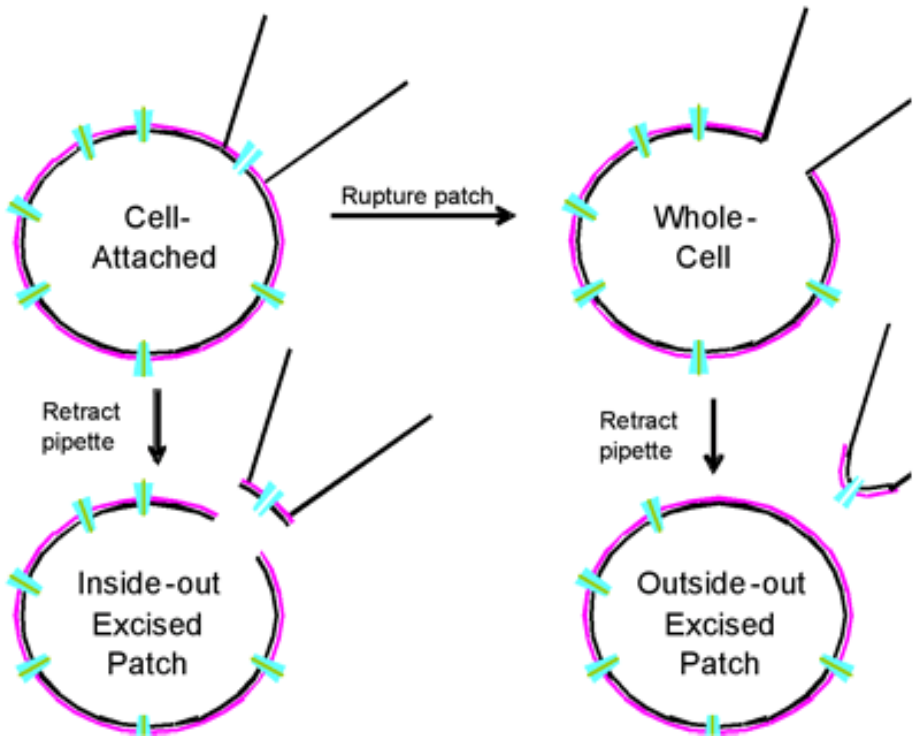

Figure 4.1 Types of patches for patch-clamping.

All results presented herein were obtained in the cell-attached configuration. This configuration better suited our needs because it is relatively facile to obtain, is more likely to isolate a single-channel for recording and allows for collection of kinetic data. The whole-cell method is not effective in oocytes given the electrical components of our electrophysiology rig and the large size of the oocytes preventing control of the cytosolic environment; it also loses much kinetic information. In addition, recordings with the semi-automated OpusXpress 6000A (Axon Instruments) in our lab provide whole-cell data for up to 8 cells simultaneously, making this configuration essentially obsolete for our purposes.

The inside-out configuration provides access to the intracellular side and is mostly used to study the gating of second-messenger-activated channels. The outside-out patch allows for superfusion of the extracellular side and thus, as in the whole-cell method, different agonist concentrations can be applied while recording on the patch. However, this type of patch is the hardest to obtain.[3]

4.3 nAChR Kinetic Model

Assuming two equivalent binding sites for the nAChR, we can write a mechanism for the interrelation of various kinetically, and presumably physically, distinct states of the receptor (Model 4.1).

$$A + R^c \underset{k_{-1}}{\overset{2k_1}{\rightleftharpoons}} A + AR^c \underset{2k_{-1}}{\overset{k_1}{\rightleftharpoons}} A_2R^c \underset{\alpha}{\overset{\beta}{\rightleftharpoons}} A_2R^o$$

Model 4.1 nAChR four-state kinetic model. Where A represents one agonist molecule, R^c receptor in the closed state, R^o receptor in the open state, k_1 agonist binding rate, k_{-1} agonist dissociation rate, β receptor opening rate and α receptor closing rate.

4.3.1 Binding and Gating Components of EC_{50}

As discussed in Chapter 2, the EC_{50} is a composite measurement of the rate at which the agonist associates with and dissociates from the receptor (binding) as well as that agonists' ability to induce the conformational changes resulting in current flow through the ion channel (gating). As with the Hill equation (see Section 1.4.1) for whole-cell data, the EC_{50} can also be related to single-channel parameters by Equation 4.1.[4]

$$EC_{50} = \frac{K_D}{\sqrt{(\Theta + 2)} - 1} \qquad \textbf{Equation 4.1}$$

This expression directly relates the macroscopic property of EC_{50} to microscopic rate constants given that:

$$K_D = \frac{k_{-1}}{k_1} \text{ and, } \Theta = \frac{\beta}{\alpha},$$

where, K_D is the equilibrium agonist dissociation constant and Θ is the gating equilibrium constant.

At high concentrations (>>EC_{50}) where the binding equilibrium is saturated, a measured P_{open} value would be $P_{open,max}$ and is an indication of efficacy, the ability of the agonist to open the channel. Single-channel recording allows for direct determination of this parameter. Furthermore, $P_{open,max}$ depends solely on gating parameters as shown in Equation 4.2.

$$P_{open,max} = \frac{\beta}{(\beta + \alpha)} \qquad \textbf{Equation 4.2}$$

Since Θ = β/α, then $P_{open,max}$ can also be expressed in terms of Θ:

$$P_{open,max} = \frac{\Theta}{(\Theta + 1)} \qquad \textbf{Equation 4.3}$$

We sought to investigate the impact of fluorination at TrpB on receptor gating when the receptor is activated by the agonist, varenicline. We therefore performed single-channel recordings of wild type as well as F_3W mutant receptors at varenicline concentrations of 10 times EC_{50} for each stoichiometry of the α4β2 receptor, A3B2 and A2B3. We applied single-channel data analysis, as detailed in

the following section, in order to determine $P_{open,max}$. As shown in Equation 4.3, $P_{open,max}$ depends solely on Θ and in turn, Θ can be used to determine the impact, if any, of the mutation on EC_{50} (Equation 4.1). Recall from previous chapters that fold-shift, FS = (EC_{50} mutant)/(EC_{50} wildtype). In order to isolate the component of the FS in EC_{50} corresponding to a change in gating (EC_{50} FS Gating), Θ of the wild type receptor ($\Theta_{wildtype}$) and Θ of the mutant receptor (Θ_{mutant}) can be related as shown in Equation 4.4. Thus, for $\Theta_{wildtype} = \Theta_{mutant}$, the corresponding FS in EC_{50} due to gating would be 1, which means that gating is unaltered and therefore, has no impact on that particular mutant's FS in EC_{50}.

$$EC_{50}\ FS\ Gating = \frac{\sqrt{\left(\Theta_{wildtype} + 2\right)} - 1}{\sqrt{\left(\Theta_{mutant} + 2\right)} - 1} \qquad \textbf{Equation 4.4}$$

4.4 Single-Channel Data Analysis: Determining $P_{open,max}$

In our analysis, defining the closed dwell times accurately was essential for determination of $P_{open,max}$, Thus, we sought a strategy that minimized the number of both misdetected channel openings and brief openings that did not reach full conductance. These openings must otherwise be manually rejected. Data were filtered offline (Gaussian, -3 dB, 2-5 kHz) and electrical interference at harmonics of 60 Hz or other frequencies was removed as necessary. Event transitions were detected with Clampfit 9.2 (single-channel search). Analyses were performed at a dead time, τ_d, of 200μs. The dead time was applied either to all events or to events from the baseline only.

Open and closed dwell time histograms were generated as described previously[5] and fitted using the predefined log-transformed exponential probability density function in Clampfit 9.2. To delineate clusters (series of events that end in desensitization), two critical closed durations based on the long components of the closed dwell time histograms were defined. These values (τ_{crit1} and τ_{crit2}) were based on the closed dwell time histograms fitted with multiple components, as previously described.[6] The longest one or more components of the closed dwell time histogram are considered as sojourns in the desensitized state for all of the channels in the patch.[7]

Closed dwell times longer than the respective τ_{crit} values were excluded from further analysis. Sojourns to a subconductance state (<70% of the full conductance level) were treated as closed and accounted for <10% of the total openings in all records when τ_d of 200μs was applied from the baseline. The time-average probability that the channel is open ($P_{open,max}$) was calculated as the total open time divided by the revised total time. The revised total time corresponds to the sum of the total open time (sum total of all the opening events) and the revised closed time (sum total of all the closing events shorter than the defined τ_{crit} value). It follows then, that $P_{open,max}$ depends strongly on the value chosen as the critical closed duration, τ_{crit}. Thus, we report $P_{open,max}$ values for τ_{crit1} and τ_{crit2} values.

Only sections of data files that showed no simultaneous activations were analyzed. For each mutant, this was ≥3 patches obtained from oocytes from ≥2 different donor frogs. Despite these rigorous analysis parameters, some events had to be manually rejected or accepted. Rejecting or accepting an event entailed

a judgment call by the person analyzing the file. Since this project was a collaborative effort between myself and Dr. Jai A.P. Shanata, we sought to ensure that our analysis method did not introduce significant variability. Thus, we each analyzed the same patch and compared our results. As shown below, in Table 4.1, while there was some variability in defining τ_{crit2}, the resulting $P_{open,max}$ values were essentially indistinguishable.

Receptor	Analysis by:	Conductance (pS)	$\tau_{crit\ 1}$ (ms)	$P_{open,max1}$	$\tau_{crit\ 2}$ (ms)	$P_{open,max2}$
A2B3 F3W	XDS	42	238	0.22	9.1	0.98
	JAPS	41	228	0.25	7.7	0.98

Table 4.1 Determining impact of subjectivity on our single-channel analysis method. The same patch was analyzed by two people (XDS and JAPS) to determine single-channel conductance in pS, two critical closed duration values, τ_{crit1} and τ_{crit2} in ms and the corresponding $P_{open,max}$ values.

4.5 Results

Single-channel recording was performed in the cell-attached configuration on the wild type A2B3 and A3B2 receptors as well as A2B3 and A3B2 receptors with F_3W introduced at TrpB by nonsense suppression. In each case, data reported here are for varenicline applied at 10 times the EC_{50}. Figures 4.2 and 4.3 show representative single-channel recording traces for the A2B3 and A3B2, respectively. Pooled closed dwell time histograms for ≥3 patches are given in Figures 4.4. Pooled open-dwell time histograms are shown for A2B3 in Figure 4.5. Finally, Table 4.2 summarizes the results showing $P_{open,max}$ values and contributions of the gating equilibrium constant, Θ, to the fold-shift (FS) in EC_{50}.

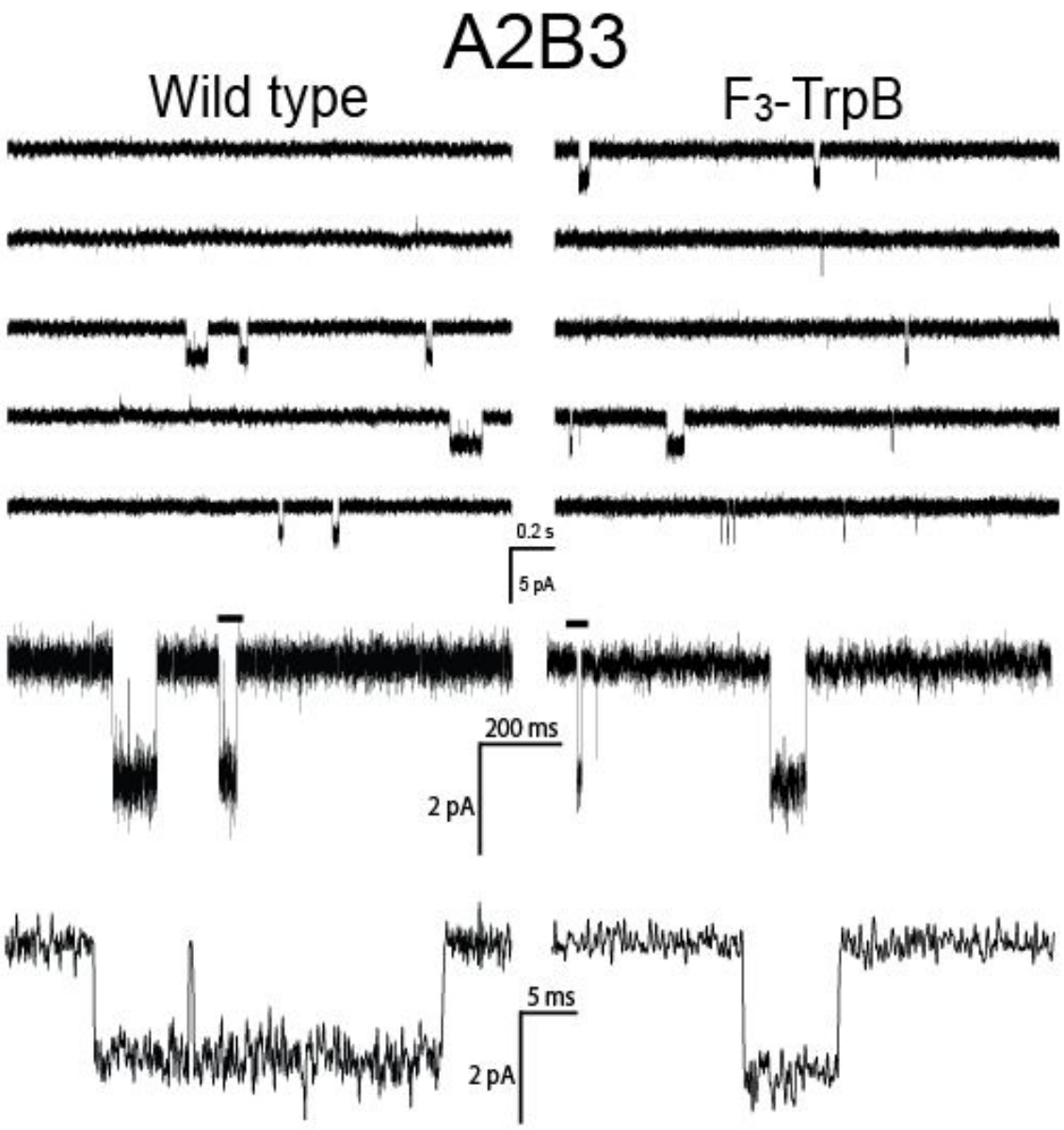

Figure 4.2 Single-channel records of A2B3 wild type (conventional expression; Left) and F_3-Trp introduced at TrpB (nonsense suppression; Right). All recordings are in the cell-attached configuration with a pipette potential of +60mV. Data are filtered at 2kHz for display and openings are shown as downward deflections. Varenicline concentrations (in the pipette) are: wild type (28.5nM) and F_3-TrpB (270nM). The single-channel conductances were 43pS and 42pS, respectively. Each set of traces represents 10s (upper), 1s (middle) and 50ms (lower). The lower traces are expansions of the regions in the middle traces designated with a bar over the trace.

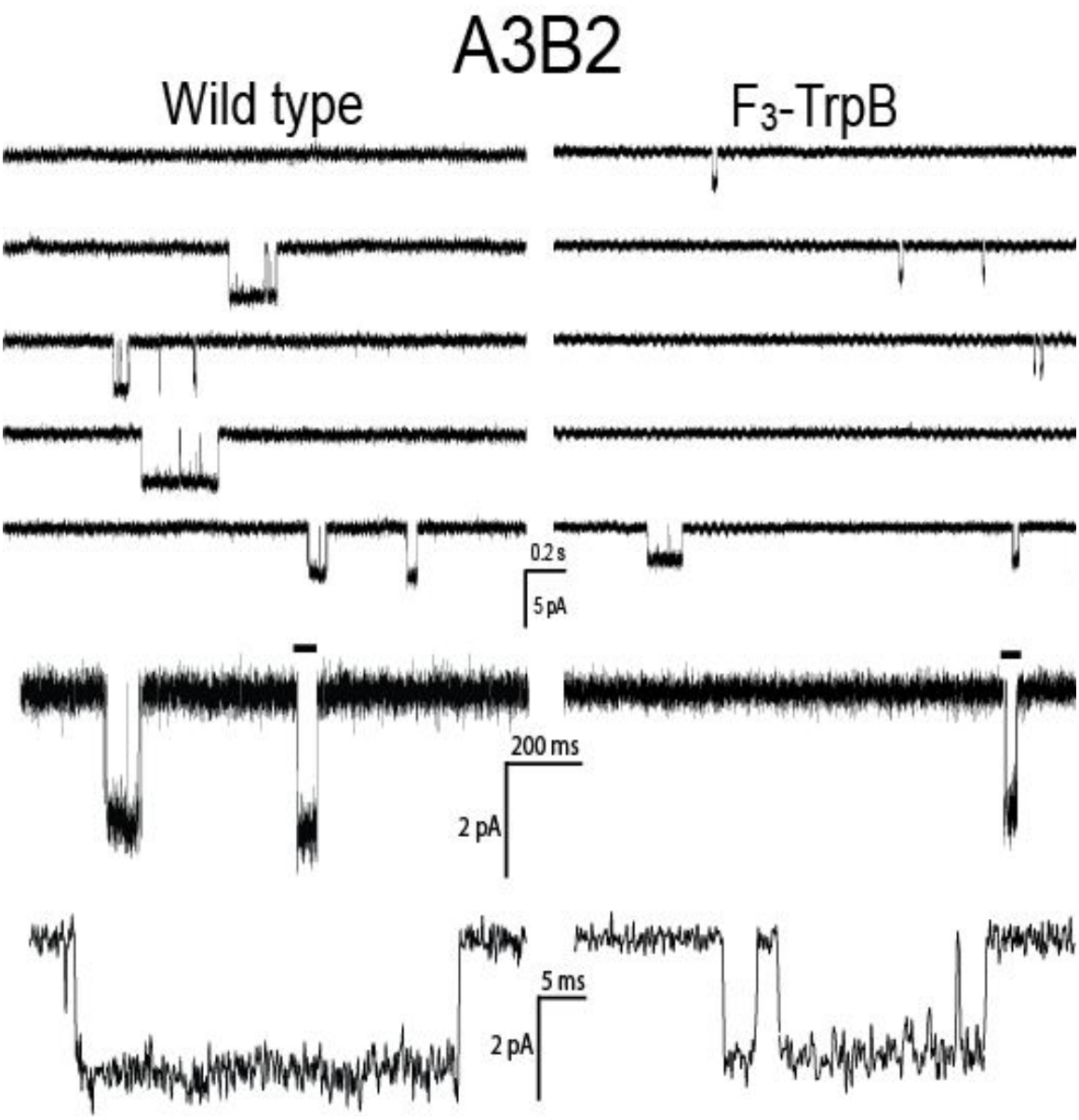

Figure 4.3 Single-channel records of A3B2 wild type (conventional expression; Left) and F_3-Trp introduced at TrpB (nonsense suppression; Right). All recordings are in the cell-attached configuration with a pipette potential of +60mV. Data are filtered at 2kHz for display and openings are shown as downward deflections. Varenicline concentrations (in the pipette) are: wild type (9nM) and F_3-TrpB (120nM). The single-channel conductances were slightly variable: wild type A3B2 (50-55pS), and ~40pS for F_3-TrpB. Each set of traces represents 10s (upper), 1s (middle) and 50ms (lower). The lower traces are expansions of the regions in the middle traces designated with bar over the trace.

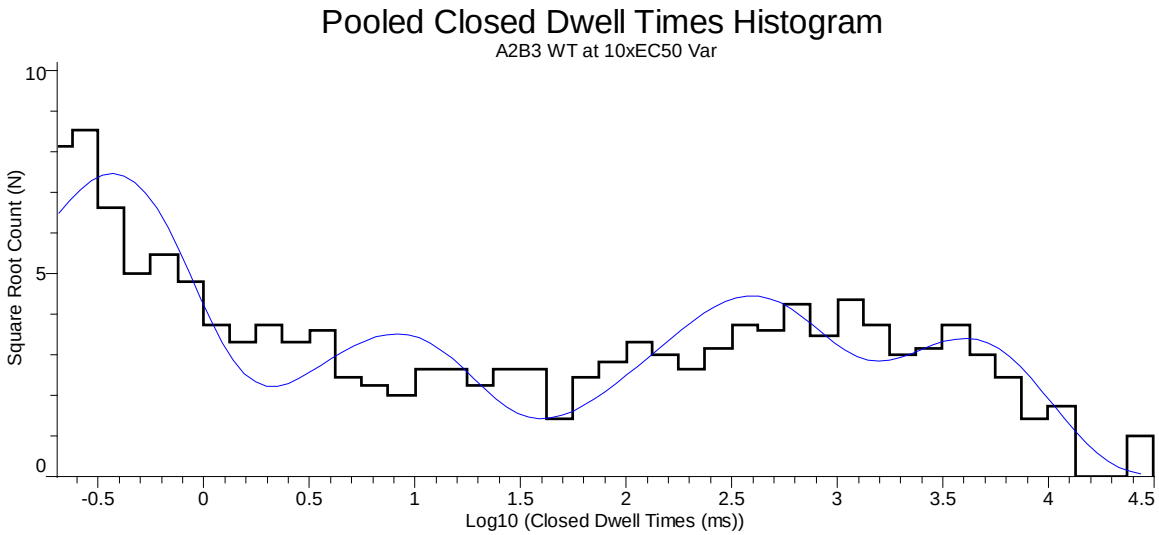
Pooled Closed Dwell Times Histogram
A2B3 WT at 10xEC50 Var
Square Root Count (N)
10
5
0
-0.5
0
0.5
1
1.5
2
2.5
3
3.5
4
4.5
Log10 (Closed Dwell Times (ms))

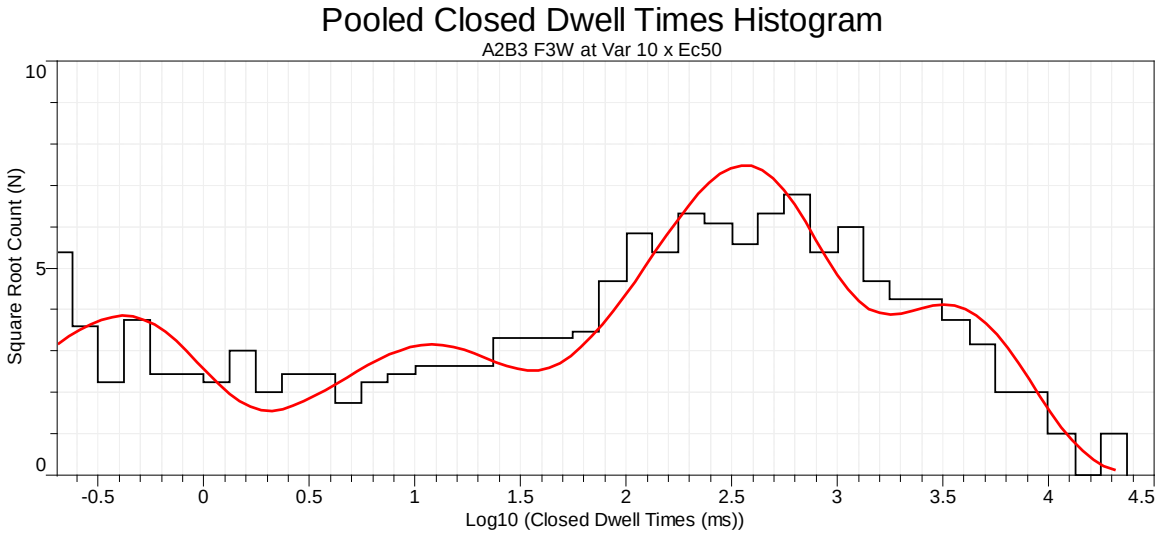
Pooled Closed Dwell Times Histogram
A2B3 F3W at Var 10 x Ec50
Square Root Count (N)
10
5
0
-0.5
0
0.5
1
1.5
2
2.5
3
3.5
4
4.5
Log10 (Closed Dwell Times (ms))

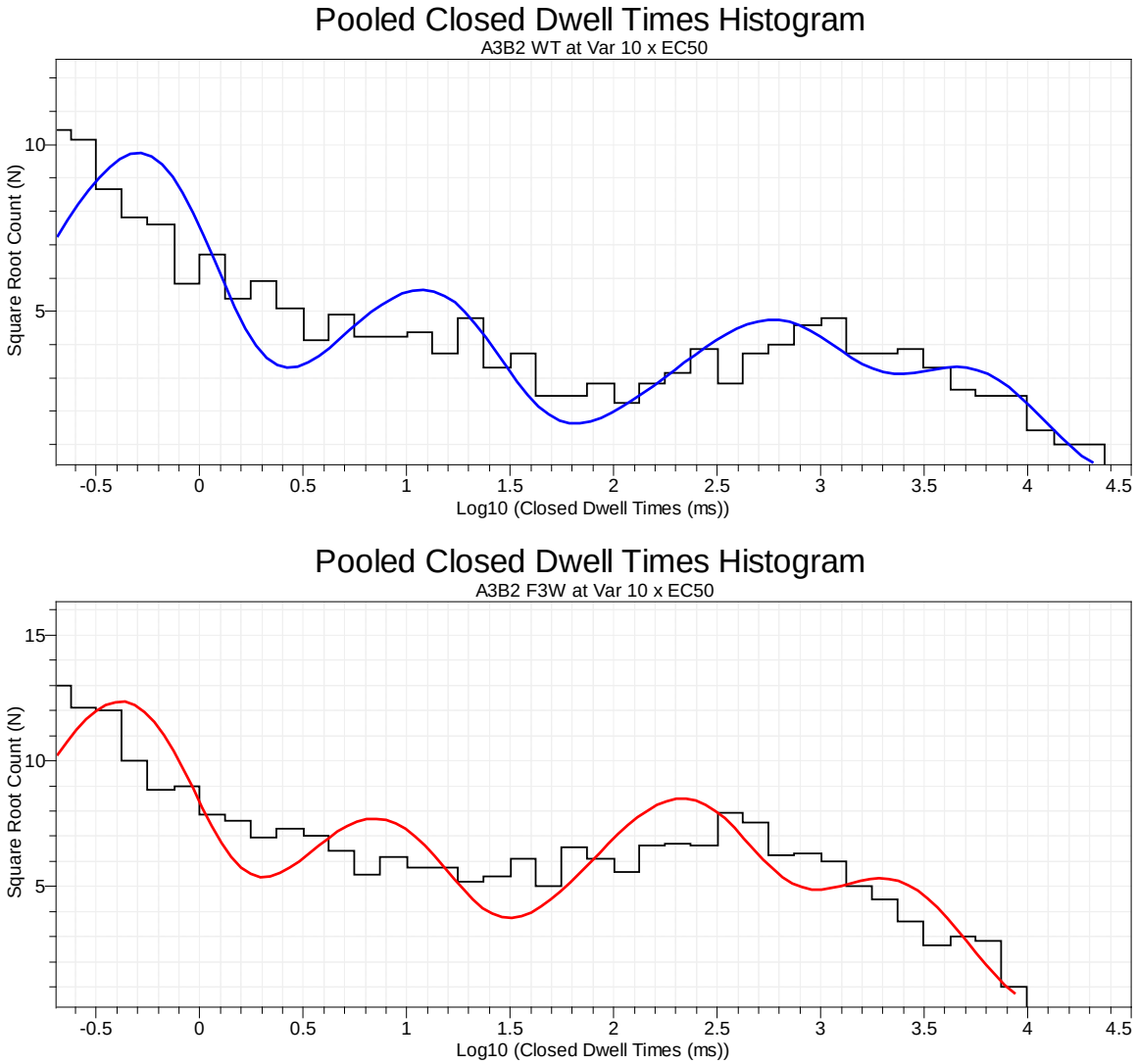

Figure 4.4 (Above and previous page) Four closed dwell time histograms, each representing data from ≥3 patches for each of the 4 receptors studied in these single-channel experiments. In each case, varenicline is applied at 10 times the respective macroscopic EC_{50} values. Each histogram is fitted to 4 components. These histograms were used to determine the values of τ_{crit}. For each A3B2 and A2B3, there is a greater contribution from the long dwell time components in the F_3-TrpB (**red**) histogram than the wild type (**blue**) distribution (see discussion).

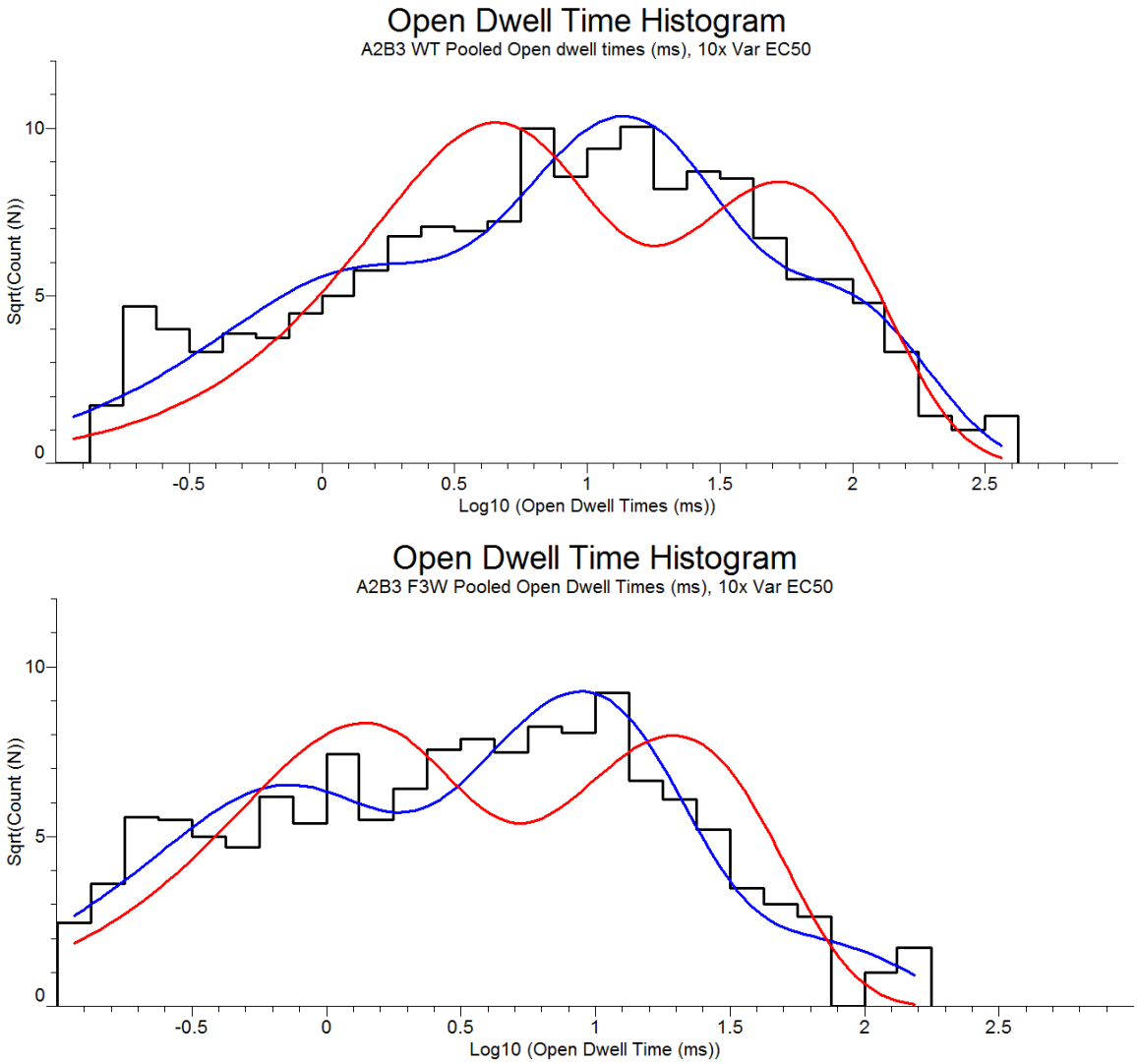

Figure 4.5 Pooled open dwell time histograms of multiple patches each at 10 times the respective macroscopic EC_{50} values for A2B3 wild type and F_3W at TrpB. Overlaying each histogram, are shown 2 component fits (**red**) and 3 component fits (**blue**). For the 2 component fit, the components (% in parenthesis) are as follows: **Upper histogram** (wild type): 53ms (50%) and 3.8ms (50%). **Lower histogram** (F_3-TrpB): 19ms (53%) and 1.2ms (47%). It is not clear what states the two or three open dwell times in the above histogram represent. However, openings of monoliganded receptors could account for at least one additional component (see discussion).

Receptor	$\tau_{crit\ 1}$ (ms)	$P_{open,max1}$	Θ_1	$\sqrt{(\Theta_1+2)} - 1$	EC_{50} FS Gating	Actual EC_{50} FS
A2B3 WT	1277	0.36	0.6	0.6	-	-
A2B3 F3W	1238	0.06	0.1	0.4	1.4	9.5
A3B2 WT	1695	0.51	1.0	0.7	-	-
A3B2 F3W	1062	0.06	0.1	0.4	1.7	12.0

Receptor	$\tau_{crit\ 2}$ (ms)	$P_{open,max2}$	Θ_2	$\sqrt{(\Theta_2+2)} - 1$	EC_{50} FS Gating	Actual EC_{50} FS
A2B3 WT	44	0.96	26.2	4.3	-	-
A2B3 F3W	44	0.88	7.1	2.0	2.1	9.5
A3B2 WT	68	0.96	26.1	4.3	-	-
A3B2 F3W	33	0.71	2.4	1.1	3.9	12.0

Table 4.2 Upper: τ_{crit1} values in ms, corresponding to the longest component of the appropriate closed dwell time histogram, for wild type (**blue**) and F_3W at TrpB (**red**) at A2B3 and A3B2 receptors. $P_{open,max1}$ values and corresponding Θ_1 values are shown. The $(\Theta+2)^{1/2}$ -1 term relates, Θ to EC_{50} as shown in Equation 4.1. EC_{50} FS Gating is the ratio of these terms for WT/F_3W and denotes how much of the actual fold-shift (FS) in EC_{50} can be attributed to a change in gating introduced by the mutation. The actual EC_{50} FS is calculated as (EC_{50} F_3W) / (EC_{50}WT). **Lower**: equivalent values based on τ_{crit2} which corresponds to the second longest component of the appropriate closed dwell time histogram (closed dwell times longer than this value are excluded from further analysis and from the revised total time used to calculate $P_{open,max}$)

4.6 Discussion

4.6.1 $P_{open,max}$ and Dwell Time Histograms

Comparison of $P_{open,max}$ values under different analysis scenarios shows some differences for wild type and F_3-TrpB A2B3 and A3B2 (Table 4.2). This holds true whether τ_{crit1} or τ_{crit2} is used. These different values of τ_{crit} impact which of the long components of the closed dwell time histogram is/are excluded from the calculation of $P_{open,max}$. Regardless, it is clear that $P_{open,max}$, which depends only on the gating equilibrium constant, Θ, is somewhat altered by incorporation of F_3W at

TrpB for each stoichiometry. As detailed in Chapter 2, we observe a systematic decrease in varenicline's potency (increase in EC_{50}) with successive fluorination of TrpB. Recognizing that EC_{50} depends on just two properties: binding and gating (Equation 4.1) we need to address how much this variation in $P_{open,max}$ (and thus gating) impacts EC_{50}. Note that EC_{50} varies directly with K_D, the equilibrium agonist dissociation constant. However, the impact of Θ on EC_{50} is lessened by the square root term in the relationship given in Equation 4.1. Consider the values for $Θ_1$ at A2B3 wild type of 0.6 and A2B3 F_3W of 0.1 (Table 4.2). Though at first glance it might seem significant, this 6 fold change in the value of Θ accounts for a mere 1.4 fold-shift (FS) in EC_{50}. Since the observed FS value for F_3W at A2B3 is 9.5, we can conclude that most of observed effect comes from a change in binding not gating. This supports our analysis of whole-cell data to show that varenicline makes a cation-π interaction, which is a binding interaction, at TrpB. Similar arguments can be made for A3B2 and for values based on $τ_{crit2}$.

Interestingly, we have observed that $P_{open,max}$ is essentially indistinguishable between wild type and F_3W for nicotine at A2B3 regardless of the value of $τ_{crit}$.[8] This poses the very interesting question as to why the same mutation slightly impacts gating for one agonist, varenicline, but not another, nicotine. One possible explanation is that varenicline, lacking nicotine's hydrogen bond to the backbone NH of the receptor, relies more on its cation-π interaction to bring about the conformational change that activates the receptor. Further studies to validate this assumption would consist of single-channel recording of *S*-(6)-chloronicotine,

which has a much weaker hydrogen bond to the receptor (similar to varenicline), to determine whether $P_{open,max}$ is affected.

A more detailed analysis of the dwell time histograms is instructive. Open dwell times provide information about the channel closing rate, α. For A2B3, the open dwell time histograms and resulting fitted distributions are quite similar for wild type and F_3W. Consider the open dwell time distributions when fitted to two components (red lines in Figure 4.5). Both components of the wild type distribution are shifted to ~3 fold longer times than in F_3W. Specifically, the longest component shifts 2.7 fold from 53ms in wild type to 19ms in F_3W and the shorter component shifts 3.3 fold from 3.8ms in wild type to 1.6ms in F_3W. Since both components contribute roughly equally (50% versus 53% and 50% versus 47%; see Figure 4.5), we can quantitatively relate these shifts to potency. Based on the quantitative relationship between EC_{50} and θ given in Equation 4.1, the decrease in open dwell time for the F_3W receptor can account for, at most, a 1.7 fold increase in EC_{50}. This is a small amount of the actual 9.5-fold EC_{50} shift (2.85 nM to 27 nM).

A similar quantitative analysis of the A2B3 closed dwell time histograms to determine kinetic parameters would require recording with varenicline across multiple concentrations. However, qualitatively and based on fairly similar τ_{crit} values, the closed dwell time histograms do not appear to indicate a significant systematic shift in the duration of any of the closed dwell time components. On the other hand, there is an increase in the relative contribution of the two longer closed components shown in Figure 4.4 from wild type to F_3W. The difference in these relative contributions to the long closed components is also apparent qualitatively

in some single-channel traces, the raw $P_{open,max}$ values in some wild type and F_3W varenicline patches appear significantly different. Although impacting apparent $P_{open,max}$, these longest closed dwells (usually 1-10s) almost certainly reflect a desensitized state for these recordings, since they are performed at 10 times EC_{50}. Additionally, the rate of entry into the desensitized state for F_3W may be faster than for wild type, producing briefer clusters. These changes to desensitization should not impact EC_{50}, so they do not factor into the quantitative analysis except for the purposes of defining τ_{crit}.

4.6.2 Nicotine, Varenicline, and Partial Agonism

Varenicline is a partial agonist, and the single-channel conductance (~40pS) does not appear to be significantly lower than what it is for nicotine. Therefore, τ_{crit1}, which produces $P_{open,max}$ values of ~0.1-0.5, is probably a more realistic value. In fact, these values concur with other data. Compare P_{open} values in this range to the relative activation achieved by saturating doses of varenicline and nicotine shown in Figure 4.6.[9]

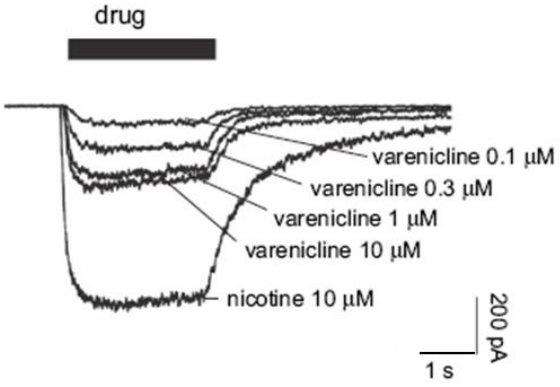

Figure 4.6 The current responses α4β2 receptors to various doses of varenicline and a high dose of nicotine. In these experiments in HEK cells, varenicline's efficacy relative to nicotine was ~45%. Adapted from [10].

In further single-channel work characterizing these agonists, it would be interesting to elucidate the mechanism of partial agonism for varenicline. This could be pursued in the context of recent models of nAChR partial agonism.[11,12] Consistent with some of these models, we observed brief closures in α4β2 single-channel data. Given that these occur even at low concentrations, nM in these experiments, they are probably not due to open channel block. A more likely explanation is that they correspond to the channel re-opening and therefore reflect the channel opening rate, β. Since these are brief closures, β is large. From the closed dwell time histograms in Figure 4.4, there is one component that is <<1ms.

4.6.3 Other Further Studies

For acetylcholine, nicotine, cytisine and varenicline, the agonist potencies are markedly different between the A2B3 and A3B2 stoichiometries (see Chapter 2). Determining the cause of this difference would be of interest. These further studies would be most interesting on wild type receptors without the L9'A mutation, which significantly impacts agonist potency. However, given that true α4β2 receptors lacking the L9'A mutation express at relatively low levels, these studies would prove challenging, especially for unnatural amino acid incorporation.

In conclusion, we have shown that even though the F_3W at TrpB mutation mildly impacts gating for both A2B3 and A3B2 in response to varenicline, the majority of the observed change in potency (over 75%) can be attributed to an impact in binding. This supports our conclusion from Chapter 2 that varenicline makes a cation-π interaction at this site.

4.7 Materials and Methods

Mutagenesis and mRNA synthesis, ion channel expression and unnatural amino acid incorporation were performed as described in Chapter 2 (see Section 2.8). Oocyte batches were characterized by whole-cell recording prior to single-channel recording and sometimes, whole-cell and single-channel recording were performed on the same oocyte as described in [13]. Whole-cell characterizations of the channels were performed as described in Chapter 2. In order to minimize reaminoacylation (see Section 1.3.2), all single-channel recording experiments were performed within 72h of the last tRNA injection.

4.7.1 Dougherty Lab Electrophysiology Rig

The components of the DAD electrophysiology rig used for all single-channel recordings reported herein are summarized below (Figure 4.7). A detailed description of the rig can be found at [13].

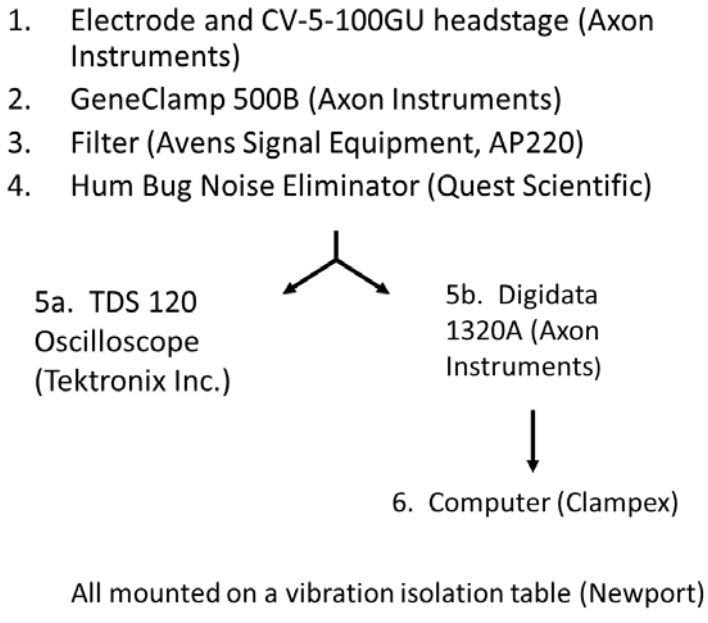

Figure 4.7 Schematic showing the components of the DAD electrophysiology rig and their connectivity.

4.7.2 Single-Channel Recording Solutions

Oocyte incubation media was prepared as described in Chapter 2. All recording solutions were stored at 4°C with parafilm around the cap with the exception of drug solutions that were stored up to several months at -20°C; freeze thaw cycles were minimized as much as possible. Oocyte stripping solution consisted of 196mM NaCl, 2mM KCl, 1mM $MgCl_2$, 5mM HEPES and was pH adjusted with either HCl or NaOH to 7.5. Bath solution consisted of 120mM KCl, 5mM HEPES, 1mM $MgCl_2$, and 2mM $CaCl_2$, pH to 7.4. As reported by Shanata,[13], this solution gives a reversal potential for agonist-induced currents of devitellinized oocytes of ~0mV. Therefore, with an applied pipette potential of +60mV, the transmembrane potential of a cell-attached patch is ~-60mV. Pipette solution consisted of 100mM KCl, 10mM HEPES, 1mM $MgCl_2$, 10mM K_2EGTA, pH = 7.4. It is desirable to perform all of a given set of experiments with a given batch of pipette solution so that single-channel conductances are more comparable (same osmolarity, pH, etc.). All single-channel recordings presented herein were performed on a single batch of pipette solution.

4.7.3 Protocol for Producing Patching Pipettes

KG-33 glass with I.D. = 0.80mm ± 0.05mm, O.D. = 1.60mm ± 0.05mm, length = 75.0mm ± 3 mm (Garner Glass Company; lots: 2544, 5596, 7687, and 8286) was cleaned by complete submersion in chromic-sulfuric acid (Fisher, SC88-1) for ~12-36 hours, followed by rinsing ≥4 times each with alternating water and methanol, then bathing ≥16 hours in methanol and drying ≥12 hours at ~110°C. Cleaned glass was stored for ~6-12 months in an airtight container.

Pipettes with final resistances of ~8-25MΩ, were pulled from cleaned KG-33 glass in two stages using a horizontal Flaming/Brown P-97 electrode puller (Sutter Instrument Company, Novato, CA). A crude estimate (bubble number) of pipette tip size was regularly made and recorded for each pipette after pulling and again after polishing. The tip size was estimated as follows: A 10mL syringe was fitted with silicon tubing (the silicon piece from Drummond Microcaps and Tygon tubing was used) and the back end of the pipette was placed firmly in the tubing. The pipette tip was then submerged in 95-100% ethanol and the plunger depressed slowly until bubbles were seen coming from the pipette tip. The syringe reading at this time was recorded and is termed the bubble number. Depression until the reading is ~4.0 to 4.5mL (i.e. depression of ~5.5 to 6.0mL from the plunger set at 10mL) typically corresponded to pipettes of ~10-20MΩ in our recording solutions. The size was never directly measured, but based on viewing at high magnification and the resistances, the pipette tips in this range were probably ~0.5-3μm in diameter.

Sylgard (World Precision Instruments, SYLG184) was then applied to within ~20-100μm of the pipette tip using the tip of a 23 gauge needle (Becton Dickinson & Co) (Figure 4.8). The Sylgard was cured by ~10-20s of gentle rotation of the pipette, with freshly coated tip up, in a stream of hot air from a heat gun. Pipettes at this stage can be stored for ~14 days in an air-tight container. Pipette tips were polished for ~15-30s on a microforge with a compound microscope providing 900x magnification (15 x eyepieces, 60 x objective, NA 0.70). Polishing was usually done immediately before recording and preferably no more than several hours

before use (Figure 4.8). At this magnification, openings in tips of pipettes with bubble number ~4.4mL or larger are clearly discernible. After polishing the pipette tip, the bubble number was again tested and recorded. The bubble number should be measurably lower than it was after being initially pulled; we found that a decrease of ~0.2 to 0.5mL best facilitates gigaseal formation. This level of decrease in bubble number is often accompanied by a visible change in the pipette tip morphology; the tip becomes slightly darker and tapers to a narrower diameter. If there was no change in the bubble number or no change in the pipette tip, the pipette tip was polished a second time. Pipettes were then stored, coated tip up, in a closed plastic box affixed in clay to prevent contamination. The high magnification of the microforge allowed for unsuitable pipettes to be identified and discarded before attempting to record with them. For example, in some cases, sylgard accidentally covered the pipette tip making it unusable. In other cases, dirt near the tip was readily visible.

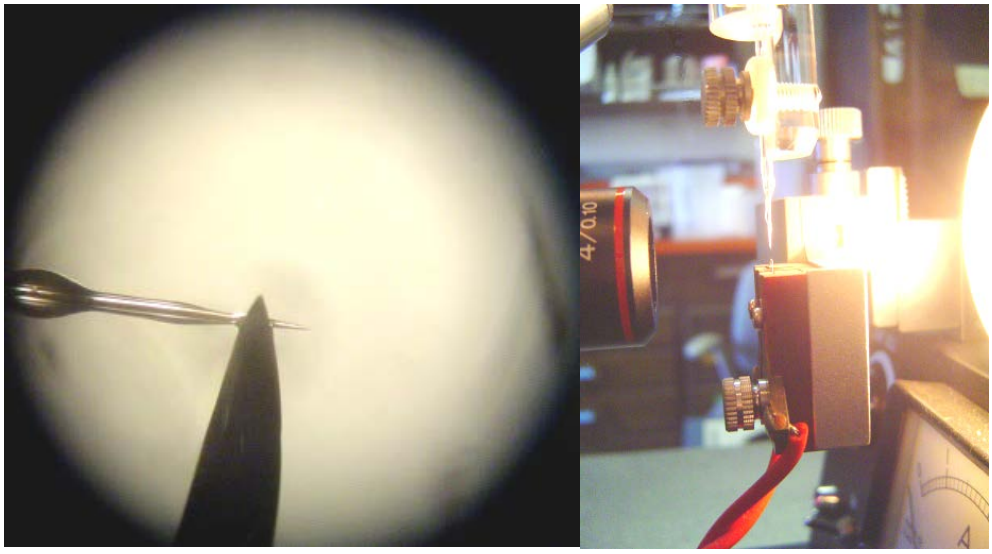

Figure 4.8 Sylgarding (**left**) and polishing (**right**) patch pipettes. Adapted from [13].

4.7.4 Single-Channel Recording

One to three oocytes were placed in hypertonic solution (oocyte stripping solution) for 15-30 minutes. The vitelline membrane was generally visible as a translucent, colorless membrane that was separated from the oocyte membrane by up to ~50-100μm. The oocyte's vitelline membrane was then gently stripped using 2 pairs of jeweler's forceps (Dumont, No. 5). The devitellinized oocyte was then transferred to a separate 35mm dish with bath solution for 1-2 minutes, then transferred to the recording chamber which was filled with bath solution (~1mL). When handling devitellinized oocytes, care was taken to avoid contact with the air-water interface, which can cause the oocyte membrane to rupture.

The tips of sylgarded, polished pipettes were filled by submerging them in the drug pipette solution and applying suction to the back of the pipette for ~30-60s. The same 10mL syringe used to test the "bubble number" can be used to apply this suction, provided that it is kept dry. During this time, the progress of filling the pipette tip was monitored by viewing the pipette against a strong light source for contrast. The back end of the pipette was then fire polished for ~3-5s in the flame of a small butane torch (~2cm-long flame) until the back end of the pipette was visibly smooth and rounded. This step is important to reduce the extent to which the pipette scratches chloride off of the AgCl wire when loading the pipette into the electrode holder. Once cooled to room temperature, the pipette is then back filled with the same drug solution as was used to fill the tip, using a 28 gauge syringe needle (World Precision Instruments, MF28G-5) and 1mL syringe with

attached 0.2μm nylon filter and flicked until all bubbles have been removed from the tip.

Once prepared, the pipette was loaded into the electrode holder with AgCl wire. Ag wire was re-chlorided prior to each recording session and any time that silver was visible on the wire (shiny as opposed to dull brown) by submersion in household bleach for 15-30 minutes, until dull brown in color. Care was taken not to chloride the entire length of the wire, as the non-pipette end must make electrical contact with the brass pin that connects to the headstage in the pipette holder. Ag wires can generally be re-chlorided 3-5 times. Once the pipette was secured on the headstage, positive pressure was applied and the solution level in the chamber was reduced to ~1-2mm above the oocyte by gently sucking off the top layer of solution with a Pasteur pipette. In our rig, this leaves ~300μL of bath solution in the chamber. The application of positive pressure to the pipette and aspiration of the top layer of solution are important steps to prevent clogging of the pipette tip before a gigaseal is formed with the oocyte.

The pipette was introduced into the recording bath at a steep angle of 60-70°. This, in addition to prior reduction of the bath solution volume, minimized the length of the pipette in contact with the solution and the resultant noise. The coarse and fine manipulators were then adjusted to place the tip of the pipette within ~200μm of the oocyte without touching it. All unnecessary AC electronics (especially lights) were then turned off and the pipette resistance was tested and recorded as the solution resistance. Final approach to the oocyte occurred with the fine manipulator (Narishige) while applying a 100μV seal test. Contact with the

oocyte was recognized as a small baseline deflection on the oscilloscope accompanied with a 1.5- to 3-fold increase in the pipette resistance.

Once the pipette was in contact with the oocyte membrane, data acquisition was initiated, then gentle suction was applied by mouth as soon as possible in order to minimize channel activity that might be missed as channels desensitize. Once a gigaseal of several to hundreds of gΩ was formed (time varied from instantaneous to several minutes), the desired pipette potential was applied. Data were collected using a GeneClamp 500B amplifier (Axon Instruments) at full bandwidth (50kHz; 4-pole Bessel, -3dB) with a CV-5 100GU headstage. The signal was then low-pass filtered (Avens Signal Equipment, AP220, 20kHz; 8-pole Bessel, -3dB), sampled with a Digidata 1320A (50kHz), and acquired in Clampex 9.2 (Axon Instruments). Channel openings and closings were observed as nearly discrete changes in the measured current when the signal was large enough with respect to the noise (usually ~3-10 fold). Once the gigaseal was lost, sufficient data (number of events) were collected, or further channel activity seemed unlikely due to channel desensitization or inactivation, the data acquisition was stopped.

4.7.5 Control for Endogenous Mechanosensitive Channels

Channels that are believed to be endogenous to oocytes were observed in some single-channel recordings. These channels generally exhibited kinetics that were different from nAChRs kinetics, a different current (at the recording pipette potentials), and were often mechanosensitive.[14,15] Application of suction to the oocyte after a few minutes of recording on the channel of interest allowed for the identification of the presence of mechanosensitive channels. When suction is

applied, the channel is probably not mechanosensitive if its activity (P_{open}, τ_{open}, conductance, etc.) continues at the same level. The presence of a mechanosensitive channel in the patch could often be identified if activity could be induced by suction in a record with no activity (or a desensitized channel). P_{open} for these mechanosensitive channels varied with applied suction: ~0.5 with light suction and nearly 1 with moderate suction. In addition to this characteristic, these channels were generally easy to distinguish from exogenously expressed channels due to their raggedy openings and closings. On several occasions, light suction was applied during channel openings; nAChRs did not display a qualitatively different P_{open} or conductance when suction was applied in this way.

4.8 Acknowledgements

This project was a collaborative effort between myself and Dr. Jai A. P. Shanata. I would like to thank Jai for working with me and for training me in the methods for single-channel recording and analysis. His unbounded enthusiasm, patience and knowledge in the field made every moment enjoyable. In addition, I thank Dr. Bruce N. Cohen for helpful discussions on single-channel recording as well as *Xenopus* oocyte health and expression.

4.9 References

1 Tavares, X. D. S. *et al.* Variations in Binding Among Several Agonists at Two Stoichiometries of the Neuronal, alpha 4 beta 2 Nicotinic Receptor. *J. Am. Chem. Soc.* **134**, 11474-11480, doi:10.1021/ja3011379 (2012).

2 Hamill, O. P., Marty, A., Neher, E., Sakmann, B. & Sigworth, F. J. Improved patch-clamp techniques for high-resolution current recording from cells and cell-free membrane patches. *Pflugers Arch.* **391**, 85-100, doi:10.1007/bf00656997 (1981).

3 Sakmann, B. N., E. *Single-Channel Recording*. 2nd edn, (Plenum, 1995).

4 Kalbaugh, T. L., VanDongen, H. M. A. & VanDongen, A. M. J. Ligand-binding residues integrate affinity and efficacy in the NMDA receptor. *Mol. Pharmacol.* **66**, 209-219, doi:10.1124/mol.66.2.209 (2004).

5 McManus, O. B., Blatz, A. L. & Magleby, K. L. Sampling, Log Binning, Fitting, and Plotting Durations of Open-and-Shut Intervals from Single Channels and the Effects of Noise. *Pflugers Archiv-Eur. J. of Physiol.* **410**, 530-553 (1987).

6 Jackson, M. B., Wong, B. S., Morris, C. E., Lecar, H. & Christian, C. N. Successive openings of the same acetylcholine receptor channel are correlated in open time. *Biophysical journal* **42**, 109-114 (1983).

7 Sakmann, B., Patlak, J. & Neher, E. Single acetylcholine-activated channels show burst-kinetics in presence of desensitizing concentrations of agonist. *Nature* **286**, 71-73 (1980).

8 Xiu, X. A., Puskar, N. L., Shanata, J. A. P., Lester, H. A. & Dougherty, D. A. Nicotine binding to brain receptors requires a strong cation-pi interaction. *Nature* **458**, 534-U510, doi:10.1038/nature07768 (2009).

9 Rollema, H. *et al.* Rationale, pharmacology and clinical efficacy of partial agonists of alpha4beta2 nACh receptors for smoking cessation. *Trends Pharmacol Sci* **28**, 316-325, doi:10.1016/j.tips.2007.05.003 (2007).

10 Rollema, H. *et al.* Pharmacological profile of the alpha4beta2 nicotinic acetylcholine receptor partial agonist varenicline, an effective smoking cessation aid. *Neuropharmacology* **52**, 985-994, doi:10.1016/j.neuropharm.2006.10.016 (2007).

11 Lape, R., Colquhoun, D. & Sivilotti, L. G. On the nature of partial agonism in the nicotinic receptor superfamily. *Nature* **454**, 722-727, doi:10.1038/nature07139 (2008).

12 Mukhtasimova, N., Lee, W. Y., Wang, H. L. & Sine, S. M. Detection and trapping of intermediate states priming nicotinic receptor channel opening. *Nature* **459**, 451-454, doi:10.1038/nature07923 (2009).

13 Shanata, J. A. P. *Single-Molecule Studies of Ion Channels Expressing Unnatural Amino Acids* Ph. D. thesis, California Institute of Technology, (2011).

14 Reifarth, F. W., Clauss, W. & Weber, W. M. Stretch-independent activation of the mechanosensitive cation channel in oocytes of Xenopus laevis. *Biochim. Biophys. Acta-Biomembr.* **1417**, 63-76, doi:10.1016/s0005-2736(98)00257-0 (1999).

15 Silberberg, S. D. & Magleby, K. L. Voltage-induced slow activation and deactivation of mechanosensitive channels in Xenopus oocytes. *J. Physiol.-London* **505**, 551-569, doi:10.1111/j.1469-7793.1997.551ba.x (1997).